FLAMMABILITY AND COMBUSTION BEHAVIORS IN AEROSOLS FORMED BY INDUSTRIAL HEAT TRANSFER FLUIDS PRODUCED BY THE ELECTROSPRAY METHOD

A Dissertation

by

PENG LIAN

Submitted to the Office of Graduate Studies of
Texas A&M University
in partial fulfillment of the requirements for the degree of

DOCTOR OF PHILOSOPHY

August 2011

Major Subject: Chemical Engineering

Flammability and Combustion Behaviors in Aerosols Formed by Industrial Heat Transfer Fluids Produced by the Electrospray Method

FLAMMABILITY AND COMBUSTION BEHAVIORS IN AEROSOLS FORMED BY INDUSTRIAL HEAT TRANSFER FLUIDS PRODUCED BY THE ELECTROSPRAY METHOD

A Dissertation

by

PENG LIAN

Submitted to the Office of Graduate Studies of
Texas A&M University
in partial fulfillment of the requirements for the degree of

DOCTOR OF PHILOSOPHY

Approved by:

Chair of Committee,	M. Sam Mannan
Committee Members,	Zhengdong Cheng
	Carl Laird
	Jerald Caton
Head of Department,	Michael Pishko

August 2011

Major Subject: Chemical Engineering

ABSTRACT

Flammability and Combustion Behaviors in Aerosols Formed by Industrial Heat Transfer Fluids Produced by the Electrospray Method. (August 2011)

Peng Lian, B.S., Liaoning University of Petroleum and Chemical Technology;

M.S., China University of Petroleum, Beijing

Chair of Advisory Committee: Dr. M. Sam Mannan

The existence of flammable aerosols presents a high potential for fire hazards in the process industry. Various industrial fluids, most of which operate at elevated temperatures and pressures, can be atomized when released under high pressure through a small orifice. Because of the complexity in the process of aerosol formation and combustion, the availability of data on aerosol flammability and flame propagation behaviors is still quite limited, making it difficult to evaluate the potential fire and explosion risks from released aerosols in the process industry and develop safety measures for preventing and/or mitigating aerosol hazards. A study is needed to investigate the relationship between aerosol combustion behaviors and the properties of the aerosols.

This dissertation presents research on the combustion behaviors of flammable aerosols. Monodisperse aerosols created by industrial heat transfer fluids were generated using electrospray. The characteristics of flame propagations in aerosols are observed in the aerosol ignition tests. Flames in aerosols are characterized by non-uniform shapes

and discrete flame fronts. Droplet evaporation was found to play an important role in the different burning modes of aerosol flames. Droplet evaporation behaviors and fuel vapor distribution are further related to aerosol droplet size, droplet spacing, movement velocity, and liquid volatility. The burning mode of a global flame with rapid size expansion is considered the most hazardous aerosol combustion scenario. When the liquid fuel has a certain level of volatility, there is an uneven distribution of fuel vapor in the system and this may cause the unique phenomenon of burning mode variations combined with enhanced flame propagation speed.

Using an integrated model, the minimum ignition energy values of aerosols were predicted. The aerosol minimum ignition energy is influenced by the fuel-air equivalence ratio and the droplet size. Higher equivalence ratios, up to 1.0, significantly reduce the minimum ignition energy, while larger droplet sizes result in a higher minimum ignition energy.

Results of the current work indicate that existence of droplets in the aerosol system can increase the severity of potential damages from aerosol fires. Preventive measures should be taken in the process industry to avoid fine atomization of leaked fluids and formation of flammable aerosols. Aerosol droplet size and the factors which influence the dispersion of aerosol droplets should be considered in the assessment of aerosol flammability and related fire hazards.

DEDICATION

To my parents, for their love and encouragement,

to my wife and son.

ACKNOWLEDGEMENTS

Looking back this last five years, I owe a deep debt of gratitude to my advisor, Dr. M. Sam Mannan, for his guidance and support throughout my research program. He has helped me through the most difficult part of my research, not only by the creative ideas about the physical science, but also by the inspirational encouragement to overcome the emotional hardships as a brave man. I will benefit from these valuable lessons and true friendship with Dr. Mannan through my life.

I am grateful to Professor Zhengdong Cheng, a member of my advisory committee, who helped me find the idea of applying electrospray method on aerosol production. Special thanks to Professor Jerald Caton and Professor Carl Laird for their advice and encouragement as my committee members.

I have been blessed to have wonderful colleagues to work together on my research. Andres Mejia's modesty and sincerity, as well as his critical mind to discover the reasons behind a minute change in an experimental observation, have been crucial for advance of our team efforts in this project. It is a pleasure to recognize the contributions to this research program from the teamwork with brilliant researchers around me, including Dr. Yingchun Zhang, Dr. Yuyan Guo, Dr. Ling Miao, Dr. Xiaodan Gao, Dr. Dedy Ng, Dr. Yi Liu, and Szu-ying Huang. Those seemingly endless discussions are all happy memories now.

Gratitude is expressed to the Department of Chemical Engineering for providing me the opportunity to advance my education for the doctorate. Help from the

administrative staff through each step, from my starting date at Texas A&M to the graduation, has eased the hassles. Special thanks to Randy Marek and his mechanical workshop and the energetic student workers, for fabricating the instruments for our lab tests.

I'm extremely fortunate to have been a member of the Mary Kay O'Connor Process Safety Center, at a time when process safety is becoming "Second Nature" for the success of our industry and future of our society.

Finally I'd like to thank my parents, my wife and all the people with whom I have been living and working together. All of them are my role models, showing me the good values to lead an honest and happy life.

TABLE OF CONTENTS

CHAPTER Page

CHAPTER Page

LIST OF FIGURES

FIGURE Page

FIGURE Page

FIGURE Page

LIST OF TABLES

NOMENCLATURE

α_g	Thermal diffusivity, m^2/s
λ	Thermal conductivity, W/K m
μ	Dynamic viscosity, N/s m^2
δ	Thickness of the flame front, m
ρ_∞	Density of air, kg/m^3
ρ_l	Density of liquid in aerosol droplet, kg/m^3
ρ_u	Density of the unburned aerosol mixture, kg/m^3
γ_f	Stoichiometric coefficient
ε	Liquid permittivity
τ_c	Characteristic time for initiation of flame front speed, m/s
Ω	Fuel-air equivalence ratio
A	The flame size, m^2
A_k	The flame kernel's outer surface area, m^2
A^*	Non-dimesionalized flame size, m^2
B_H	Non-dimensional energy transfer number
C_{pa}	Specific heat of air, J/kg K
C_D	The drag coefficient
C_{pl}	Specific heat of liquid in aerosol droplet, J/kg K
$D_{[10]}$	10% percentile droplet diameter, μm
$D_{[50]}$	50% percentile droplet diameter, μm

$D_{[90]}$	90% percentile droplet diameter, μm
$D_{[3][2]}$	Surface area moment mean diameter or Sauter Mean Diameter (SMD), μm
d_1	Produced aerosol droplet size in non-ignition environment, m
d_2	Measured aerosol droplet size in ignition test environment, m
E	Electric field, N/C
E_1	Fuel evaporation rate per unit length from droplets passing through the height the aerosol system, kg/m s
E_2	Evaporated fuel vapor from an aerosol droplet averaged by its travel distance in the flame, kg/m
E_{min}	Aerosol minimum ignition energy, J
g	Gravitational constant, m/s^2
H_c	Heat of combustion, J/kg or J/mol
H_{evp}	Heat of evaporation, J/kg or J/mol
k'	Non-dimensional positive coefficient
k_a	Thermal conductivity of air, W/K m
k_l	Thermal conductivity of liquid fuel in aerosol droplets, W/K m
L_S	Overall travel distance of a droplet traveling inside the flame, m
M	Total amount of evaporated fuel from a droplet traveling inside the flame, kg
M_f	Average molecular weight of the heat transfer fluid, kg/mol
M_k	Mass of the flame kernel, kg
M^*	Non-dimensionalized evaporated fuel vapor from aerosol droplets
$\dot{m}$	Droplet evaporation rate, kg/s

P_f	Vapor pressure of the heat transfer fluid, Pa
P_k	Flame kernel pressure, Pa
P_S	The number of droplets passing through the height in the aerosol system per second, 1/s
P_r	Prandtl number
P^*	Non-dimensionalized vapor pressure of liquid fuel in aerosol droplets
Q_{comb}	Combustion heat release rate in the flame kernel, J/s
Q_{cond}	Conduction heat loss from the flame kernel to surrounding environment, J/s
Q_{cp}	Heat to raise temperature of the fresh mixture entering the flame front, J/s
Q_{vap}	Aerosol droplet evaporation heat in the flame front, J/s
S	Flame front propagation speed, m/s
S_{La}	Laminar flame front propagation speed in the aerosol system, m/s
S_{Lg}	Laminar flame front propagation speed in the gaseous mixture, m/s
R	Ideal gas constant
R_e	Reynolds number
R_k	Flame kernel radius, m
R_s	Aerosol droplet radius, m
T_∞	Gaseous phase temperature around aerosol droplets, K
T_{am}	Ambient gaseous phase temperature, K
T_b	Boiling point temperature of the heat transfer fluid, K
T_k	Flame kernel temperature, K
T_L	Liquid temperature in aerosol droplets, K

t_c	Characteristic time for chemical reaction in the vapor phase, s
t_e	Characteristic time for fuel droplet evaporation, s
t_q	Characteristic time for flame zone quenching, s
U^*	Non-dimensionalized flame propagation speed, m/s
u	The flame propagation speed, m/s
ΔV	Volume of evaporated liquid from aerosol droplets in the aerosol system, m^3
V_k	Flame kernel volume, m^3
v	Kinematic viscosity, m^2/s
v_∞	Gas phase flow velocity, m/s
v_s	Droplet movement velocity in the aerosol system, m/s
Y_f	Droplet travel distance in the aerosol system before entering the flame, m
Y_s	Vertical position of the droplet's center in the aerosol system, m
$y_{O,\infty}$	Oxygen concentration in air

CHAPTER I

INTRODUCTION

The existence of flammable aerosols presents a high potential for fire and explosion hazards in the process industry. Various industrial fluids, most of which operate at elevated temperatures and pressures, can be atomized when released under high pressures through small-diameter orifices. 54 accidents involving fires and explosions, and an estimated loss of $150 million due to aerosol releases were reported during the last ten years (Febo & Valiulis, 1996). The potential existence of aerosols and related fire hazards can be found in the reported hydrocarbon releases and fire cases which frequently occurred in the offshore environment (HSE, 2000). One of the contributing causes of these accidents was the misconception of aerosol hazards, which assumed that combustible liquids were safe when operating below their expected flash point (Krishna et al. 2003a; Krishna et al. 2003b; Krishna et al. 2004).

Because of the complexity of the process of aerosol formation and combustion, the availability of data on aerosol flammability and flame propagation behaviors is still quite limited, making it difficult to evaluate potential fire and explosion risks of released aerosols and develop safety measures for preventing and/or mitigating aerosol hazards in the process industry. Investigation of aerosol flammability and combustion behaviors will not only be of practical importance to the process industry, but will also contribute

---

This dissertation follows the style and format of the *Journal of Loss Prevention in the Process Industries*.

to a fundamental understanding of aerosol combustion.

STATEMENT OF THE PROBLEM

Flammable aerosols can be formed in the process industry through the pressurized release of industrial hydrocarbons, creating a fire hazard in the surrounding area. Unfortunately, fire hazards of flammable aerosols have not been fully recognized. In order to assess the hazards, a study is needed to investigate the relationship between aerosol combustion behaviors and the properties of aerosols. This study should provide information to answer to the following two questions on flammable aerosols:

1. How flammable is an aerosol system with a certain fuel concentration and droplet size?
2. When the aerosols are ignited, how different are the flames of aerosols from the flames of flammable gaseous mixtures?

Together with the knowledge of aerosol formation and dispersion, an understanding of aerosol combustion behaviors gained from this study can be used to establish a system for assessing aerosol fire hazards and providing guidance on preventive and protective measures in the process industry.

METHODOLOGY

In order to assess fire hazards of aerosols, the current research focuses on two topics, the combustion behaviors of aerosols and the flammability of aerosols. Research on the first topic investigates characteristics of aerosol flames, such as different flame

burning modes, related flame sizes and flame propagation speeds. Research on the second topic tries to predict the minimum ignition energy of aerosols. The influences of properties of the liquid droplets in the aerosol system are studied for both topics. Knowledge from the current study on aerosol flammability and combustion behaviors can connect to previous knowledge on aerosol formation and dispersion, so that a comprehensive assessment methodology on aerosol fire hazards can be established, as shown in Figure 1-1. Using knowledge of aerosol formation and dispersion, the process areas where aerosols with certain properties can be formed can be identified. Knowledge of the properties of aerosol droplets and their contribution to the appearance of lager flames or faster flame propagation will lead to protective measures in the process area that will reduced the destructive impact of aerosol fires on the surrounding environment. Knowledge of the energy required for the ignition of aerosols with certain properties will lead to preventative measures that avoid potential ignition sources.

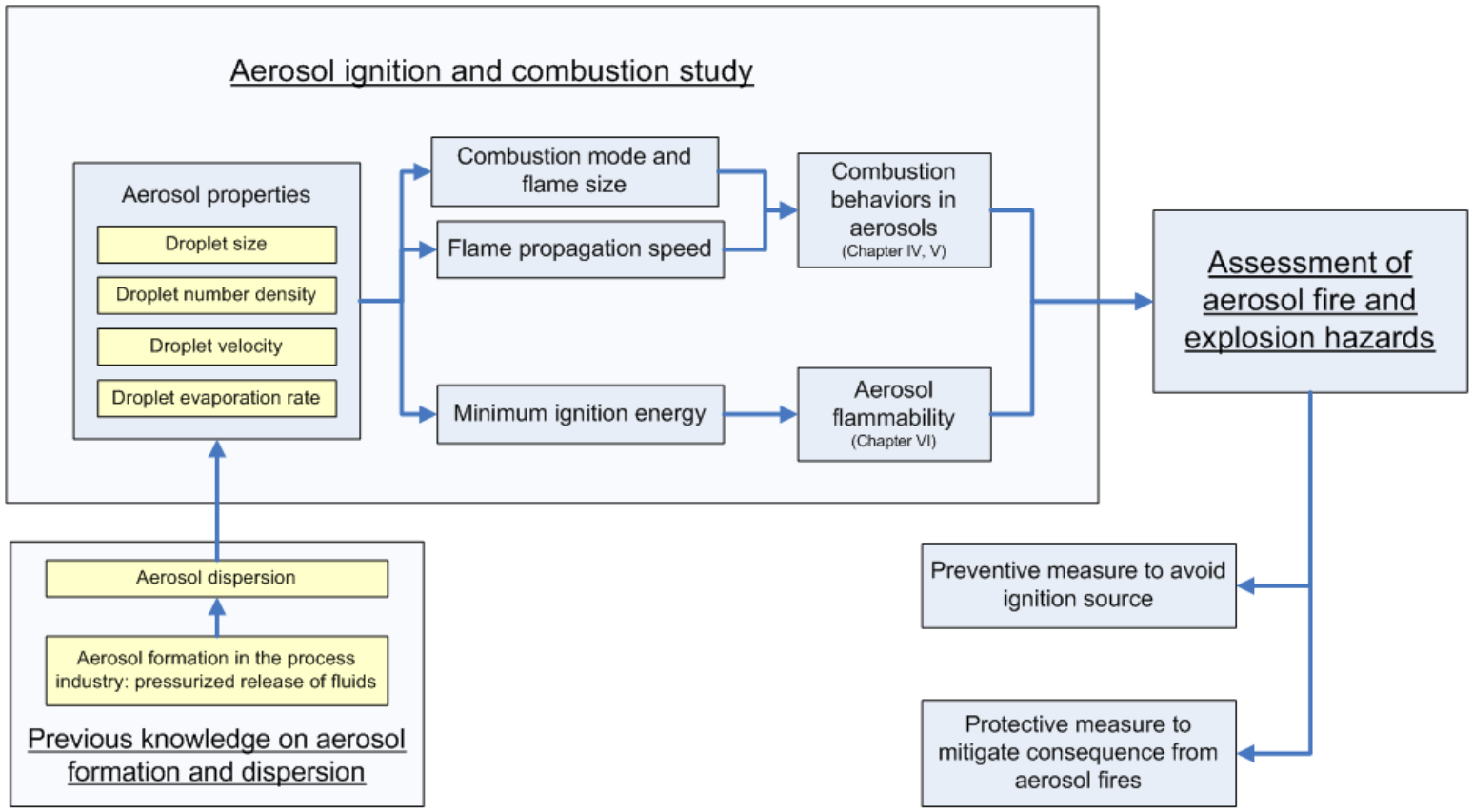

Figure 1-1 Research methodology on aerosol flammability and combustion behaviors

OBJECTIVES

The objective of this research is to study the flammability and combustion behavior of aerosols from industrial heat transfer fluids. The current work aims to lay the foundation for a framework for systematic evaluations of potential fire and explosion hazards from aerosols. The framework needs to address two basic issues: aerosol flammability and potential consequences from aerosol fires. The indicator used to represent the flammability of aerosols is the aerosol minimum ignition energy. Important parameters used to characterized fires in aerosols include the burning mode, flame size, and the flame propagation speed.

Specific aims of the research include:

1) Designing a system to produce monodisperse aerosol droplets with the electrospray method using industrial heat transfer fluids. Studying the influence of electrospray conditions, including nozzle voltage and liquid flow rate, on aerosol droplet size;
2) Observing characteristics of aerosol flames through the heat transfer fluids. Studying the applicability of flame movement speed and flame area for characterization of the flame propagation process in aerosol systems, and studying the influence of aerosol properties on characteristics of the flame propagation process;
3) Studying the influence of droplet evaporation and movement on flame propagation in the aerosol systems using numerical modeling.

4) Developing a model to predict the minimum aerosol ignition energy as an indicator for aerosol flammability.

ORGANIZATION OF THE DISSERTATION

This dissertation is based on a current, ongoing research program in the aerosol laboratory of the Mary Kay O'Connor Process Safety Center at Texas A&M University. Parts of the work in the dissertation were published in peer-reviewed publications.

This dissertation includes seven chapters. Following this chapter, a literature review is presented in Chapter II. The literature review represents the current state of knowledge on the topics in this research, including formation and dispersion of aerosols in the process industry, and research progress in flammability and combustion behaviors of aerosols. This knowledge is considered necessary for understanding the methodology in the current research program. Chapter III introduces the method electrospray and its application in the current work for aerosol production using industrial heat transfer fluids. The study shows that the droplet size of the aerosol produced by electrospray can be finely controlled.

Chapter IV and Chapter V focus on combustion behaviors in aerosols of industrial heat transfer fluids. Chapter IV includes information on aerosol ignition tests and experimental observations on flame characteristics in aerosols. Unlike combustion of gaseous mixture, different burning modes exist in aerosols. Chapter V discusses the reasons for the phenomena observed in the aerosol ignition tests. Both non-dimensional analysis and numerical modeling of the aerosol droplets' aerodynamics and behaviors

are used to address the issues of flame size and flame propagation speed. The study intends to establish a relationship between flame behaviors in aerosols and aerosol properties.

Chapter VI focuses on aerosol flammability. An integrated model of the flame kernel for flame initiation in aerosol systems is established to predict the minimum aerosol ignition energy. The integrated model combines the kernel growth process with the flame front theory, and uses the kernel temperature as the criterion for successful ignition. The minimum ignition energy of tetralin aerosols is studied. Chapter VII concludes the work from Chapter III to Chapter VI and proposes directions for future development of the research program.

CHAPTER II

BACKGROUND

Hydrocarbon fluids are widely used in the process industry under various operating conditions. The fluid's flash point, fire point and auto-ignition point temperatures are the three main indicators for assessment of the fluid's safe operating conditions when considering fire safety.

Flash point is the temperature under which the fluid is capable of producing sufficient vapor through evaporation to support a flash fire which exists momentarily on the liquid surface. A liquid flash point is usually measured according to the ASTM standard D92, the Cleveland Open Cup method, or the ASTM standard D93, the Penske Martens Closed Cup method. The fire point is a higher temperature under which the fluid is capable of producing vapor through evaporation that is sufficient enough to support sustained fire on a liquid surface.

A fluid with lower flash point or fire point is usually considered easier to ignite; this needs to be considered in the design of the operation conditions for the fluid. Then there is the general concept that liquid fluids are safe at temperatures below their flash point. The concept might be wrong or even dangerous to the process industry, because it does not consider when fluids are atomized and exist in the form of aerosols.

The flash point and fire point temperatures mainly depend on the liquid's volatility. But when the liquids are atomized into fine droplets which are suspended in the air, the surface area of the liquid becomes significantly larger than surface area of the

same liquid with the same volume which exists in form of a liquid pool. The larger liquid surface area of an aerosol greatly enhances the liquid evaporation, which may produce sufficient vapor to support a fire at a temperature far below the liquid's flash point.

AEROSOL FIRE HAZARDS IN THE PROCESS INDUSTRY

A liquid in the form of an aerosol can be flammable at temperatures below the flash point. The existence of flammable aerosols presents a high potential for fire and explosion hazards in the process industry. The pioneering work on the combustion behavior of monodisperse aerosol droplets, by Burgoyne and Cohen (1954), reveals the influence of aerosol droplet size on the burning characteristics of aerosols. In regards to the process industry, Eichhorn (1955) initially proposed the concept of an aerosol flammability limit based on the temperature and fuel/air weight concentration ratio. He questioned the generally held notion that the handling of flammable liquids at temperatures below their flash points is safe. He pointed out that mists of flammable liquids at temperatures well below their flash points are capable of supporting flame propagation. Although his conceptualization of the aerosol flammability limit diagram is over-simplified for today's standards, it still caused concern over the potential fire and explosion hazards of flammable aerosols.

Febo (Febo, 1995; Febo & Valiulis, 1996) first raised the issue of fire and explosion hazards from the heat transfer (HTF) system; a system that is widely used in the chemical process industry. The heat transfer fluids in the HTF system are usually

considered chemically stable. With flash points usually between 300 ºF and 500 ºF, most heat transfer fluids fall into the category of Class IIIB liquids, according to the NFPA 30 ratings for flammable and combustible liquids, and are considered as benign under normal operating conditions. But according to the statistics by Factory Mutual Engineering and Research (FME&R), 54 fire and explosion accidents related to organic and synthetic heat transfer fluids were reported during a 10 year period (until 1995), and resulted in a gross loss of $150 million. They adopted Eichhorn's concept of the aerosol flammability limit and compared aerosol explosions to dust explosions in terms of the flame initiation and subsequent flame propagation. Because droplets of smaller sizes can be suspended in the air and have a higher volatility, they can support faster propagation of the flame front. This pointed out the necessity of finding correlations based on liquid properties and their operating conditions to predict the properties of the aerosol droplets upon their release and atomization.

Bowen and Shirvill (1994) also discussed the classification of areas in petroleum installations that use industrial fluids which operate below their flash points but can be potential sources of flammable aerosols. These areas might receive non-hazardous classifications under the Institute of Petroleum Model Code of Safe Practice. They mentioned an example of emergency drivers using diesel fuel at offshore facilities. Flammable aerosols can be formed due the pumping pressure at a leakage point in a flanged joint, posing fire and explosion hazards to the facility.

The offshore hydrocarbon release statistics by HSE (Witlox & Bowen, 2002) recorded cases of hydrocarbon releases on offshore facilities in the North Sea during the

ten-year period from October 1992 to March 2002. The total number of hydrocarbon release cases is 2312 (Figure 2-1). The cases are divided into five types based on the form of the hydrocarbon: gas release, liquid or oil release, 2-phase release, condensate, and non-process release. The non-process liquids refer to liquids used in utilities, including diesel, helifuel, lubricants, and methanol.

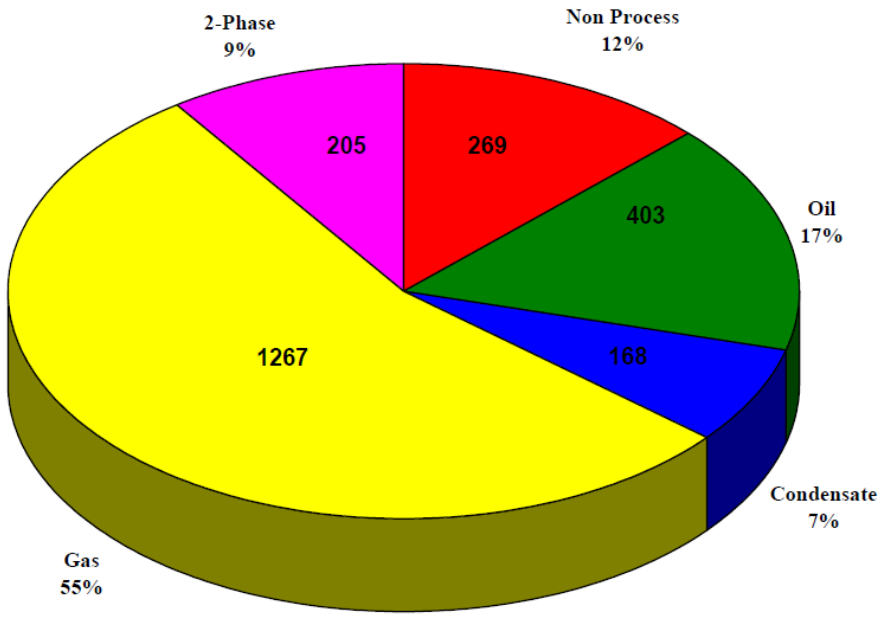

Figure 2-1 Offshore hydrocarbon release cases breakdown by hydrocarbon type (HSE, 2000)

Table 2-1 Selected ignition cases of offshore hydrocarbon release (HSE, 2000)

No.	Hydrocarbon type	Severity	System	Release amount /kg	Release pressure /bar	Release duration	Equivalent hole /mm	Ignition
1	Non-process heat trans oil	Significant	Utilities, fixed facility	1044.0	10.34	10	9.53	Contact with a hot, unlagged flange
2	Non-process lub oil	Significant	Gas compression, fixed facility	964.8	70.00	2	12.70	Contact with hot surfaces of running machinery within turbine enclosure
3	Non-process hydraulic oil	Significant	Power generation turbines, fixed facility	163.8	81.00	5	3.20	N/A
4	Non-process lub oil	Significant	Power generation turbines, fixed facility	85.0	10.00	20	1.90	Hot surface within the enclosure

Aerosols were not included as a form of release, but formation of aerosols might occur in some of the cases. Some of the non-process fluid release cases are listed in Table 2-1. Some of the cases resulted in ignition and fire incidents. The release pressures are above 10 bars, and the sizes of the leaking holes are in the scale of millimeters. The release conditions can be considered pressurized releases of liquids through small openings, and aerosols can be formed from the mechanical breakup and atomization of these liquid streams. The hydrocarbon fluids released in these cases are all characterized by high boiling points. Since they are usually expected to have low vapor pressures, the vapor concentrations are low due to liquid evaporation upon release. The cases which resulted in ignition and fire incidents may not be simple cases of vapor fuel ignition, and flammable aerosols might have been involved in the ignition and combustion process. Similarly, flammable aerosols may also exist in other types of release cases, such as liquid or 2-phase releases.

Using heat transfer fluids, which can be categorized as non-process fluids according to HSE, Sukmarg (Sukmarg et al. 2002) and Krishna (Krishna et al. 2003a; Krishna et al. 2003b) show that aerosols can be formed when the heat transfer fluids are pressurized and released from small orifices. The aerosol droplet size can be as low as 30 μm. Singh (1986) shows that the minimum ignition energy for low volatile tetralin droplets of 40 μm can be lower than 10 mJ. This further indicates that aerosols can be formed in the process industry and can create fire and explosion hazards.

The insufficient recognition of aerosol's flammability may be the reason that flammable aerosols were not considered a major form of hazardous hydrocarbon release.

With the advance of knowledge of aerosols, fire and explosion hazards from flammable aerosols are receiving more attention. There are four stages in the development of aerosol fire hazards:

(i) Formation of aerosols;

(ii) Dispersion of aerosols;

(iii) Ignition of aerosols;

(iv) Combustion of aerosols.

In the following sections of this chapter, background knowledge on these four stages is introduced in further details.

FORMATION OF AEROSOLS

Formation of aerosols involves the breakup of a released liquid jet and the further breakup of liquid ligaments or large droplets into fine aerosol droplets. Witlox and Bowen (2002) gave a comprehensive description of different aerosol formation scenarios. According to the liquid release temperature, the scenarios are put into two categories, non-flashing breakup and flashing breakup. In non-flashing breakups, the liquid temperature is below its boiling point and mechanical atomization dominates the aerosol formation process. Flashing breakups are further divided into three sub-categories, according to the degree of liquid superheat. At low superheat conditions, mechanical breakup still prevails. At intermediate superheat, flashing or bubble formation was observed in the liquid jet outside the releasing point. The external flashing atomization mode starts to prevail. At high level superheat, the flashing of

liquid stream begins in the path of flow before the releasing point. The current work tries to address scenarios of pressurized releases with high flash point industrial fluids, so scenarios with non-flashing breakups or mechanical breakups will be the focus of discussion in the next sections.

Primary and secondary breakup

In the process industry, aerosols can be formed by the accidental release of liquid fluids, which are under pressurized conditions in normal operating situation. The process of aerosol formation, also known as the atomization process, refers to the disintegration of the liquid stream, which goes through the exit nozzle/orifice on the process unit formed in the pressurized release scenario.

The aerosol formation process is characterized by different regimes of spray breakup. According to the classification of the spray breakup regimes by Faeth (1990), there are six major regimes, including Rayleigh breakup, first and second wind-induced breakup, and atomization breakup, based on the properties of the aerosol. Following the same order from the Rayleigh breakup regime to the atomization breakup regime, both the droplet size and the breakup distance became smaller. Among the regimes, the atomization breakup regime is capable of producing fine atomized liquid droplets.

When there is atomization in the breakup regime, two types of sprays are formed, dense and dilute. According to Faeth's description of the flow near the exit of the pressure-atomized spray injector, a dense spray region was formed by the primary breakup of the liquid flow upon exiting the injector nozzle (Figure 2-2). During the

dense spray process, two multiphase flow regions exist within the dense sprays, the liquid core and the dispersed flow region around the surface of the liquid core. The dispersed flow region is further divided into two minor regions, the multiphase mixing layer and the multiphase jet. The multiphase mixing layer exists close to the surface of the liquid core, where the primary breakup occurs and liquid ligaments of irregular shapes are formed. The multiphase jet exists around the multiphase mixing layer, where the dense spray evolves through the secondary breakup and a dilute spray flow is formed.

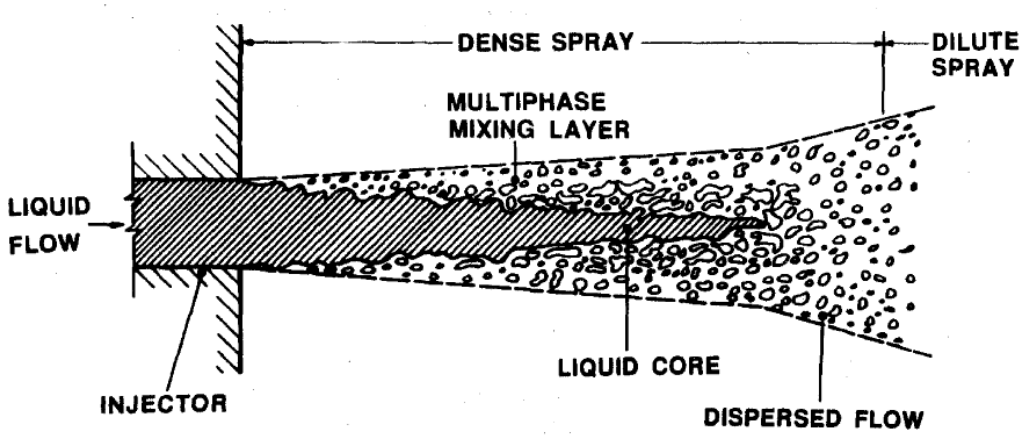

Figure 2-2 Schematic illustration of the atomization breakup regime (Faeth et al. 1995)

Characteristics of the primary breakup process, such as length of the liquid core, liquid volume fraction in the dense spray, and liquid drop size, depend on the liquid flow conditions of the release point, including the liquid flow rate, turbulence in the flow, etc.

The dense spray transitions into the diluted spray phase through the secondary breakup. The secondary breakup mainly involves the deformation and breakup of liquid droplet in the gas stream. The breakup process was studied by researchers using different experimental systems (Krzeczkowski, 1980). Based on a systematic experimental study of the disintegration of falling droplets in a wind tunnel, Krzeczkowski (1980) found that the Weber number plays an important role in the mechanisms of droplet deformation and the breakup process, as well as the breakup duration. According to the visual observations, he further divided the breakup process into four cases (Figure 2-3): the bag mechanism, the bag-jet mechanism, the transition mechanism, and the shear mechanism. Following the same order from the bag mechanism to the shear mechanism, the Weber number increases, and the breakup process evolves towards the mechanism of greater chaos.

Mechanisms of secondary breakup

Before Krzeczkowski (1980), Hinze (1955) proved that different secondary breakup mechanisms were mainly determined by the Weber number and the Ohnesorge number. The Weber number represents the ratio of drag force on the droplet to the surface tension force. The Ohnesorge number represents the ratio of the surface tension force. Further research shows that, if the Ohnesorge number is low, a breakup

mechanism can have a higher chaotic level with a lower Weber number. As the Ohnesorge number increases, a larger Weber number value is required to achieve a breakup mechanism of the same chaotic level.

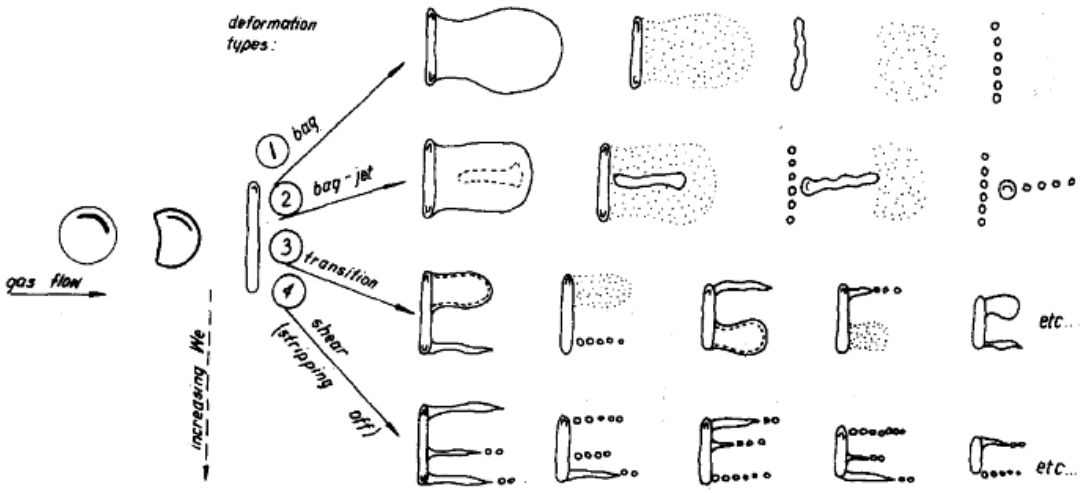

Figure 2-3 Mechanisms of droplet deformation and breakup in secondary breakup (Krzeczkowski, 1980)

Hsiang and Faeth (1995) further mapped out the regimes for different droplet deformation and breakup mechanisms (Figure 2-4). Additional parameters which may influence the breakup mechanism include the Reynold's number, the Laplace number, the ratio of kinematic viscosity of the liquid phase to the gas phase, and ratio of the density of the liquid phase to the gas phase.

Aerosol formation by pressurized release of industry fluids

Although the spray formation process has been of particular interest to researchers in the area of liquid fuel combustion and has been widely studied for many years, study of the aerosol formation process considering the potential scenarios in the process industry has been limited.

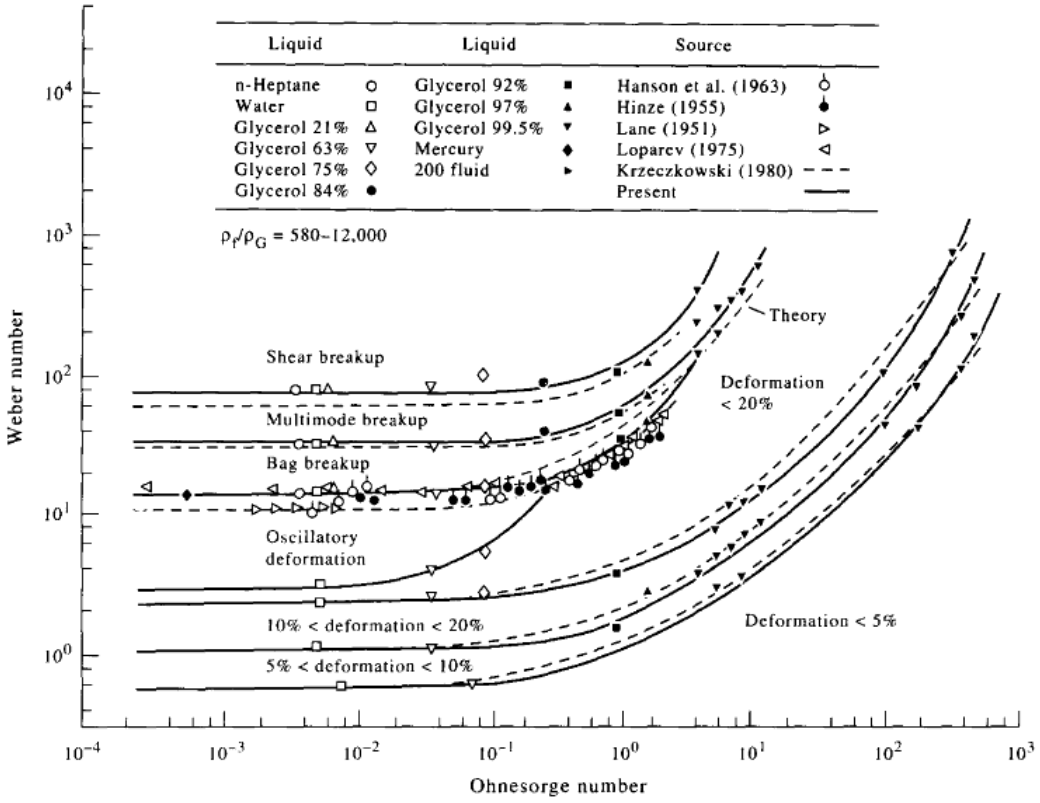

Figure 2-4 Regimes of droplet deformation and breakup in secondary breakup (Hsiang & Faeth, 1995)

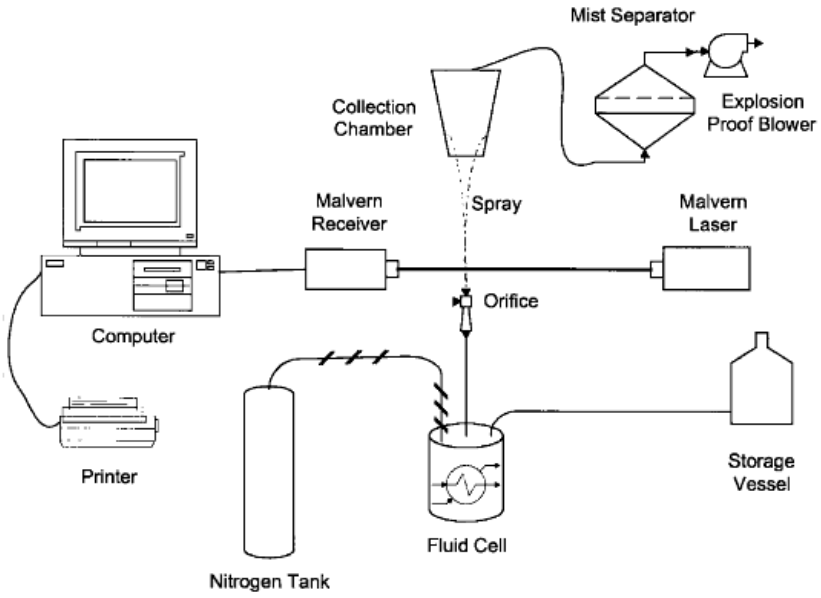

Figure 2-5 Experimental setup for aerosol formation and characterization tests
(Sukmarg et al. 2002)

Sukmarg (Sukmarg et al. 2002) and Krishna (Krishna et al. 2003a) investigated the aerosol formation process with pressurized releases of industrial heat transfer fluids through small orifices. The purpose is to study the characteristics of aerosols, particularly the aerosol droplet size, in a scenario which simulates a potential situation of fluid leakage in process equipment. An illustration of the experimental setup is shown in Figure 2-5. The heat transfer fluids used in the experiments had high flash points and boiling points. The fluids were contained in the fluid cell and were pressurized by nitrogen. Upon opening the orifice on the end of the container outlet, a liquid stream or jet was formed, which was captured by high speed camera, as shown in Figure 2-6.

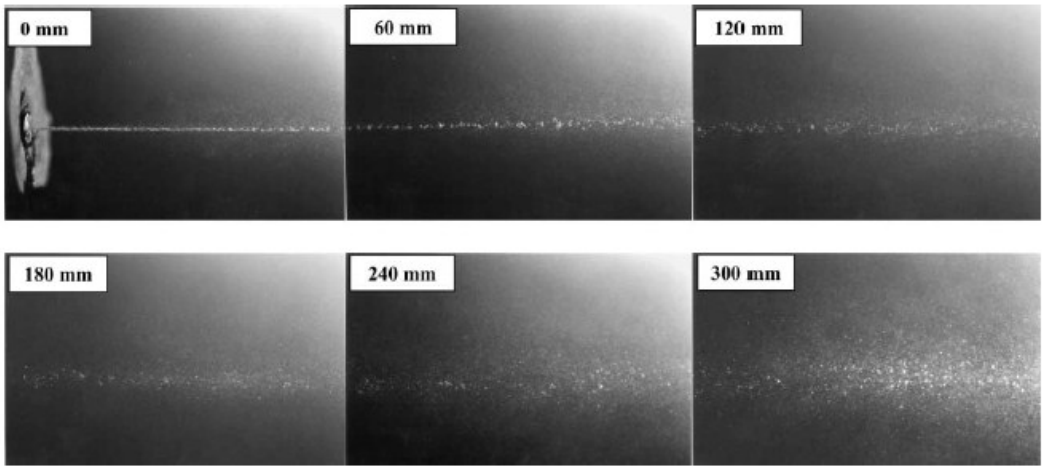

Figure 2-6 Photographs of the atomization of heat transfer fluid by pressurized release through small orifice (Sukmarg et al. 2002)

Based on their observations, jet disintegration stages similar to Elkotb's (1982) descriptions were observed. Instability and disintegration of the liquid stream was induced by a disturbance in the gas phase due to the velocity of the liquid jet and the friction between the jet surface and air. As shown in Figure 2-6, the jet went through the stages of jet oscillation and disintegration into ligaments or large droplets (the primary breakup). Then the ligaments and large droplets further deformed and disintegrated into fine droplets with a stable size. They had conclusions similar to those by Faeth (Faeth, 1990; Faeth et al. 1995; Faeth, 1996) and Hsiang (Hsiang & Faeth, 1995), that there exist a range of critical Weber number values to realize the atomization process for fine aerosol droplets.

It is quite difficult to establish universal theories to predict the properties of aerosols because of the great complexity of the aerodynamic process during the liquid break up caused by the pressurized release of a liquid jet through an injector exit or nozzle. Predictions of aerosol properties need to consider the specific spray conditions, as well as the liquid properties.

In experimental tests by Krishna (Krishna et al. 2003a), fluid release conditions and the fluid properties were considered important to the spray formation process and the aerosol droplet size. Fluid release conditions include diameter of the release orifice, axial distance from the orifice, and initial velocity of the exiting liquid stream. The fluid properties include liquid surface tension, liquid density, gas phase density, dynamic liquid viscosity, and dynamic gas phase viscosity. The initial velocity of the exiting fluid stream depends on the pressure drop across the orifice. The aerosol droplet size was represented by the Sauter Mean Diameter, and was measured at a certain distance from the orifice, so that liquid jet had been completely atomized, and only the fine droplets after the secondary breakup were measured. Through dimensional analysis, correlations based on non-dimensional parameters, which consist of the above listed experimentally obtained variables, were developed to predict the aerosol droplet size. There is good agreement between the predicted droplet size and those measured in the experiments (Figure 2-7).

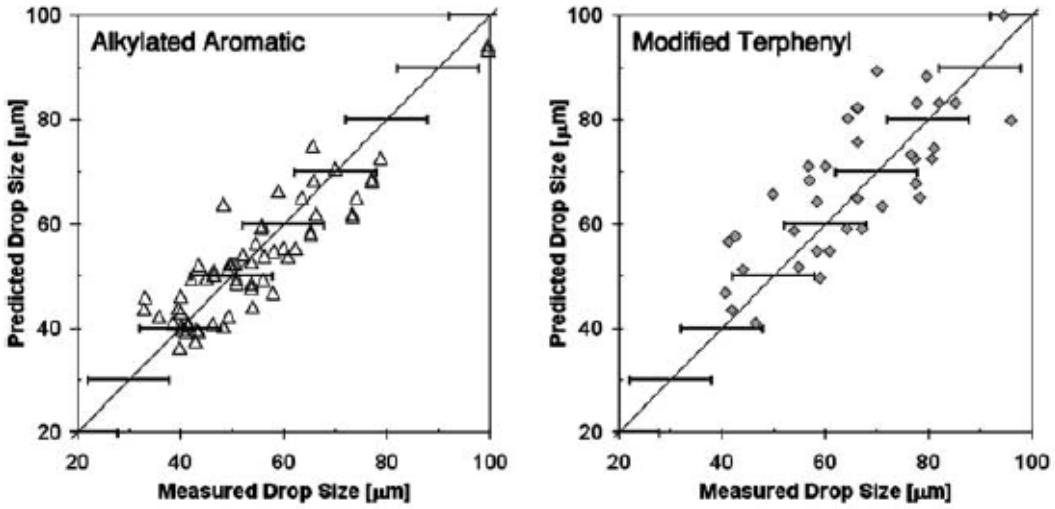

Figure 2-7 Measured vs. predicted aerosol droplet size by correlations from dimensional analysis (Krishna et al. 2003a)

According their results, the influences of the liquid properties were studied. Under the same spray conditions, liquids with higher dynamic viscosities or surface tensions tend to form larger sized droplets. Liquids with larger densities tend to form aerosol droplets of smaller sizes. The atomization process tends to happen in a shorter distance from the nozzle, because of the higher kinetic energy in the liquid stream.

Understanding the aerosol formation process and relationships between the spray conditions and aerosol droplet size can help define the aerosol source terms for the study of the aerosol dispersion process, which will be introduced below.

DISPERSION OF AEROSOLS

When aerosol is formed, the aerosol liquids suspended in the vapor cloud will go through the dispersion process. During the dispersion process, liquid evaporation becomes the controlling factor in determining the aerosol droplet size. The mass, momentum and heat transfer between the liquid and gas phase determines the overall properties of the dispersing two-phase mixtures. All these factors pose a huge challenge to carry out comprehensive experimental program on aerosol cloud dispersion, as well as development of relevant model for prediction of the aerosol dispersion behaviors.

The aerosol research program at the Center for Chemical Process Safety (CCPS) (Johnson & Woodward, 1999; Woodward et al. 1995; Woodward & Papadourakis, 1995) focused on accidental scenarios of pressurized releases of toxic or flammable liquids. The research program aimed to develop a model for predicting the dispersion and rainout behaviors of aerosols formed during accidental liquid discharges. A series of liquid release tests using different fluids were carried out to validate the model. The RELEASE model developed by the program contains the sub-models from aerosol formation to droplet dispersion and liquid rainout.

A sectional view of the modeled liquid discharge scenario and the subsequent two-phase cloud is shown in Figure 2-8. Upon liquid discharge and formation of the two-phase aerosol cloud, the cloud further expands due to the turbulent entrainment with air in the downstream. During this process, the continuous interaction between the liquid and gas phase in the cloud, and the transfer phenomena between the cloud and the environment, properties of the liquid droplets in the cloud keep changing. The droplets

continuously evaporate, following different trajectories according to their sizes, momentum of movement, and the turbulence in the cloud. Some droplets will rainout in the near-field from the release source. Some droplets will remain airborne for a longer period of time, and disperse with the cloud for a longer distance. The rainout droplets will form a liquid pool on the ground, which continues to spread and re-evaporate along the droplet rainout. The modeled scenario includes the sub-process of aerosol formation, dispersion, liquid rainout, and the liquid pool spread and evaporation.

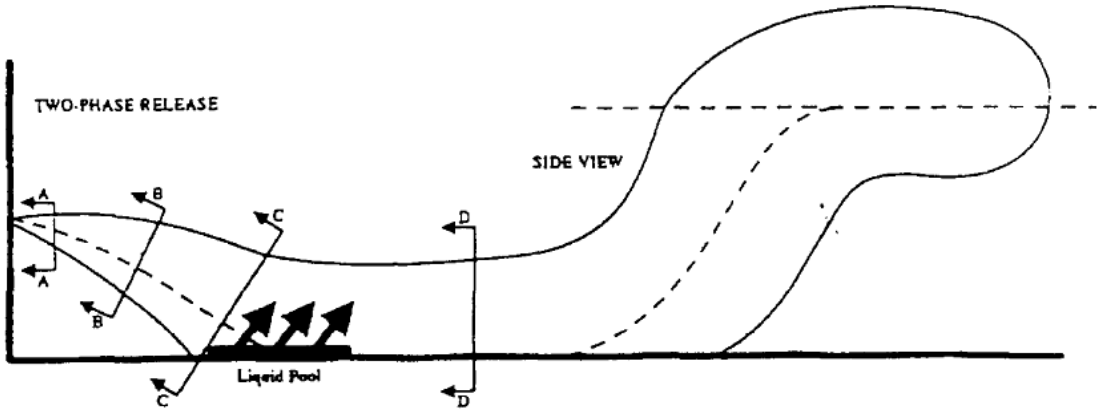

Figure 2-8 Sectional view of the modeled scenario of liquid release, aerosol dispersion and rainout (Woodward & Papadourakis, 1995)

The sub-model of the aerosol source term computes the aerosol droplet size. The sub-model considered the breakup mechanisms introduced in the previous section, such as the critical Weber number for initiation of liquid jet breakup. Computation of the

aerosol droplet from the source term is based on the liquid storage temperature, pressure, liquid density, surface tension, viscosity, heat capacity, enthalpy, release orifice diameter, wind speed in the ambient conditions, etc. The sub-model also considers the flashing of superheated liquids and flashing breakup by the mechanism of internal droplet boiling. Droplet diameters in the aerosol system generated by the source term modeling follow the log normal distribution.

The sub-model for aerosol dispersion and rainout calculates the fraction of the liquid which will fall to the ground. The fractions are obtained by computing the critical droplet diameter below which the aerosol droplets will remain in the air. The RELEASE model was then validated by liquid rainout collection and measurement of the rainout fraction. By correcting the experimental data regarding the initial aerosol droplet size due to flashing and the actual rainout fraction considering the re-evaporation of the collected liquid, the model was proved to achieve a certain level of accuracy. At the time of the model development, the model still needed further improvement for the calculation of liquid droplet trajectory, coupled with droplet evaporation.

IGNITION AND FLAMMABILITY OF AEROSOLS

Pidoll (2001) divided the burning of flammable mixtures into three classes: self-sustaining burning (class a), non-self-sustaining burning (class b), and non-burning (class c). Class a burning refers to a situation where the flame front, after separating from the ignition source, will continue its propagation over the whole volume of the flammable mixture until being extinguished upon complete consumption of the fuel in

the system or by extinguishing factors such as turbulence. In class b burning, the flame is not self-sustainable. It will extinguish right after removal of the ignition source. In class c burning, no flame front develops from the ignition source. Different modes of burning are distinguished by whether the energy released from the flame front's chemical reaction is larger than the energy loss to the surround mixture. For class burning, the energy gained from reaction needs to be larger than the energy lost. For class b and c, the energy gained is smaller than the energy lost.

The minimum ignition energy, one of the most important indicators for the flammability of fuel-oxidizer mixtures, has been widely used to assess the fire and explosion hazards of existing flammable materials. The concept of the minimum ignition energy (MIE) was discussed by Lewis and Von Elbe (1987). The MIE values they provided for a wide range of flammable gas mixtures have been widely used for several decades, and are thought to be constant for gas mixtures of fixed compositions and thermodynamic states.

Measurement of the minimum ignition energy is usually related to the ignition of aerosols by electric sparks. The scenario in which aerosols are ignited with an electric spark as the ignition source has been widely studied by many researchers due to the wide application of the spark ignition process in engines and turbines. The spark ignition process involves the growth of a hot kernel. Characteristics of a hot kernel depend on the spark discharge mode, the setup of electrodes, which produce the spark discharge, and the electric circuit configuration, through which the electric energy in the spark is

recorded. The minimum ignition energy values obtained are also influenced by these factors.

During the spark discharge, a plasma channel is established between the two electrodes, and electrons flow through the channel. The spark discharge process consists of two steps, the breakdown discharge followed by the arc or glow discharge. The two modes of spark discharge breakdown were discussed by Singh (1986). The capacitance discharge is characterized by its short duration (usually within 1.0 μs) and the corresponding high voltage and current peak values across the gap of the electrodes. The rapid increase of temperature and pressure inside the plasma channel result in a shock wave being emitted from the channel. Within the channel, the gas molecules are ionized. The mode of discharge generated by the circuit, consisting of capacitance, resistance and inductance, has a longer discharge duration. By distributing the same amount of energy in a longer time period, the level of molecule ionization is reduced and molecule activation is enhanced. Avoidance of rapid temperature and pressure increase reduces the energy loss carried by the shock wave emitted from the channel. After the breakdown discharge, the gap between the electrodes is bridged, and further discharge takes the form of an arc or glow discharge. The subsequent arc or glow discharge can last for several milliseconds according to configuration of the circuit.

The energy lost from the spark kernel includes the heat conduction lost to the electrode materials and surrounding mixtures, thermal radiation loss, diffusional and convective heat lost to the surroundings. The mode of the spark discharge can influence the spark kernel's energy loss. The spark kernel from the glow discharge is smaller than

that from the arc discharge. The conduction heat lost to the electrode material is larger in the glow discharge mode, resulting in a higher minimum ignition energy.

The spark duration has two effects on the spark kernel (Ballal & Lefebvre, 1975; Rao & Lefebvre, 1976). A shorter spark can reduce the energy lost to the surrounding environment. But a shorter spark of the same energy level is usually accompanied by a stronger shock wave, which can result in a larger energy loss by the shock wave emission. For each flammable mixture there exists an optimum spark duration when the best ignition results can be achieve using a fixed ignition energy level. The optimum spark duration can range from around 60 μs to 100 μs. A lower minimum ignition energy can be found for a specific mixture by using an electric spark with a duration within the optimum range.

The spark gap, the distance between tips of the two electrodes, also influences the spark kernel and the corresponding minimum ignition energy. A closer electrode tip configuration may increase the heat conduction lost to the electrodes, thus increasing the minimum measured ignition energy (Kono et al. 1977). When the spark gap is wider than the quenching distance, a further increase in the spark gap may result in a higher minimum ignition energy (Ko et al. 1991).

As discussed above, electric sparks with different durations, gap widths, and electrode configurations can have profound influence on the spark discharge process, resulting in different minimum ignition energy values for fixed mixtures. The so-called "absolute" minimum ignition energy refers to the minimum ignition energy obtained under the optimum combination of spark duration and gap width, which can bring about

the lowest minimum ignition energy for a flammable mixture of fixed properties (Rao & Lefebvre, 1976; Singh, 1986; Danis, 1987; Ko et al. 1991).

The minimum ignition energy of an aerosol is also influenced by the properties of the aerosol system. Among them, the three properties aerosol droplet size, fuel-air equivalence ratio, and mixture flow velocity are considered the most important factors (Ballal & Lefebvre, 1979), because they are the controlling factors that determine the vapor fuel concentration in the ignition zone, assuming that the ignition process is controlled by droplet evaporation. Due to difficulties in the experimental conditions for aerosol generation and flow, these factors are often interrelated to each other, which create certain difficulties in interpreting the effects of a single parameter.

Ballal and Lefebvre (1979) tested the influence of the droplet size and fuel-air equivalence ratio on the minimum ignition energy of aerosols created from different types of fuels. They use the Sauter Mean Diameter to characterize the aerosol droplet size. They showed that the minimum ignition energy increased drastically as droplet size increased (Figure 2-9a), up to 100 μm, and the minimum ignition energy decreased as the equivalence ratio increased to 1.0 (Figure 2-10). Singh (1986) tested the effects of droplet diameter on the minimum ignition energy of tetralin aerosols (Figure 2-9b). The droplet size in his test is within the range of 6.7 μm to 40 μm. An interesting phenomenon he observed is an optimum droplet size range of 20 μm to 30 μm for the lowest minimum ignition energy. The explanation he gave is that droplets of smaller sizes were pushed away from the initial spark kernel by the shock wave, which resulted in a lean fuel region around the kernel.

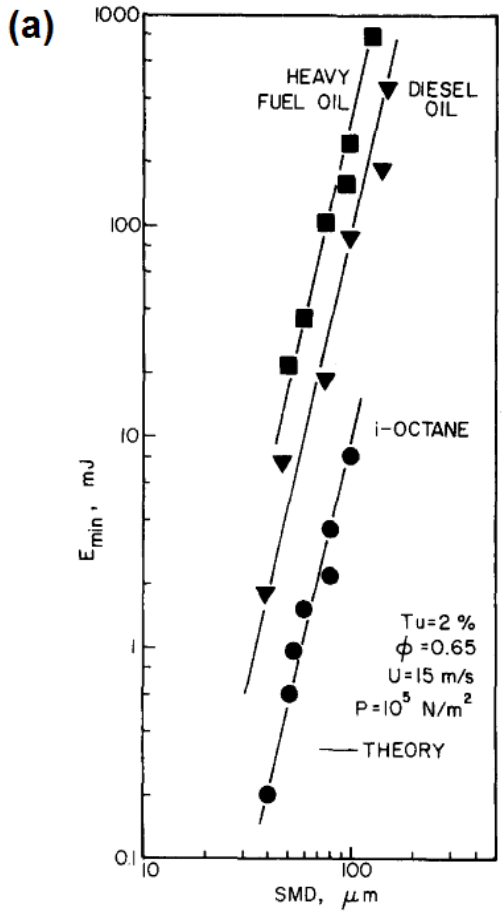

Figure 2-9 Influence of aerosol droplet size on minimum ignition energy. (a) Ballal and Lefebvre, 1979; (b) tetralin aerosols (Singh, 1986)

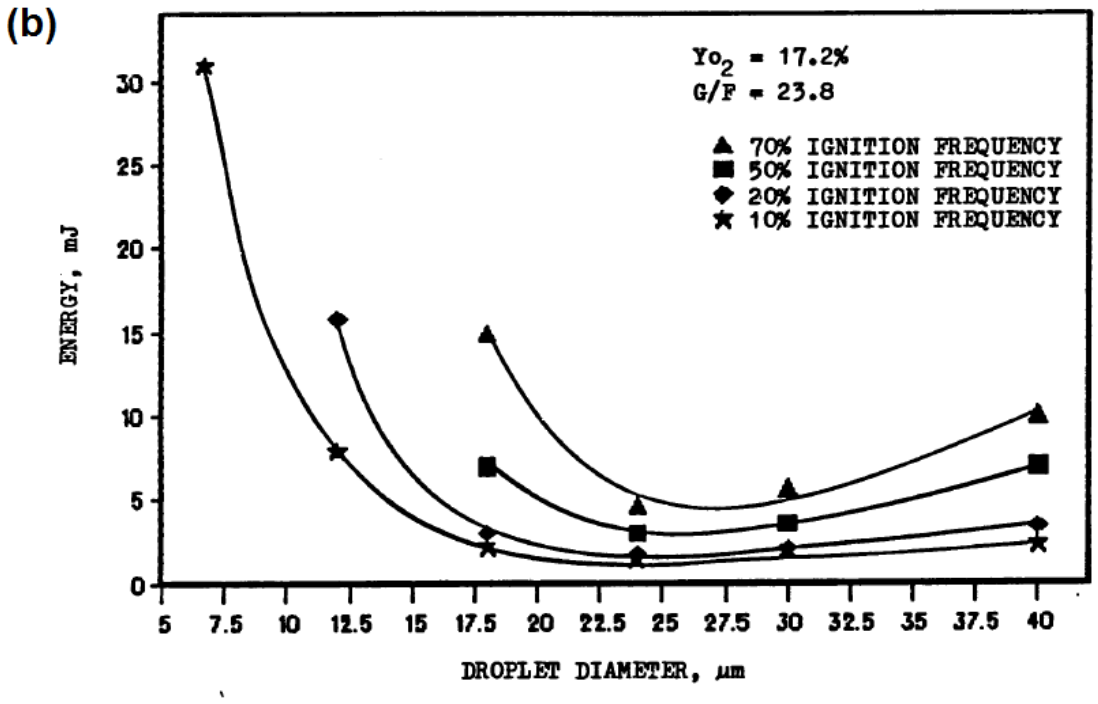

Figure 2-9 Continued

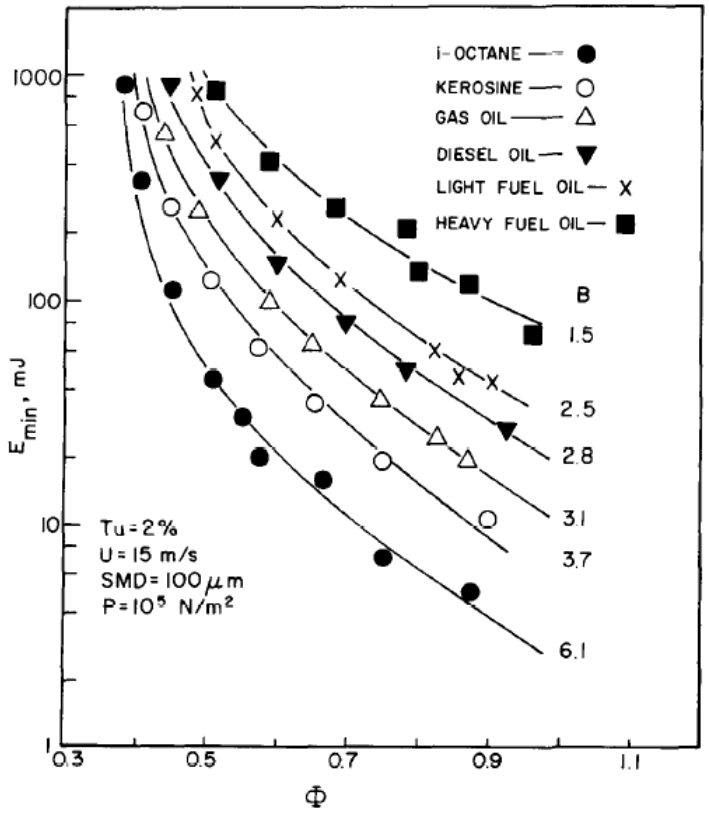

Figure 2-10 Influence of fuel-air equivalence ratio on aerosol minimum ignition energy (Ballal & Lefebvre, 1979)

COMBUSTION BEHAVIORS OF AEROSOLS

Upon ignition of a flammable gaseous mixture, a flame front will be produced and will flash through the vapor cloud. Thermal effects from the fire and subsequent heat damage to people and equipment in the surrounding area depend on the size of the flame front and the duration of the contact between the flame front and the affected objects (Muñoz et al. 2007; Leung & Halliday, 2010). Due to its rapid propagating speed in

gaseous mixtures, fire's thermal effects in vapor mixtures are usually considered relatively small compared to other effects, such as overpressure caused by vapor cloud explosions, because of the flame front's short contact period with the affected objects.

When flammable aerosols are ignited, fires exhibit different characteristics (Sukmarg et al. 2002; Maragkos & Bowen, 2002; HSE, 2000). The simple scenario of a flame front flashing through the flammable mixture is not applicable to fires in flammable aerosols, because fuel vapors are continuously evaporating from aerosol droplets to support the combustion reaction in the flame. Therefore, heat release rates from aerosol fires are expected to be significantly higher than those from fires of vapor mixtures, which may result in more severe damage to the surrounding areas. Unfortunately, because of the complexity of aerosol formation and ignition, knowledge of the characteristics of flames of aerosols is quite limited in previous literature, making it difficult to assess the fire hazards of flammable aerosols in the process industry (Ballal & Lefebvre, 1981; Polymeropoulos, 1984; Myers & Lefebvre, 1986; Suard et al. 2001; Lawes et al. 2002).

Two aspects of characteristics are considered important for aerosol flames. One aspect of the characteristics involves the size and shape of the flames. The other aspect involves movement of the flame, or the flame propagation speed.

Burning modes in aerosols

For the first aspect, the size and shape of the flames are closely related to the mode of combustion in aerosols. Researchers have made different sets of classifications for the burning modes based on their experimental observations, with both similarities and differences. The different burning modes are mainly attributed to overall fuel concentration, aerosol droplet size, and droplet number density or spacing.

The classifications by Hiyashi (Hiyashi et al. 1981), based on experimental observations using n-decane aerosols, include three burning modes, mis-propagation, propagation of isolated diffusion flames surrounding droplets, and propagation of interacting yellow-flames which spread over the cross section of the aerosol stream. The criteria in his classification are whether flames can propagate vertically through the aerosol stream, or horizontally through the cross section of the aerosol stream. The isolated diffusion flames surrounding the droplets are capable of propagating vertically through the aerosol stream, but are not large enough to spread horizontally over the entire cross section of the aerosol stream. The interacting yellow flames can spread over the cross section as they propagated vertically through the aerosol stream. Hiyashi further proposed that there is a relay ignition mechanism in aerosols. When the droplet size is above a certain value, droplet evaporation becomes weak and the fuel vapor concentration in the space between droplets becomes lower. When droplets are ignited, they are enveloped by the small diffusion flames around them. In order to realize the propagation of flames, unburned droplets in the space around the burning droplets needs to be ignited successively, resulting in the propagation of isolated diffusion flames. The

spacing between aerosol droplets should be lower than a certain value to enable the successive ignition of droplets.

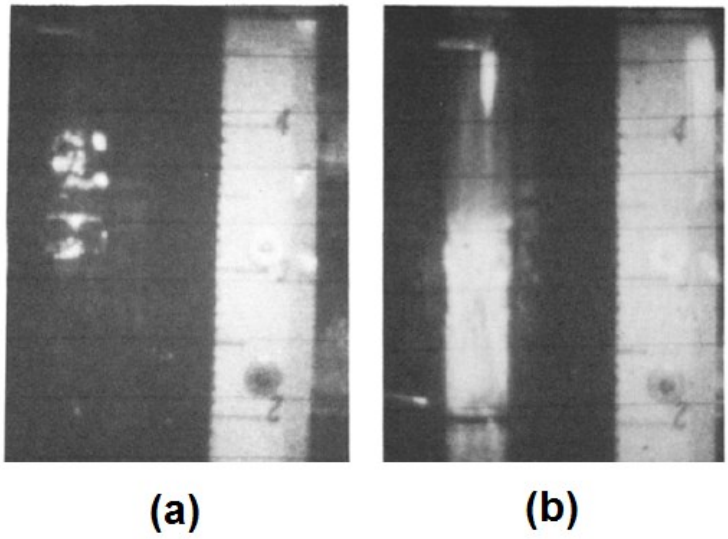

Figure 2-11 Different flame propagation modes in tetralin aerosols. (a) Propagation of diffusion flames surrounding droplets; (b) flame propagation mode close to that in premixed gaseous mixture (Chan & Jou, 1988)

In the tests by Chan and Jou (1988) using monodisperse tetralin aerosols, different modes of burning, which follow the classification by Hiyashi, were observed (Figure 2-11). By controlling the fuel-air equivalence ratio and varying the droplet size, he observed the transition from diffusion flames around droplets (Figure 2-11a) to the flame propagation mode which is close to flame propagation in premixed gaseous mixture

(Figure 2-11b). The transition happens as the aerosol droplet size decreases to a certain range, around 15 μm. When the droplet size is above the range, the propagation happens through the droplet-droplet relay mechanism, due to the large space between droplets. When the droplet size is below the range, the rapid evaporation of liquid droplets and close distance between droplets bring about a flame front similar to the flame fronts in homogeneous mixtures.

In another set of classification (Williams, 1973; Chigier, 1983; Aggarwal, 1997), there are three different modes: burning in the vicinity of an individual droplet, cluster of droplets, or globally in a spray. Ignition of an individual droplet occurs when the droplet is surrounded by a flame whose dimension is in the order of the droplet's diameter. A global flame appears if the flame has a dimension several orders of magnitude larger than an individual droplet. Burning of a droplet cluster is the intermediate situation between the previous two modes. The global flame is similar to the burning mode in Chan's classifications, which is close to burning in homogeneous mixtures.

Because the aerosol combustion process is complex and various phenomena are involved, researchers have been trying to describe the process using different models. The models focus on different phenomena in the aerosol combustion process. Some researchers focused on the burning of droplets (Williams, 1973, 1990; Chigier & McCreath, 1974; Chigier, 1983; Faeth, 1977; Chiu et al. 1982; Law, 1982; Faeth, 1983). For example, in the review by Chigier and McCreath (1974), the flame around a single droplet is categorized as either an envelope flame or a wake flame, depending on the distribution of fuel vapor and the oxygen concentration around the droplets. Distribution

of the species is influenced by the relative velocity of the gas phase around the droplet and the turbulence inside. This type of models can be used on dilute aerosol systems with low volatility fuel droplets.

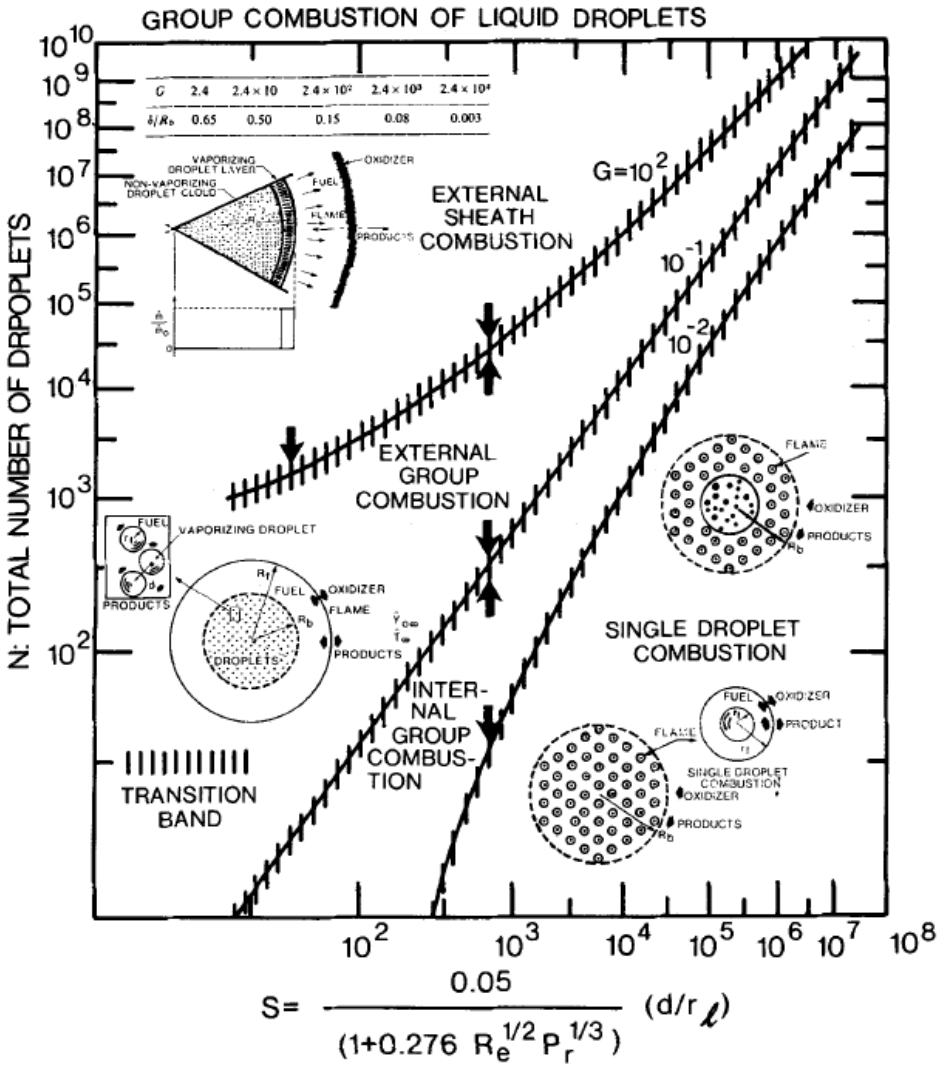

Figure 2-12 Types of aerosol combustion according to the group number (Chiu et al. 1982)

Another type of model focused on the combustion of droplet groups. The so-called "group combustion" theory was proposed by Chiu (Chiu et al. 1982). There are four different regimes for the group combustion mode: the isolated droplet combustion, the internal group combustion, the external group combustion, and the sheath combustion (Figure 2-12). In the isolated droplet combustion regime, each droplet in the aerosol is engulfed in a flame separately. In the internal group combustion regime, a core is formed in the aerosol and is surrounded by a flame. Evaporation continuously happens in the core. In the external group combustion regime, the core's size increases, and more droplets are enveloped into the single flame surrounding the core. Transitions between different burning regimes are correlated to the group combustion number, a dimensionless number that is the ratio of the droplet evaporation rate over the diffusional transport rate of gaseous species. As the group combustion number becomes larger, the burning regime transitions towards a regime with larger droplet groups and flame sizes.

Flame propagation speed in aerosols

The second aspect of combustion characteristics in aerosols is the flame's propagation speed. As discussed above with the various burning modes of aerosols, it is obvious that the classical flame front theory about a plane shaped flame front cannot be simply applied to all the scenarios of aerosol burning. In previous attempts to measure the flame front propagation speed, researchers faced the challenge of complex flame shapes in different burning modes. Measures are taken to achieve flame fronts close to the plane shape (Ballal & Lefebvre, 1981; Chan & Jou, 1988). So far the results for

flame front propagation speeds of aerosols can be seen as the propagating front speed of global flames. Other burning modes are not fully represented in the reported results.

An interesting phenomenon in the flame front propagation process is the accelerated flame front speed due to the existence of aerosol droplets. This phenomenon has been reported in previous tests (Chan & Jou, 1988; Atzler & Lawes, 1998; Atzler et al. 2007; Suard et al. 2001; Suard et al. 2004; Lawes et al. 2002), and theoretical studies have been used to find possible explanation (Polymeropoulos, 1984; Greenberg et al. 1999). This phenomenon is not yet fully understood.

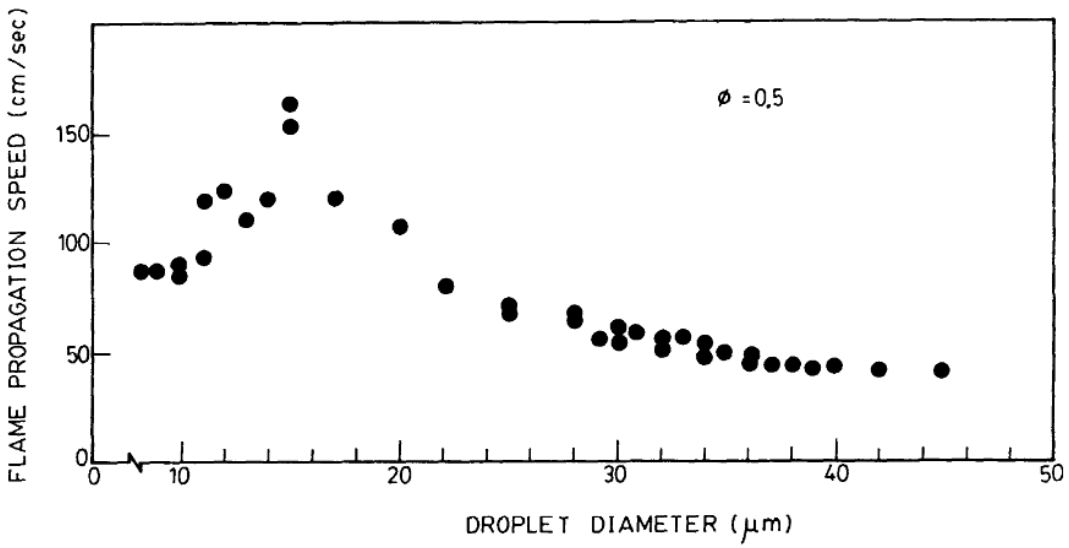

Figure 2-13 Flame speed enhancement during the burning mode transition in tetralin aerosols (Chan & Jou, 1988)

In Chan's observations (Figure 2-13), during the transition between burning modes, the flame front propagation speed is enhanced to above 1.5 m/s for a transition droplet size range of around 15 μm. Atzler and Lawes (1998) also reported an enhanced flame propagation speed, which is larger than the speed in gaseous mixtures with the same fuel concentration (Figure 2-14). Later on, Atzler (Atzler et al. 2007) reported the oscillation of flame front propagation speed in iso-octane aerosols (Figure 2-15a). Different from the previous study, this system has a certain fuel vapor concentration, as well as fuel in the form of liquid droplets. Observation of the flame front structure by high speed photography (Figure 2-15b) shows that the flame front takes a cellular shape when the flame front speed reaches the climax.

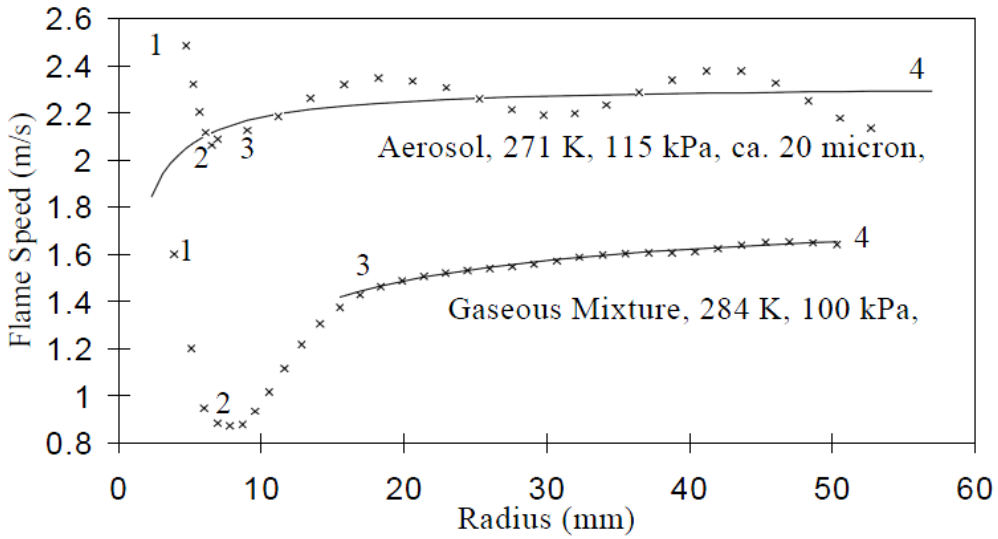

Figure 2-14 Flame speed enhancement in iso-octane aerosols (Atzler & Lawes, 1998)

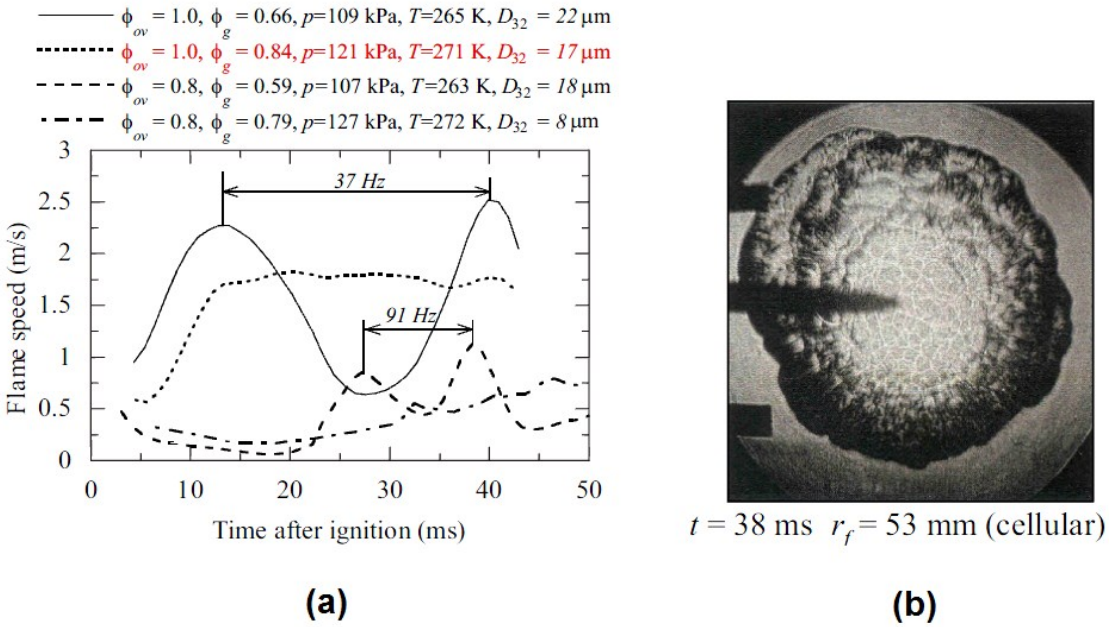

Figure 2-15 Flame speed oscillation in iso-octane aerosols (Atzler & Lawes, 1998)

SUMMARY

Compared with combustion of gaseous mixtures, the combustion of aerosols is a topic of huge complexity. Due to the existence of liquid droplets, droplet evaporation is involved in both the ignition and combustion processes of aerosols. Instead of solely considering the fuel vapor concentration for gaseous flammable mixtures, the properties of liquid droplets, their sizes, number density, and movement need to be considered. The properties of the aerosol droplets not only influence the aerosol's ignitability, they also determine the burning characteristics of aerosol flames. As introduced in Chapter I, the methodology for assessment of aerosol fire hazards, includes two major topics,

observation of aerosol combustion behaviors and estimation of aerosol flammability. Both topics try to probe the impacts of the properties of liquid droplets in aerosol systems. Knowledge from the current study on these two topics, which will be introduced in the upcoming chapters, can be related to previous knowledge on aerosol formation and dispersion to identify the process areas where aerosols with certain properties can be formed. Knowing how properties of aerosol droplets contribute to the appearance of larger flames or faster flame propagation speed means protective measures can be taken in the process area where aerosols with similar properties might be formed, so that destructive impacts of aerosol fires can be reduced. Knowing the energy required for the ignition of aerosols with certain properties means preventive measures can be taken in the process area to avoid potential ignition sources.

CHAPTER III

AEROSOL PRODUCTION BY ELECTROSPRAY*

INTRODUCTION

Electrospraying as a method of fine particle production has been used in many application fields, including gas cleaning, liquid fuel micro-combustor, electrospray ionization mass spectrometry for investigation of macromolecules, and automatic pipeting of biological samples in massively paralleled drug discovery and DNA arraying (Jaworek et al. 2006; Jaworek, 2007; Kim et al. 2006; Si et al. 2007). The electrospray system applies electrostatic means to liquid to create dispersion of minute droplets. The system works by feeding a liquid with sufficient electric conductivity through a small nozzle. The top of the nozzle is maintained at a few kilovolts relative to a ground electrode, which is positioned at a certain distance from the nozzle.

The most important issues in aerosol generation by electrospray are the droplet size control and spray stability. Although the droplet size is mainly controlled by the voltage applied to the liquid stream in the spray nozzle and the liquid flow rate, many other factors can affect the droplet size, such as the geometry of the electric field around

*Part of this chapter is reprinted from "Flammability of heat transfer fluid aerosols produced by electrospray measured by laser diffraction analysis" by Lian, P., Mejia, A. F., Cheng, Z., and Mannan, M. S. (2010). *Journal of Loss Prevention in the Process Industry*, *23*(2), 337-345, Copyright 2009, with permission from Elsevier.

the nozzle and the properties of the liquid. Researchers have been trying to identify the range of the physical parameters of the liquid so the liquid can be atomized by electrical forces. For example, a liquid with high surface tension cannot be atomized by electrospray. And liquids with conductivity higher than 10^{-12} S/m and a dipole moment less than 3×10^{-25} $N^{1/2}m^2$ cannot be sprayed by electrospray (Jaworek, 2007). For semi-conductive liquids, electrospraying in cone-jet mode is widely assumed to be possible when the liquid conductivity falls within the range of 10^{-4} to 10^{-8} S/m. But there is still difficulty in theoretically determining the droplet size of electrospray. In the correlations based on experiments predicting droplet size produced by electrospray by different researchers (Tang & Gomez, 1996; Juan & de la Mora, 1997; Turetsky et al. 2000; Jaworek, 2007), the liquid properties considered are the most important factors in determining droplet size, including liquid conductivity, permittivity, surface tension, viscosity, as well as electrospray configurations and conditions including the liquid flow rate, the voltage applied to the nozzle, and the distance between the spray nozzle tip and the ground electrode. Dimensionless variables in various forms include the Reynolds and Weber numbers.

Another issue in electrospray is spray stability, which is quite a complicated phenomenon, and can be related to multiple factors in the configuration of electric fields (Tang & Gomez, 1996; Duby et al. 2006). Based on Taylor's classical cone theory, characteristics of the interfacial forces on the Taylor's cone surface during the electrospray are the most important factors controlling generation of minute droplets (Wilm & Mann, 1994; de la Mora, 2007). Two ratio numbers have been considered by

previous researcher (Kim et al. 2006), one is the gravitational Bond number, which is the ratio of the gravitational force to the surface tension of the droplet, and the other is the electrical Bond number, which is the ratio of the electrical force to the surface tension.

In the current work, electrospray is applied through aerosol generation and ignition tests to study aerosol flammability and related safety problems in the process industry, which can create fire and explosion hazards in the presence of an ignition source and result in fatalities and huge economic losses.

This chapter experimentally addresses the dependence of aerosol droplet size on electrospray operating conditions, and tries to find suitable electrospray conditions for production of monodisperse aerosol droplets, which will be applied in the aerosol ignition tests. Special focus is on electrospray using industrial hydrocarbons with low conductivity and high viscosity, and the conditions for stable cone-jet mode spraying. Currently the biggest challenge in applying the electrospray technique to the aerosol ignition tests is increasing droplet concentration (Almekinders & Jones, 1999; Bocanegra et al. 2005; Deng et al. 2006). Before developing a multiple nozzle system with an array of capillaries, it is necessary to predict the performance of electrospray nozzles under the geometrical influences, such as varied electric field distributions due to existence of neighboring nozzles, and the configuration of the nozzles with the ground electrode (Snarski & Dunn, 1991; Rulison & Flagan, 1993; Regele et al. 2002; Duby et al. 2006; Deng & Gomez, 2007). Based on experimental results, the current research established a multiphysics model using the finite element method to study the formation process of the Taylor's cone and liquid jet by studying the equilibrating effects between

the electric field force and the surface tension on the liquid-air surface. Influence of a specific electric field distribution on the characteristics of the cone-jet mode and the stability of the droplet size are studied.

MATERIALS AND METHODS

Electrospray setup

Three commercial heat transfer fluids, HT-D, P-NF, and P-HE, are applied in the current work for production of monodisperse aerosols. The main properties of the fluids are summarized in Table 3-1.

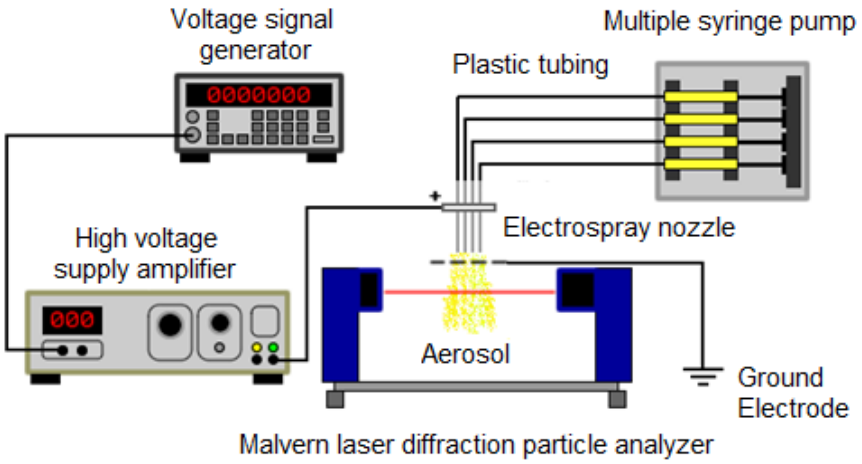

Figure 3-1 Experimental setup for aerosol generation by electrospray

Electrospray is characterized by its capability of fine control over aerosol droplet size distribution (Mejia et al. 2009). Figure 3-1 shows a schematic of the electrospray setup for the production of uniform aerosol droplets from the heat transfer fluids. The electrospray system applies an electrostatic field for dispersing the liquid into minute droplets (Deng et al. 2006; Deng & Gomez 2007). The electrospray setup consists of a function generator (Stanford Research System, Ds-345) to generate a voltage signal, and a high voltage amplifier (Trek Inc. 610E) to raise the signal to the desired high voltage level. An electric wire connects the high voltage amplifier output to the top of the nozzles. The nozzles are maintained at several kilovolts relative to a ground electrode, which is positioned at a certain distance down from the nozzle tips. The nozzles used in the experiment are stainless steel capillary tubes of 0.01" i.d. and 0.02" o.d. The heat transfer fluid is pumped from an infusion syringe pump (KDS 220). The volume of each syringes is 2.5 mL. The liquid meniscus at the outlet of each capillary takes a conical shape (cone-jet) under the influence of the electric field between the nozzles and the electrode on the ground. The jet breaks up downstream further into a spray of fine, charged droplets. Aerosol droplet sizes are mainly controlled by liquid flow rate from the nozzles, and the voltage applied to the nozzles.

Prior to electrospray, the Stadis 450 additive was added to the fluid to enhance its electrical conductivity, so that the electrospray can stably produce monodisperse aerosol droplets. The samples were stirred for 5 minutes to ensure proper mixing of the additive. The fluid cells containing the samples were then allowed to stand for 60 minutes until air bubbles were no longer visible.

Table 3-1 Industrial hydrocarbon for the tests and the properties

Heat Transfer Fluid	HT-D	P-NF	P-HE
Appearance	Crystal clear	Transparent colorless	Transparent pale yellow
Composition	Paraffinic hydrocarbon	Hydrotreated mineral oil	Hydrotreated heavy paraffinic hydrocarbon
Recommended operating range	121-315˚C 250-600˚F	49-343˚C 120-650˚F	66-316˚C 150-600˚F
Average Molecular Weight	372	350	445
Flash Point	224˚C (435˚F)	174˚C (345˚F)	227˚C (440˚F)
Fire Point†	240˚C (464˚F)	196˚C (385˚F)	260˚C (500˚F)
Density	0.850g/ml (38˚C)	7.25 lb/gal (24˚C)	7.22 lb/gal (24˚C)
Viscosity	32.1 cSt as 40˚C	11.0 cSt at 40˚C	40.25 cSt at 40˚C

Droplet size measurement

A laser diffraction particle analyzer (LDPA, SprayTec, Malvern Inc.), which consists of a 2mW Helium-Neon laser tube and a ring diode detector, was used to characterize the aerosols formed from the heat transfer fluid. The aerosol droplets that pass through the laser beam will scatter light at angles directly related to their sizes (Figure 3-2). As the droplet size decreases, the observed scattering angle increases logarithmically. The laser beam was a collimated monochromatic beam of wavelength

632.8 nm and 10mm in diameter. Intensities of the diffracted light on the diodes in the detector were converted into droplet-size data online by a computer.

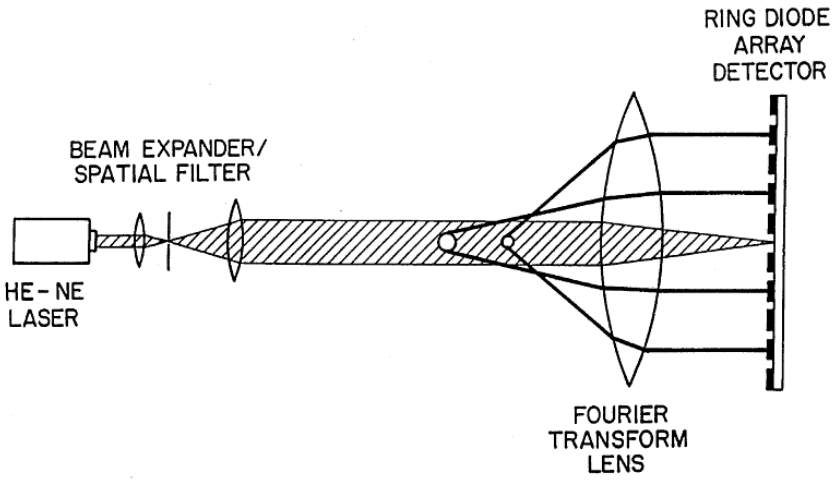

Figure 3-2 Droplet size measurement by Malvern LDPA (Krishna et al. 2003a)

Parameters calculated by the laser diffraction particle analyzer include the percentile diameters $D_{[x]}$, which are the sizes in μm that specifies x% percent of the aerosol droplets whose sizes are below the value. In this paper the $D_{[10]}$, $D_{[50]}$ and $D_{[90]}$ values are used to indicate the aerosol droplet size distribution. The Surface Area Moment Mean Diameter $D_{[3][2]}$, also known as the Sauter Mean Diameter (SMD), is used to represent the droplet size of the aerosols produced by the electrospray. The

Sauter Mean Diameter is the volume-to-surface-area mean diameter. It is calculated based on the droplet size distribution at every sampling moment.

$$SMD = D_{32} = \frac{\sum_{i=1}^{m} D^3 \Delta n}{\sum_{i=1}^{m} D^2 \Delta n} \tag{3-1}$$

where D is the droplet diameter, and Δn is the number of droplets in the aerosol system with the diameter D.

The Sauter Mean Diamter is the most common mean diameter used to represent droplet size in aerosol systems because of its applicability to the study of important phenomena related to aerosol droplets, such as droplet penetration, and heat and mass transfer (Krishna et al. 2003a). Obtaining the SMD for an aerosol system created by electrospray follows the procedures as stated below:

1) Start Malvern laser diffraction particle analyzer (LDPA), and finish the automatic electrical and optical background alignment before the measurement.
2) Start the electrospray, adjust the nozzle voltage and the fluid flow rate in the nozzles to the desired values, and fix the spray conditions.
3) Start the droplet size measurement with the LDPA. The laser sampling rate on the aerosols system should be set at 1 Hz. For each sample, the laser light signal obtained by the LDPA receiver is processed to give the droplet size distribution. The D_{32} (SMD) value is calculated based on the distribution.

4) Continue the aerosol production and droplet size measurements for at least 5 minutes, so that a data set containing more than 300 calculated D_{32} (SMD) values is obtained for the aerosol system produced under fixed electrospray conditions. The 300 calculated D_{32} (SMD) values are averaged to represent the droplet size of the aerosol system under electrospray conditions.

The Mie theory is used by the laser diffraction particle analysis for the evaluation of the extinction cross section, which is defined as the difference between the incident and transmitted light energy. The theory starts from Maxwell's electromagnetic equations and proceeds to exact solutions for the equations for the interaction of lasers with aerosol droplets.

One shortcoming of using the Mie theory for laser diffraction droplet size analysis is its reliance on the exact refractive index values of the materials. The real part of the complex refractive index describes the amount of light scattered as a result of light interacting with the droplets, and the imaginary part describes the amount of absorption that takes place as the light enters the droplet. But in practice, the accurate refractive indices for hydrocarbons of various compositions are hard to obtain (Chigier, 1991; Schwar & Weinberg, 1969). Large saturated hydrocarbons usually have a value between 1.4 and 1.5. Because the heat transfer fluids are mainly composed of hydrotreated mineral oil, n=1.5 is selected in the current measurements. A variation of the imaginary part k is very complicated. It depends on both the molecular structure of different components and the wavelength range of the light. For the current work, since the combustion process is involved, k is set at 0.5 as that is the default value for standard

opaque particles in the Malvern LDPA particle library. With air as a dispersant, the real refractive index is set at 1.0.

The liquid volume concentration of the aerosol droplets obtained by the Malvern laser is calculated from the Beer-Lambert law, with:

$$C_V(ppm) = \frac{-2000Ln(T)}{3b\sum \frac{Q_i v_i}{d_i}}$$

where T is the relative transmission of the laser beam; Q_i is the efficiency of light extinction by scattering and absorption, and is calculated from the Mie theory for a particle of radius r_i; n_i is the number of particles of radius r_i; d_i is the diameter of the particle; and b is the path length of the laser beam through the aerosol.

EXPERIMENTAL RESULTS

The Taylor's cone

In the current work, the droplet size from electrospray is controlled predominantly by the liquid flow rate and secondarily by the applied voltage. For a given liquid, the Taylor's cone can only be established in a certain range of liquid flow rates and voltages. Formation of a stable Taylor's cone by the liquid meniscus upon exit of the nozzle is observed by high speed digital camera, as shown in Figure 3-3.

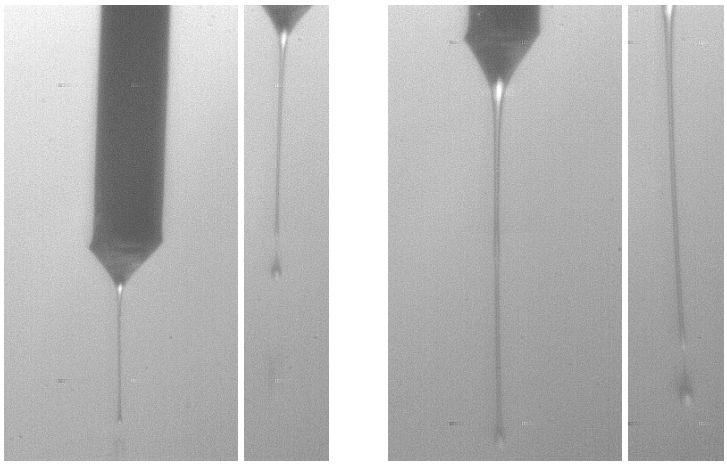

Figure 3-3 Formation of stable Taylor's cone in electrospray by digital camera

Droplet size distribution

A picture of the electrospray aerosol particle size distribution is shown in Figure 3-4. The histogram displays the results in the form of "in band" percentages. Each bar in the graph represents a size band of particles and their height represents the percentage of the spray that is within that size band. The cumulative total of the heights of all the fractions is equal to 100%. The histogram can be replaced by a continuous curve as shown in Figure 3-4, representing the frequency or the probable density of the volume fraction of a certain droplet diameter. The $Dv_{(x)}$ value of aerosol, the percentiles, is the size in microns which the specified x% of the aerosol droplets are smaller than. The $Dv_{(10)}$, $Dv_{(50)}$, and $Dv_{(90)}$ values for the aerosols in the histogram are 96.27, 120.1, and

148.3 μm respectively. And the SMD is 118.4 μm. Mono-dispersity of the aerosol by electrospray is evident.

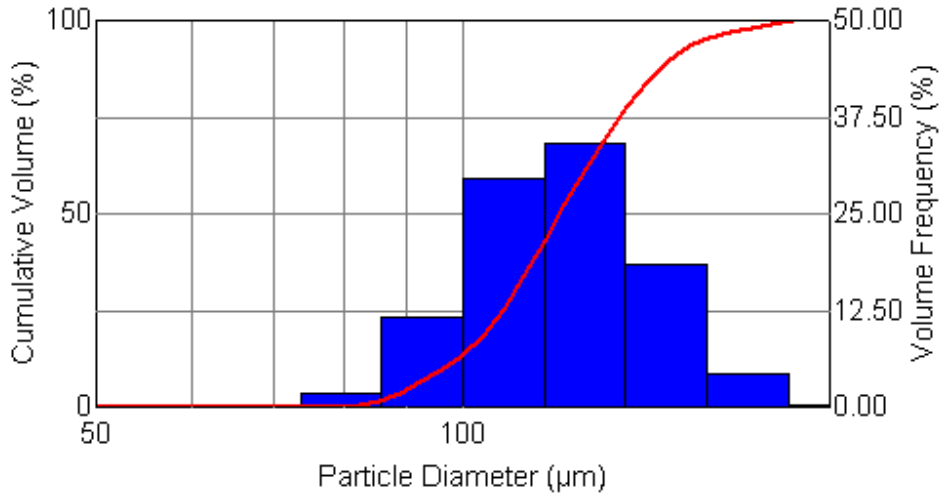

Figure 3-4 Histogram of particle size distribution in electrospray aerosol (HT-D heat transfer fluid, 400 ppm additive,5mL/h flow rate, 9200 V nozzle voltage)

Droplet size of aerosols by electrospray

Figure 3-5 shows the effects of the liquid flow rate and the voltage applied to nozzle on the aerosol droplets from the P-NF fluid. Under the same nozzle voltage, the liquid droplet size is decreased by lowering the liquid flow rate. The droplet size deceases as the voltage to the spray nozzles becomes higher. Each data point in the figure represents an average SMD value for the aerosols produced under fixed

electrospray parameters for a certain period of time. The error bar on each data point shows the standard deviation for the average SMD value. A higher error bar indicates that there are larger fluctuations in the SMD values during the aerosol production period. It is observed, based on the standard deviations, that there exist two unstable regions for the P-NF aerosols, below 7.75kV and from 8.75 to 9.75kV. The first unstable region for the lower applied voltage seems to be significant for high liquid flow rates above 1.0mL/h. The second unstable region tends to appear for the liquid flow rate of 1.0 to 2.5mL/h and the applied voltage range of 8.00kV to 8.75kV. And as the liquid flow rate increase, this unstable region tends to become narrower in terms of the applied voltage range.

Figure 3-6 shows the effects of liquid flow rate on aerosol droplets by the HT-D fluid. The liquid droplet size is decreased under the same electrospray conditions for the lower liquid flow rate. Similar to Figure 3-5, there exist two unstable regions according to the standard deviation values, applied voltage below 7.75kV and from 8.75 to 9.75kV.

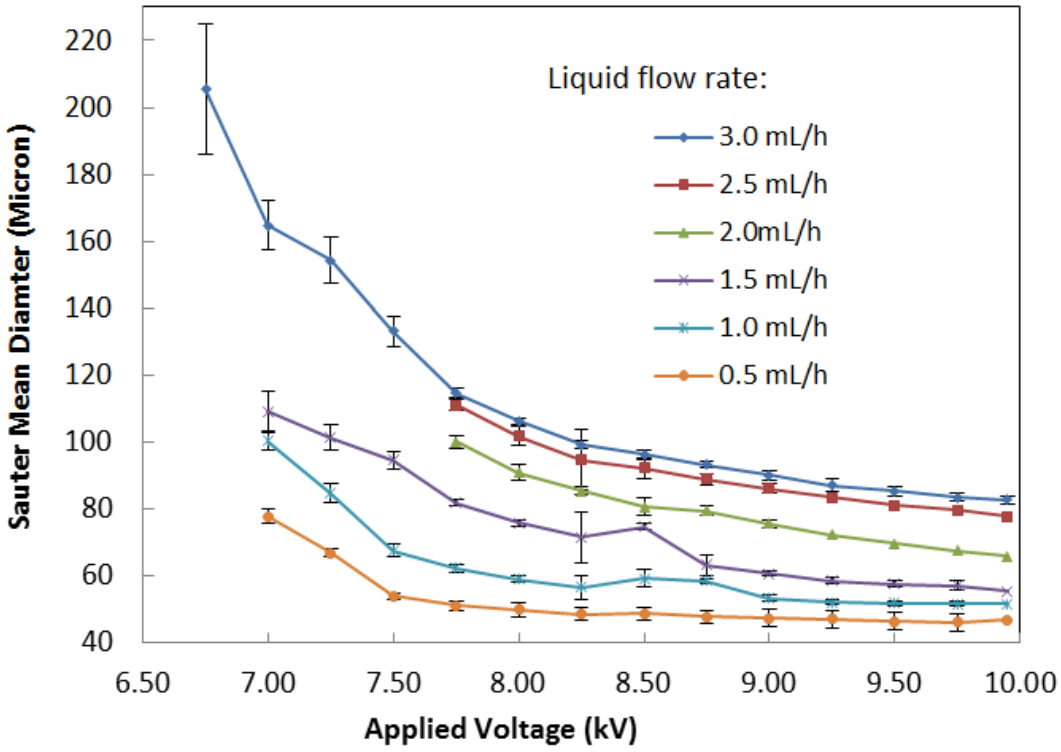

Figure 3-5 Influence of applied voltage and liquid flow rate on aerosol droplet size (P-NF). P-NF aerosol, 800 ppm additive

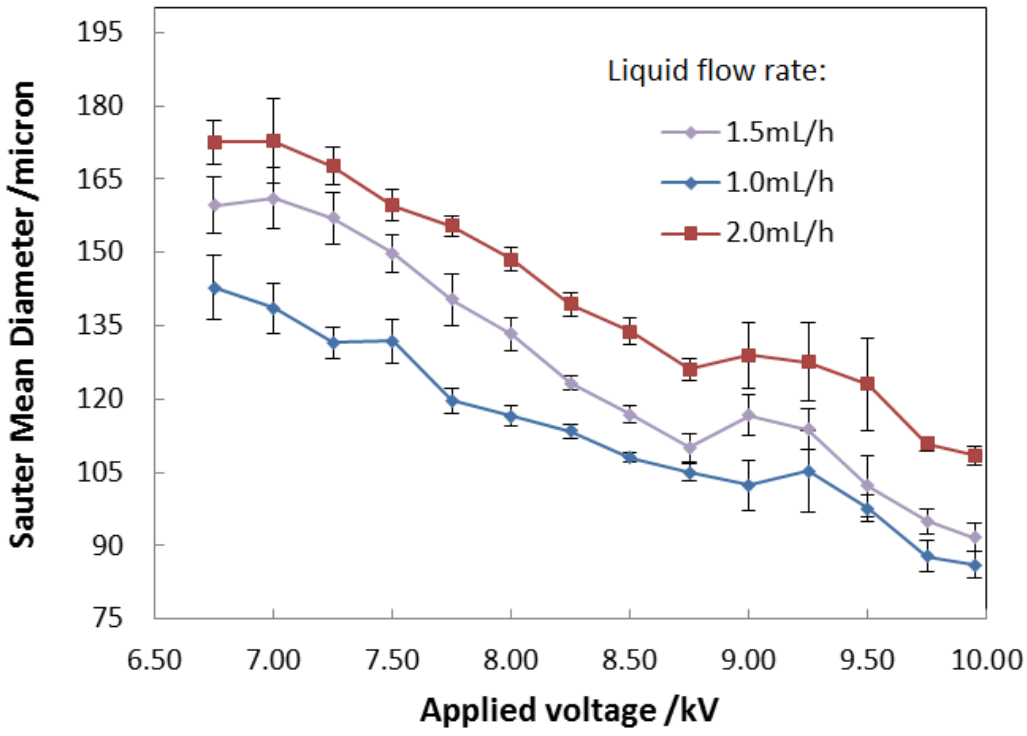

Figure 3-6 Influence of applied voltage and liquid flow rate on aerosol droplet size (HT-D). HT-D aerosol, 800 ppm additive

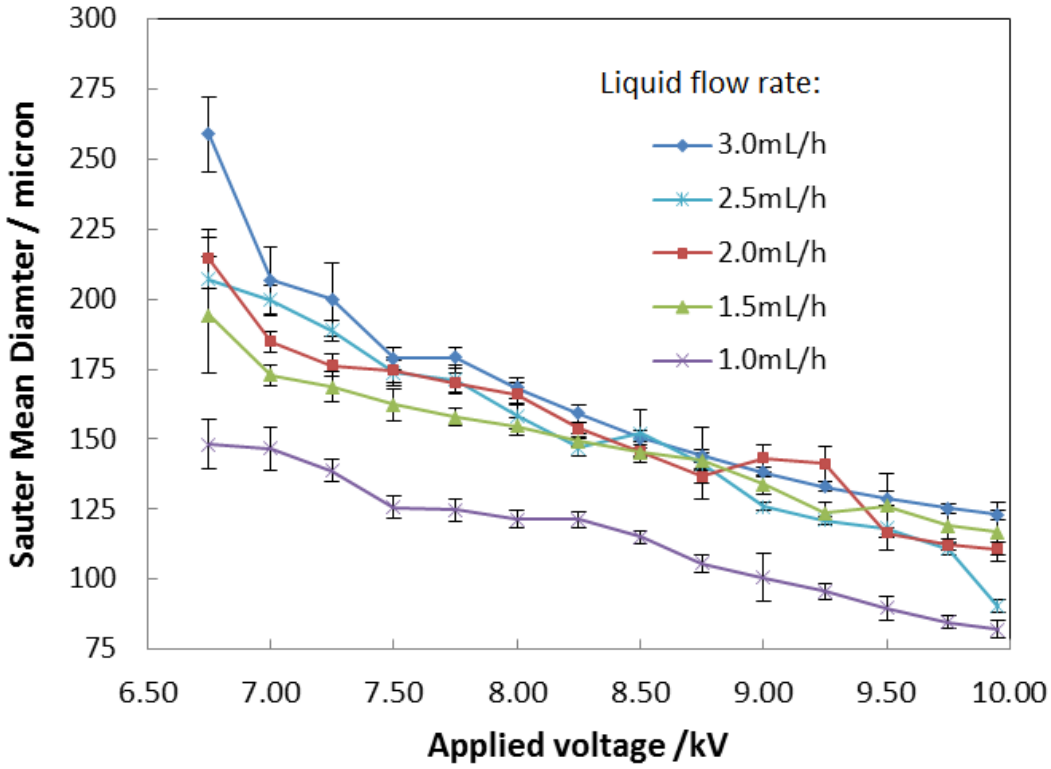

Figure 3-7 Influence of applied voltage and liquid flow rate on aerosol droplet size (P-HE). P-HE aerosol, 800 ppm additive

Figure 3-7 shows the effects of liquid flow rate on aerosol droplets from the P-HE fluid. It can be seen that for a liquid flow rate of 1.5mL/h to 3.0mL/h, a decrease in droplet size under the same electrospray conditions is not significant. For a liquid flow rate of 1.0mL/h, the droplet size noticeably decreases. The error bars indicate the values of the standard deviations from the sampling data under the corresponding electrospray conditions. The standard deviations are relatively higher in the two voltage regions

below 7.25kV and from 8.5 to 9.5kV, which are assumed to be the unstable regions for the electrospray.

Unstable electrospray regions

A closer look at the unstable spray conditions in the detailed droplet size sampling data by LDPA shows an interesting phenomenon in the droplet size fluctuation pattern. The droplet size fluctuation patterns under the unstable spray conditions for the HT-D and P-HE aerosols are shown in Figures 3-8 and 3-9 respectively. Under each unstable spray condition, there appears to be two droplet size ranges where the SMD values fluctuated within a range of 10 μm for a short period of time before migrating to another one. For example, in Figure 3-8b, the two droplet size ranges are 105 μm ~ 115 μm and 95 μm ~ 105 μm. The two ranges appeared alternately. The alternating pattern became quite obvious for Figure 3-9b. The alternating of droplet sizes between the two ranges results in a larger standard deviation for the average SMD values of the aerosol systems under unstable spray conditions.

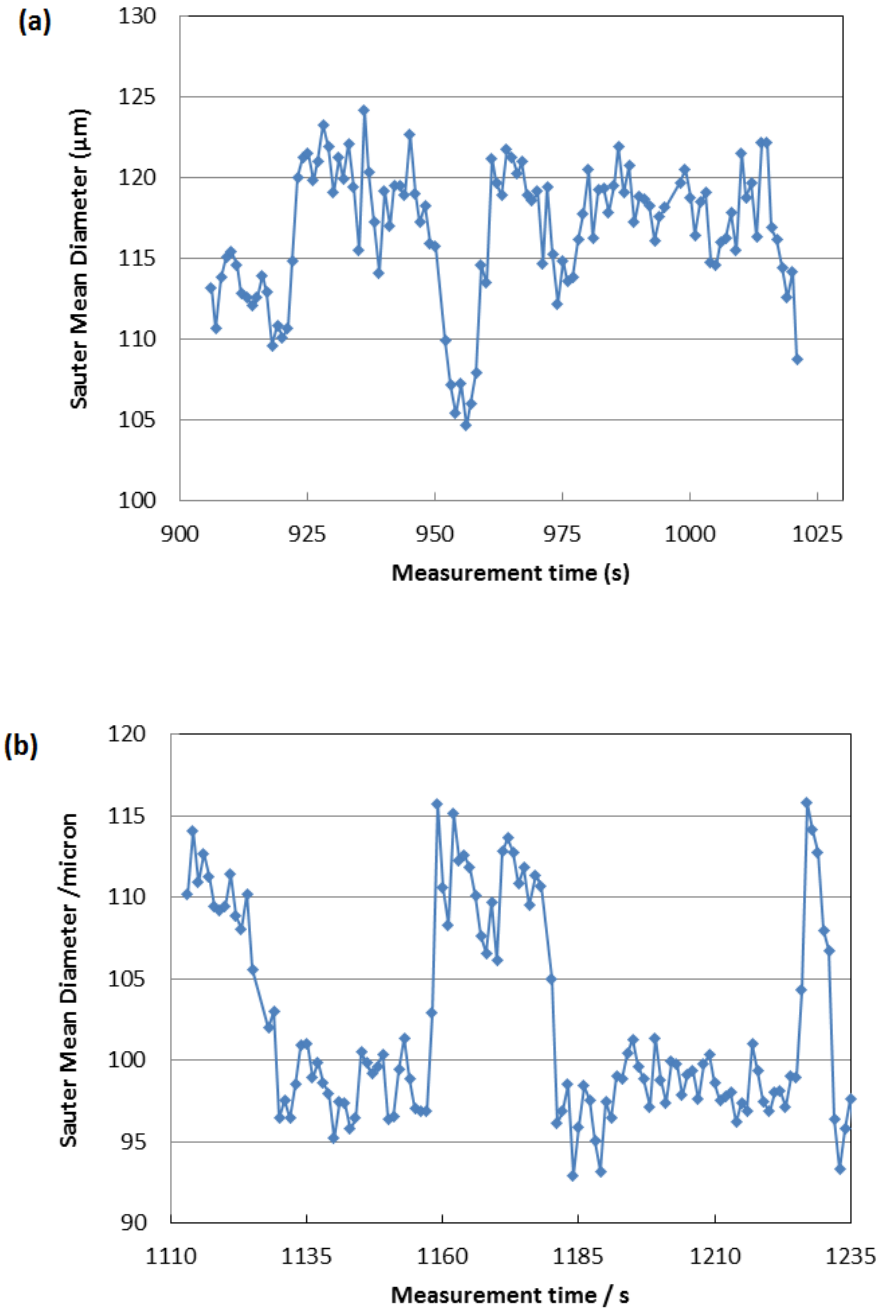

Figure 3-8 Appearance of unstable spray mode (HT-D). HT-D aerosol, 800 ppm additive, 1.5 mL/h) (a) 9.0 kV applied voltage; (b) 9.50 kV applied voltage

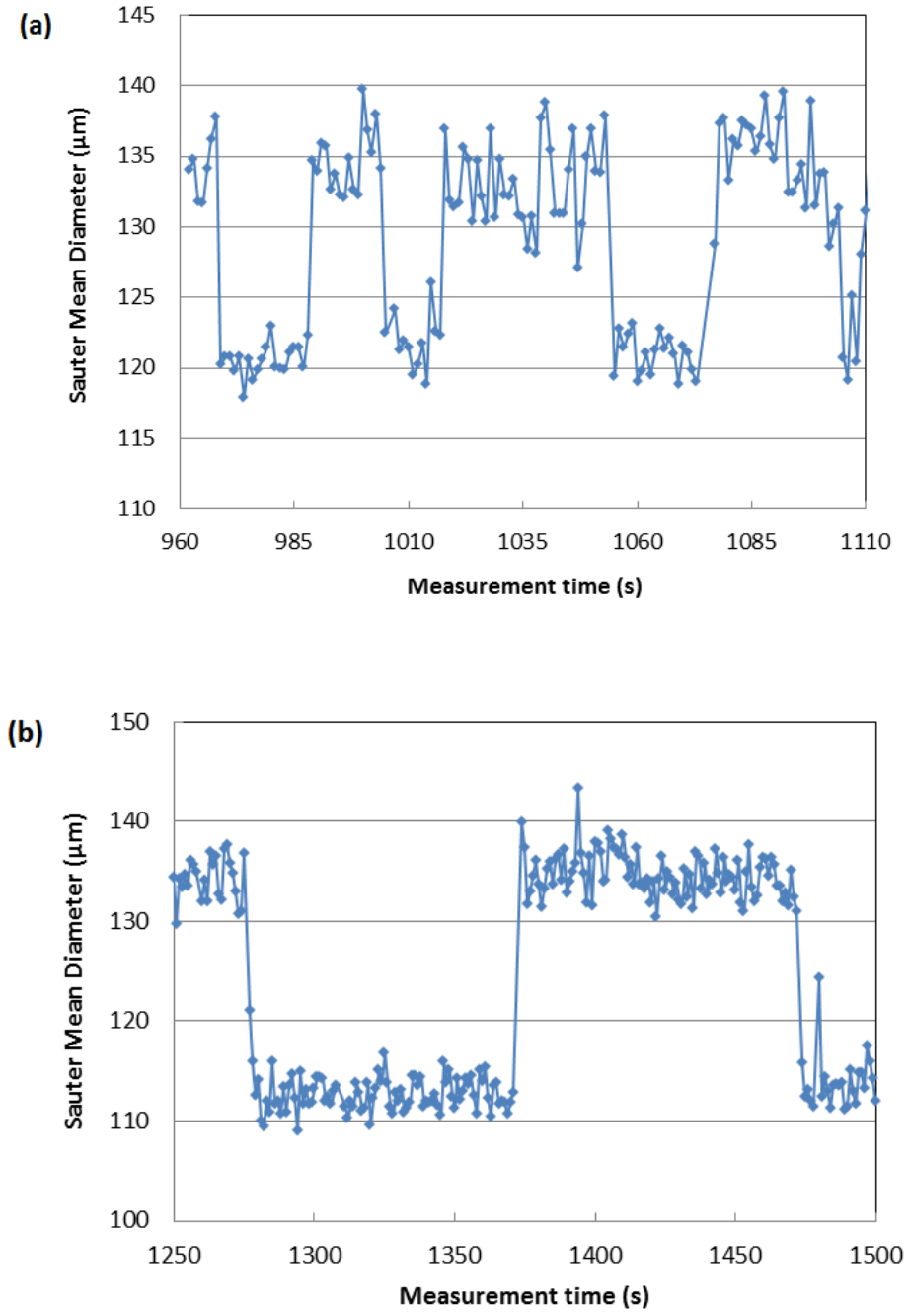

Figure 3-9 Appearance of unstable spray mode (P-HE). P-HE aerosol, 800 ppm additive, 2.0 mL/h) (a) 9.0 kV applied voltage; (b) 9.50 kV applied voltage

STUDY OF ELECTROSPRAY USING FINITE ELEMENT MODELING

Introduction

Due to the complexity of electrospray behavior of industrial hydrocarbons because of the great variety in their compositions and physical properties, a method capable of predicting electrospray characteristics of hydrocarbons based on their properties is necessary to facilitate future efforts for finding optimum spray conditions for higher spray stability and mono-dispersity in aerosol droplet sizes. A model using the finite element method is set up as an initial trial for the prediction of electrospray performances, and will be introduced below.

Modeling of electric field around spray nozzles

In electrospray, a conductive Taylor's cone surface is assumed. When the nozzles are made of non-conductive materials, aerosol droplet formation is mainly controlled by the electric field between the surface of the Taylor's cone and ground level electrode. In the current work, stainless steel tubing with good conductivity is used for the spray nozzles. The electric field between the spray nozzles and the ground level electrode is mainly determined by the voltage applied on the nozzles and the distance between the nozzles and the ground level ring. To study their influences on electric field strength and distribution, a 3-D simulation of an electrostatic field between the spray nozzle and the ground level is carried out with COMSOL Multiphysics 3.5a (COMSOL inc.). The electrostatic application mode in MEMS module, which is governed by Poisson's

equation, is applied in the models. Voltages applied to the nozzles varied from 7.5kV to 8.5kV, and the distance between the nozzle tips and the ground level varied from 10mm to 30mm.

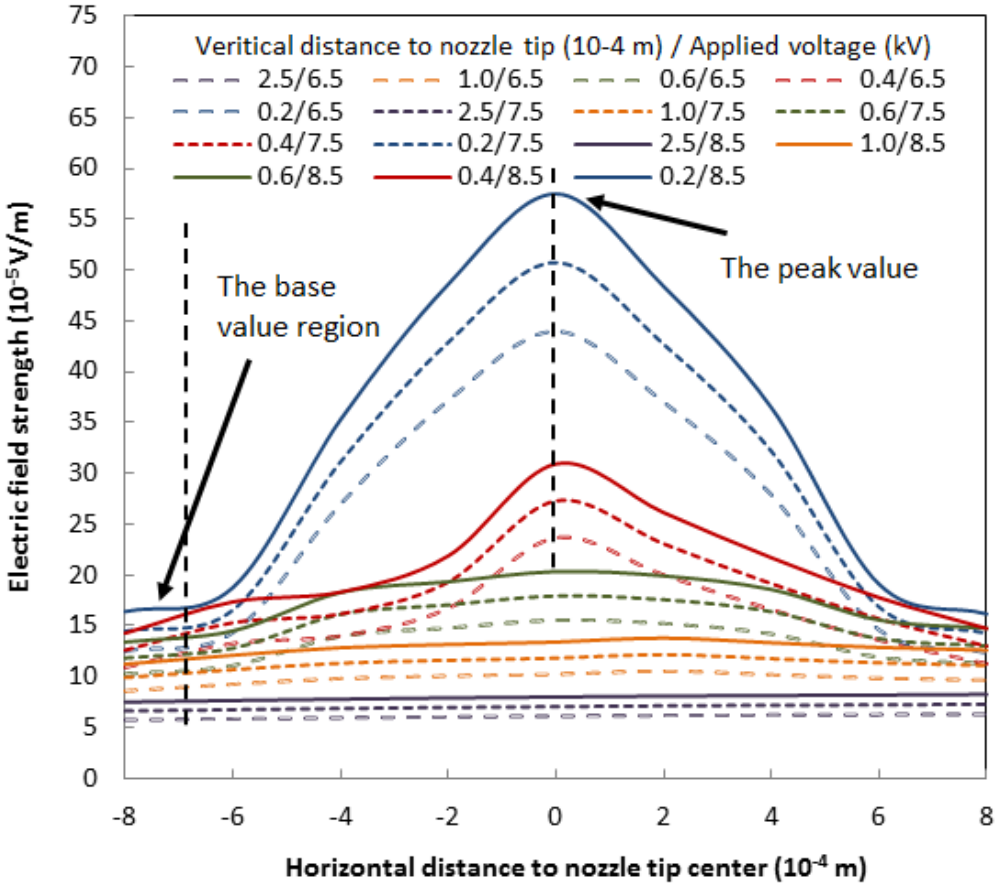

Figure 3-10 Electrostatic field strength below spray nozzle

Figure 3-10 shows the impact of applied voltage on the distribution of the electric field below the spray nozzle. The electric field varied in both the horizontal and vertical directions. The electric field below the nozzle increases with higher nozzle voltage. The electric field lines have different peak shapes at different distances below the nozzle tip, indicating different trends in the variation of the electric field in the horizontal direction. The electric field lines at 0.2 mm and 0.4 mm below the tip exhibit near triangular shaped peaks around the nozzle's center line at x=0. As the distance became longer the peaks gradually decrease in height to a near oval shape. For distances beyond 2.0 mm the lines become flat, showing little variation in the electric field along the horizontal direction. The lines can be generally characterized by two parameters, a peak value in the center and a base value for the flat regions on both sides, as shown in Figure 3-10. As the nozzle voltage is increased, both the peak and base values become higher, though the increase seems to be more significant for the peak values, particularly for the lines closer to the nozzle tip.

Modeling of droplet generation

A two-dimensional axisymetrical numerical simulation with COMSOL Multiphysics 3.5a (COMSOL inc.) is carried out to investigate the effects of the electric field on droplet generation in electrospray. The two-phase flow, laminar, level-set mode in the MEMS module, which is governed by the incompressible Navier-Stokes equation (u), the continuity equation, and the level-set function (φ), are applied. The level set method is a technique to model moving interfaces between two fluids with fixed mesh.

A level set function is defined to represent the position of the interface. As in the current model, the liquid-air surface is located at the isocontour of ø=0.5, and a smooth transition from ø=0 to ø=1 represents the transition from the air phase to the liquid phase.

The model consists of two sub-domains, as shown in Figure 3-11a. Initially domain 1 was filled with the high-density fluid, representing a nozzle filled with heat transfer fluid. The inner diameter of the nozzle is 100 μm. The interface between domain 1 and domain 2 is set as the initial liquid-air interface resting at the nozzle tip (Figure 3-11a right). The domains were dicretized into 11176 rectangular elements of consistent size for numerical stability during computation. Liquid will flow through the top of domain 1 downward into the domains. The interface between the liquid and air will experience a strong electrical field force upon applying the electric field.

Although the COMSOL Multiphysics package features the capability to combine electrostatic and level-set multiphase flow physics together, due to the vast difference in the length scales of the domains between the electrostatic field models discussed before and the electrospray nozzle models here, such a multiphysics combination will bring about unnecessary computational inefficiencies. Based on characteristics of the electric field distributions by electrostatic modeling and the expression of electric field forces on the liquid-air surface $F = \varepsilon R E^2$ (ε the liquid permittivity, R the surface shape factor), a simplified distribution of an electric field force on the surface is applied in domains of the electrospray nozzle model, as shown in Figure 3-11b.

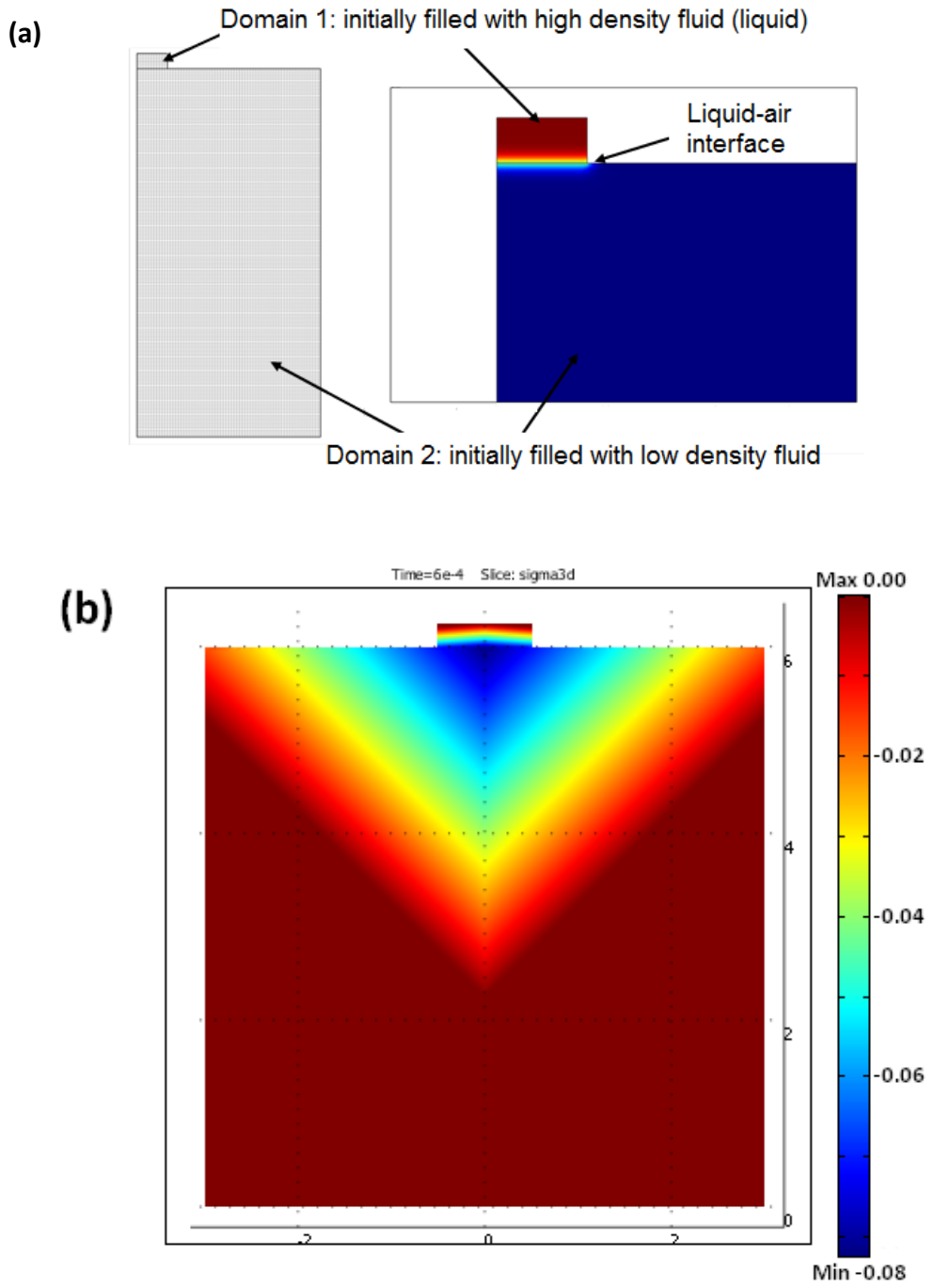

Figure 3-11 Finite element modeling of electrospray. (a) System geometry and initialized liquid-air interface in the model; (b) electric field strength distribution in the initialized model

The electric field force varied from 0 to a negative value of highest force intensity; the negative sign represents the opposite direction of the force against the surface tension. The electric field force degraded linearly from the center of the nozzle tip in both the horizontal and vertical directions, which results in the triangular isocontours of the electric field force in Figure 3-11b. The application of the electric field force to the cone-jet mode is realized through adding the expression of the force distribution to the original liquid surface value in the model. By exerting the electric field force on the liquid-air surface, the process of the Taylor's cone formation and droplet generation from the liquid jet can be simulated. By changing the minimum value of the force, effects of adjusting nozzle voltages are simulated.

Droplet sizes from liquid jets under the influence of electric field force by finite element modeling are shown in Figure 3-12. As shown in Figure 3-12a**,** the sizes of the droplets from the nozzle under a specific electric field force configuration decreased as the electric field force on the liquid-air surface increased, exhibiting a trend similar to what is observed in experiments. Also similar to experimental observation, droplet sizes in two electric field force height ranges are unstable, one below 0.06 N/m and the other one above 0.075 N/m, as indicated by a large fluctuation in droplet sizes and higher standard deviation values.

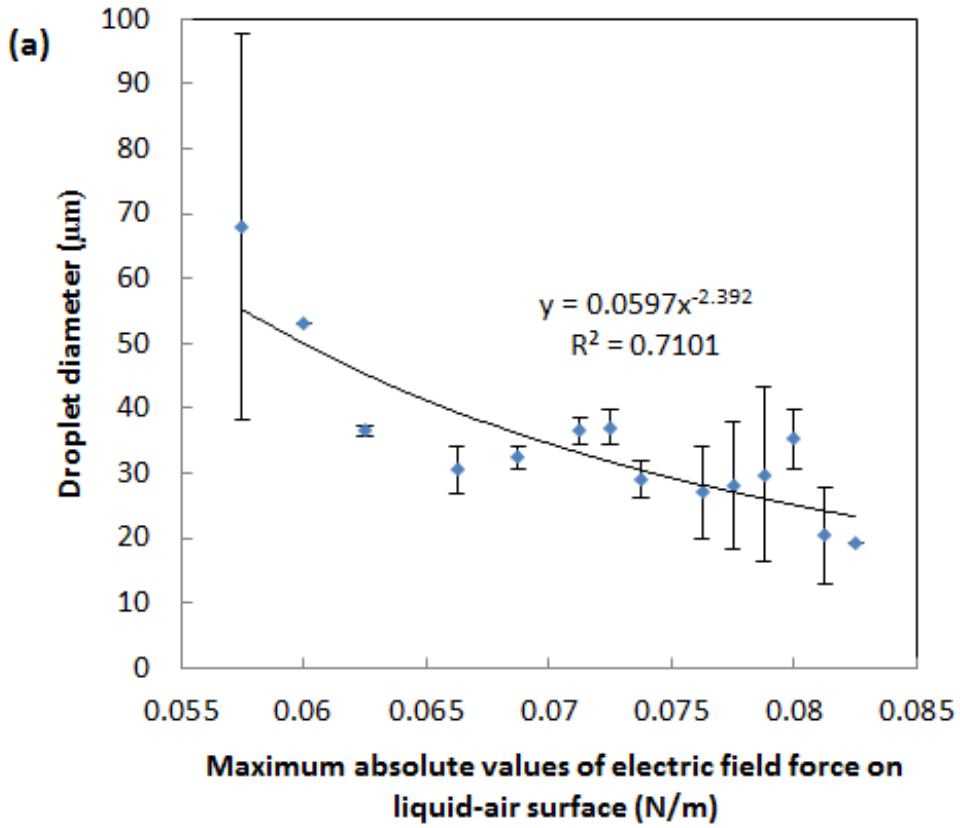

Figure 3-12 Comparison of droplet formation in finite element modeling of electrospray with experimental observation. (a) Simulated droplet size against increasing electric field force on the liquid-air surface; (b) liquid cone-jet formation and droplet generation along time (6 mL/h liquid flow rate, 0.078 N/m electric field force); (c) comparison of experimental observation of stable (1 mL/h flow rate, 3.6 kV nozzle voltage) and unstable (5 mL/h, 3.6 kV) cone-jet spraying modes; (d) development of Sauter Mean Diameter of aerosols along time under different nozzle voltage as characterized by laser diffraction particle analysis (HT-D, 5 mL/h flow rate; nozzle applied voltage (I) 7.2 kV, (II) 7.5 kV, (III) 8.0 kV, (IV) 8.5 kV, (V) 8.7 kV

(b)

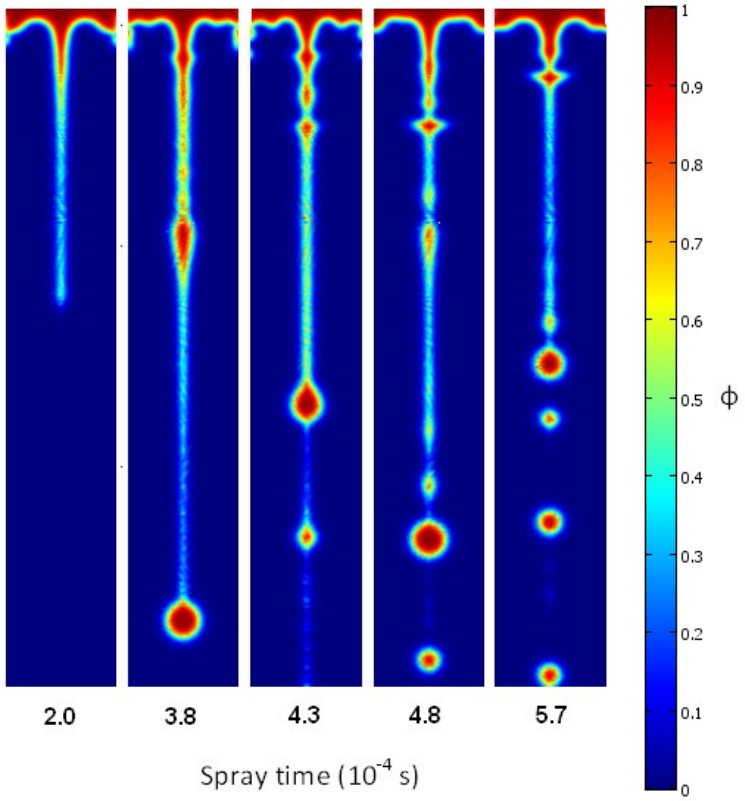

(c)

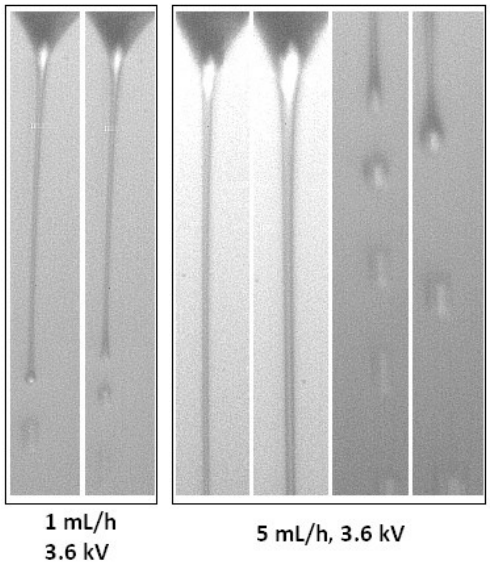

Figure 3-12 Continued

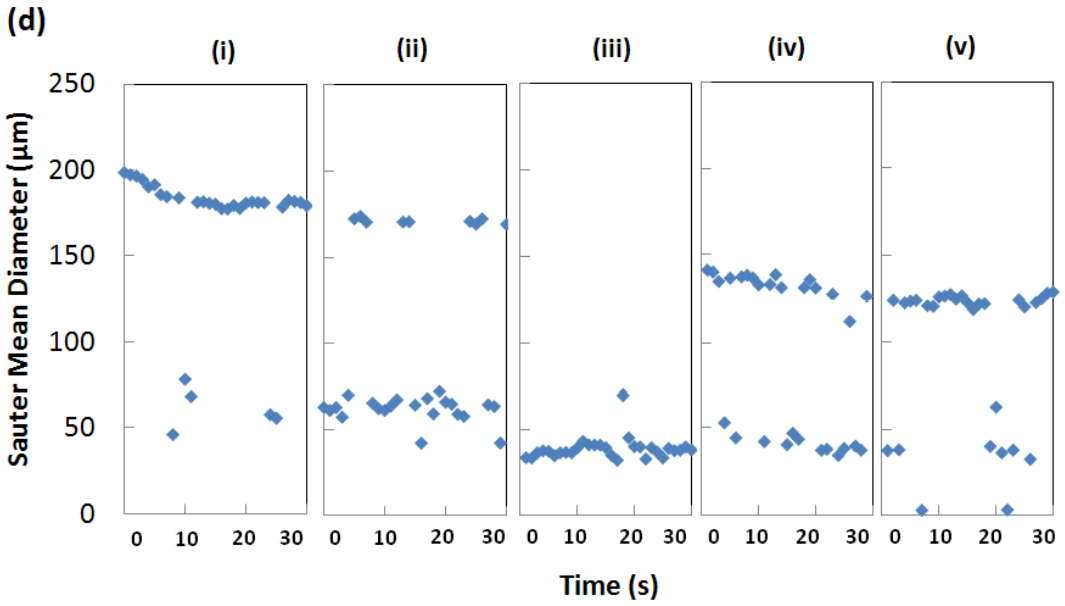

Figure 3-12 Continued

Figure 3-12b shows the modeled process of liquid cone-jet formation and droplet generation under a 0.078 N/m electric field force height in the unstable spraying mode. A liquid cone jet with a smooth liquid-air surface in the shape of Taylor's cone has been formed at 0.2 mS. Balance between the liquid surface tension and electric field force was reached by the curvature of the surface. The length of the jet increased until the first droplet was formed at 0.38 mS. More droplets were generated from 0.38 mS to 0.57 mS. Although the sizes of the droplets were different, they can be grouped into two main size ranges, one around 50 µm and the other one around 20 µm. Within each group the droplet sizes are quite stable. This is similar to the phenomenon observed in the electrospray experiments. As shown in Figure 3-12d**,** during the unstable spraying mode

there exist two main droplet size ranges, the higher one above 100 μm and the lower one around 50 μm. Droplet sizes within each range are quite stable. As the nozzle voltages are increased from 7.5 kV to 8.0 kV, the amount of droplets in the lower size range continued to increase, resulting in a lowered average Sauter Mean Diameter over time. When the nozzle voltage was further increased, the proportion of larger size droplets became higher again.

It can be seen that the frequency of droplet generation in the modeling of unstable electrospraying also changes along time, depending on the size of the formed droplets. This is also similar to experimental observations of the Taylor's cone-jet as indicated in Figure 3-12c by pictures from a high speed camera. For the stable cone-jet spraying mode with a 1 mL/h HT-D flow rate and 3.6 kV applied nozzle voltage, both the shape of the Taylor's cone-jet and droplet size remain stable. For the unstable spraying mode with a 5 mL/h HT-D flow, both the droplet generation frequency and droplet size kept changing, and the liquid jet changed in its intersectional area by alternately swelling and shrinking.

There are also some differences between the modeling and experimental observations. The droplet sizes from the numerical modeling are smaller than the actual electrospray. Since the model addresses the surface force phenomenon in an ideal electric field condition with simplified electric field force distribution, even under a higher liquid flow rate of 6 mL/h, the dimensions of the spray are significantly smaller, and the droplet generation frequency is much higher than in the actual system. There are also some differences in the phenomena between the modeling spray and the

experimental system. Because of the small dimension of the liquid cone-jet, instead of swelling and shrinking alternatively, the liquid jet kept pulsating with liquid flowing downward into the cone-jet.

SUMMARY

Using the method of electrospray, monodisperse aerosol droplets are produced using three types of commercial heat transfer fluids. Aerosol droplet size is measured using a laser diffraction technique. The main findings are summarized below:

1) Aerosol droplet size is mainly determined by the voltage applied to the spray nozzles and the liquid flow rate in the nozzles. The applied voltage ranges from 6.5 kV to 10.0 kV. The liquid flow rate in each nozzle ranges from 0.5 mL/h to 3.0 mL/h. The droplet size of the P-NF aerosols ranges from 40 μm to 220 μm; the droplet size of the HT-D aerosols ranges from 80 μm to 180 μm; the droplet size of the P-HE aerosols ranges from 75 μm to 275 μm. Under the same nozzle voltage, liquid droplet size decreases with a lowered liquid flow rate. The droplet size deceased as the voltage on the spray nozzles increased.
2) There exist unstable spray conditions for electrospray using heat transfer fluids. Under the unstable spray conditions, the Sauter Mean Diameters of the aerosols from electrospray keep fluctuating between two droplet size ranges, resulting in large standard deviations in the average SMD values.
3) The electrospray process is modeled by the finite element method. The size of the droplets from the spray nozzle decrease as the electric field force on the

cone-jet liquid-area surface becomes larger. The electrospray model shows unstable spraying phenomenon similar to the experimental observations. The mechanism for the unstable spraying phenomenon still needs further study.

CHAPTER IV

AEROSOL IGNITION TEST AND FLAME CHARACTERISTICS IN AEROSOLS *

INTRODUCTION

Because of the complexity of aerosol formation and ignition, knowledge of the characteristics of flames in aerosols is quite limited in previous literature, making it difficult to assess the fire hazards of flammable aerosols used in the process industry (Ballal & Lefebvre, 1981; Polymeropoulos, 1984; Myers & Lefebvre, 1986; Suard et al. 2001; Lawes et al. 2002). To assess the fire and explosion hazards of aerosol systems, it is necessary to gain more knowledge on the characteristics of flames produced by aerosols, especially the flame size and flame propagation speed.

The purpose of the work in this chapter is to study how the characteristics of a flame, such as its size and propagating speed, are determined by the existence of aerosol droplets, their evaporation behaviors, and their properties, such as droplet size and number density. Industrial heat transfer fluids, which have an extremely wide range of applications in the process industry, are used.

---

* Part of this chapter is reprinted from "Flammability of heat transfer fluid aerosols produced by electrospray measured by laser diffraction analysis" by Lian, P., Mejia, A. F., Cheng, Z., and Mannan, M. S. (2010). *Journal of Loss Prevention in the Process Industry*, *23*(2), 337-345, Copyright 2009, with permission from Elsevier. Part of this chapter is reprinted from "Study on flame characteristics in aerosols by industrial heat transfer fluids" by Lian, P., Ng, D., Mejia, A. F., Cheng, Z., and Mannan, M. S. (2011). *Industrial & Engineering Chemistry Research*, *50*, 7644-7652, Copyright 2011, with permission from American Chemical Society.

Starting from a small-scale laboratory experiment setup, a different approach to characterizing the propagating flames in aerosol systems is presented. Electrospray was used for the production of aerosol droplets with uniform size and initial velocity to simulate those from actual pressurized release scenarios. High-speed photography was used to capture the aerosol flame propagation and to address the complexity of the flame shapes. The numerical modeling of droplet movements and evaporation behaviors was carried out to explain the phenomena observed in the experiments.

Knowledge from current work on how the flame characteristics in aerosols are influenced by the droplet size and speed may help connect the aerosol fire consequences to the aerosol formation and dispersion conditions in the pressurized release scenarios of industrial fluids, since they determine the droplet size and movement (Sukmarg et al. 2002). From this, relevant safety measures for preventing or mitigating aerosol fire hazards can be developed in the process industry. Investigations of such systems will not only be of practical importance to the process industry, but will also contribute to the fundamental understanding of combustion in aerosols.

MATERIALS AND METHODS

Aerosol production and droplet size measurement

A commercial heat transfer fluid with a high flash point, P-NF, was used to produce aerosol droplets through electrospray. The fluid's properties are listed in Table 3-1. Prior to electrospray, the Stadis 450 additive was added to the fluid at a volume

percent of 0.4% to enhance its electrical conductivity, so that the electrospray can stably produce monodisperse aerosol droplets. The samples were stirred for 5 minutes to ensure proper mixing of the additive. The fluid cells containing the samples were then allowed to stand for 60 minutes until air bubbles were no longer visible.

Setup of the electrospray system follows that in previous works (Lian et al. 2010), as shown in Figure 4-1. The electrospray system consisted of an array of ten metal nozzles acting as the droplet manifolds, which were energized by high voltage signals supplied from a function generator (Stanford Research System, Ds-345) through a voltage amplifier (Trek Inc. 610E). A grounded aluminum mesh was positioned 20 mm below the nozzle tips to create an electric field. The heat transfer fluid sample was pumped from an infusion syringe pump (KDS 220). When the fluid samples flowed through the capillaries, the liquid meniscus at the outlet of each capillary took a conical shape under the influence of the electric field. The liquid jet further broke up into monodisperse aerosol droplets which traveled downward into the space below. In electrospray, the produced droplet size is mainly controlled by the liquid flow rate in the nozzle and the voltage applied to the nozzle (Deng et al. 2006; Jaworek, 2007; Mejia et al. 2009). In this work, the liquid flow rate per nozzle was fixed at 3 mL/hr. The droplet size produced was adjusted solely by changing the voltage applied to the spray nozzles. Aapplying a higher voltage to the spray nozzle can reduce the droplet size.

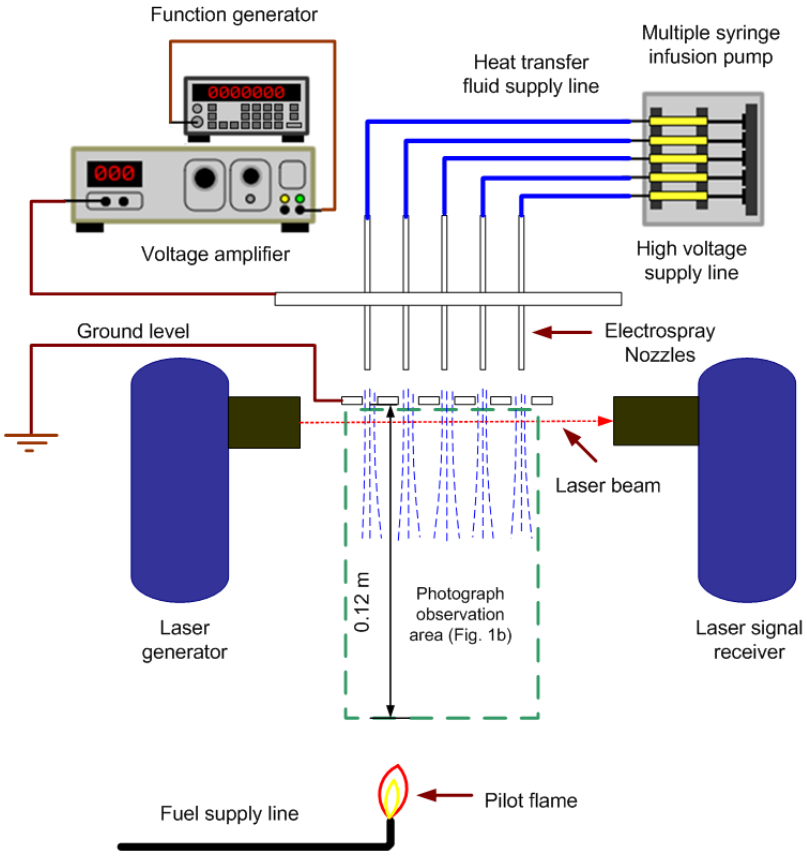

Figure 4-1 Aerosol ignition test setup

The droplet size produced was monitored by a laser diffraction particle analyzer (SprayTec, Malvern Inc.), and the droplet size was recorded as the surface area moment mean $D_{[3][2]}$ or the Sauter Mean Diameter (SMD) (Sukmarg & Krishna, 2002). The electrospray was turned on and the aerosol droplet size was sampled by Malvern LDPA at the 500 Hz sampling frequency. The electrospray was kept on for a certain period of time under the same set of electrospray conditions, so that no less than 1500 $D_{[3][2]}$ values were obtained for the aerosol system produced under the same set of electrospray

parameters (i.e. applied voltage, liquid flow rate). An average $D_{[3][2]}$ value with its standard deviation was further calculated. For example, the average $D_{[3][2]}$ value and its standard deviation for the electrospray condition of 8.75 kV and 3 mL/h liquid flow rate is 85.91 μm and ± 2.43 μm respectively. In the present work, the produced aerosol droplet size, as represented by the $D_{[3][2]}$ value, ranges from 82 μm to 96 μm. The uncertainty of the SMD values measured by the Malvern laser is estimated to be < ±5 μm.

Aerosol ignition

Aerosols formed in the open space below the grounded aluminum mesh, where ignition of the aerosols was carried out (Figure 4-1). The ignition source flame was positioned 150 mm below the mesh, and was controlled at about 10 mm in length.

Flame observation by high speed camera

To observe characteristics of the propagation process, a high speed camera (Phantom v4.2, Vision Research) was used to capture the movement of the flames through a space below the mesh with a height of 120 mm (Figure 4-1). The series of flame movement pictures was processed and analyzed using the ImageJ software (v1.43, National Institutes of Health). Two parameters from the image analysis, the flame size and the flame propagation speed, were used to characterize the combustion propagation process.

Flame size based on flame image analysis

The following is a description of the steps in the image processing and analysis used to obtain the flame size. For most of the pictures, there were multiple flames observed at a single moment. First, the bright areas of the flames in each picture were highlighted by adjusting the threshold values of brightness, so that all pixels in the flame areas had the same brightness and all other background objects in the picture were set to dark. The total number of pixels in the flame area of the picture were then converted to the actual size of the flame for that moment according to the scale. The flame size in the current work is defined as the total size of the flames, and it changed along time as the flames propagated upward.

Flame propagation speed based on flame image analysis

The steps to obtain the flame propagation speed are described as follows. The mass center of the flames in a picture was the average position of all pixels in all the flame areas. The y-coordinate value of the mass center is used to represent the vertical position of the flames in the picture, which was further converted to the actual height in the space. The actual height of the flames' mass center was also plotted as a function of time. Then, the combustion propagation speed was defined as the slope of the linear fitting line to heights of the flames' mass centers along time.

Flame detection by laser diffraction technique

A new way to study the flame behavior of the heat transfer fluid aerosols fabricated by electrospray is also introduced here. The method is based on detection of the aerosol combustion flame using Laser Diffraction Analysis (LDA), which is used for droplet size measurements in the current work.

Before the ignition tests, the instrument alignment was automatically checked by the laser diffraction particle analyzer (the instruments are aligned to ensure that the maximum intensity of the laser light is focused upon the central diode), before propane gas is allowed to flow through the gas line and ignited at the flame tip by the ignition source. Then the electrospray was started and the laser diffraction measurement was manually triggered at the same time. The time for each ignition measurement is 30 sec and the laser sampling rate is 500 Hz.

Characteristic changing patterns along time in the droplet size measurement data taken by the LDA were identified, which correspond to the moments flames appeared in the aerosol and its propagation through the laser beam measurement area. Analysis of each pattern yielded the propagation velocity of the flame front, which was further compared with the velocity visually observed by the high speed camera. Meanwhile, the frequency of the flame pattern appearances can also be related to the flammability of the aerosol. By changing the properties of the aerosols a new trend in frequency of the flame appearance is revealed, as will be discussed below.

EXPERIMENTAL RESULTS AND DISCUSSION

Three stages of flame propagation in aerosols by P-NF fluid

Flames in an aerosol system can take three modes: individual burning droplets, burning of droplet clusters, and the global flame. A global flame appears if the flame has a dimension several orders of magnitude larger than an individual droplet (Aggarwal, 1997; Chigier, 1983). During the ignition tests of aerosols produced by the P-NF heat transfer fluid, the first few droplets were ignited as the aerosol droplets approached near the ignition flame. Flames further developed from the ignited droplets or droplet clusters, and propagated upward through the aerosol system, as illustrated in Figure 4-2. The flames in the aerosol finally quenched when they reached the mesh at the top. Different burning modes were visually observed during development of the flame. In the aerosols near the open ignition flame, droplets seem to be burning individually, or burning in small clusters, accompanied by smoke production. As the flames propagated upwardly, larger flames evolved from burning droplet clusters, spreading over the cross section of the aerosol stream, and propagating quickly through the aerosol profile before quenching. These flames are considered global flames. The criterion for a successful ignition is the appearance of a global flame, the front of which is capable of propagating upward through the aerosol system.

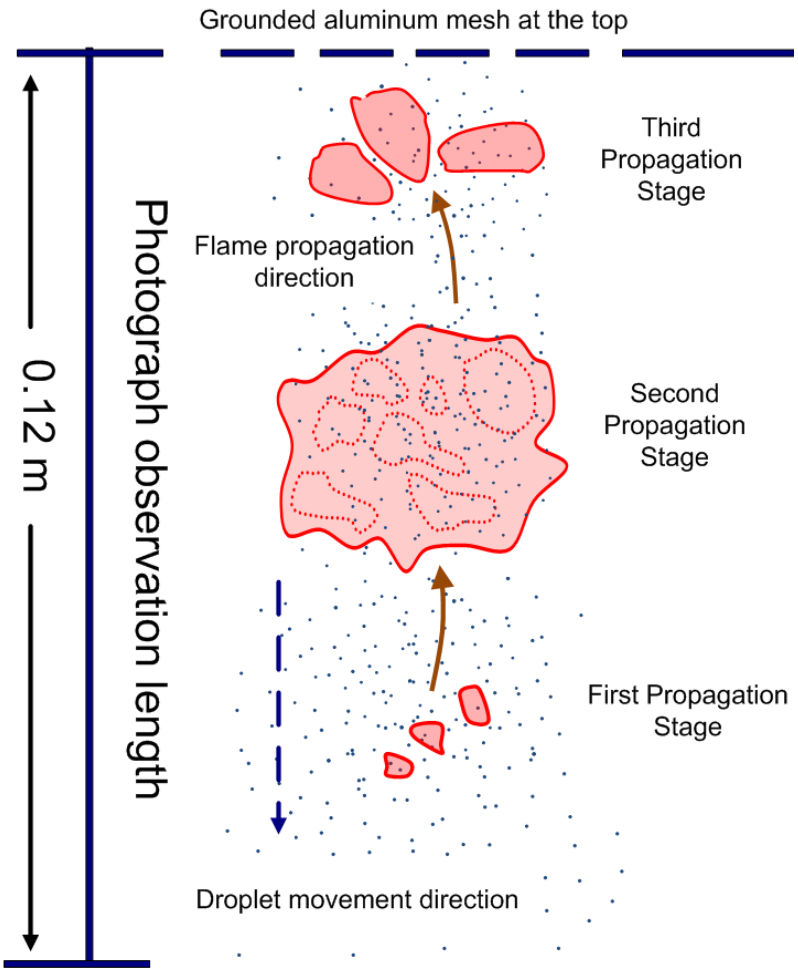

Figure 4-2 Schematic illustration of flame propagation stages in aerosol systems

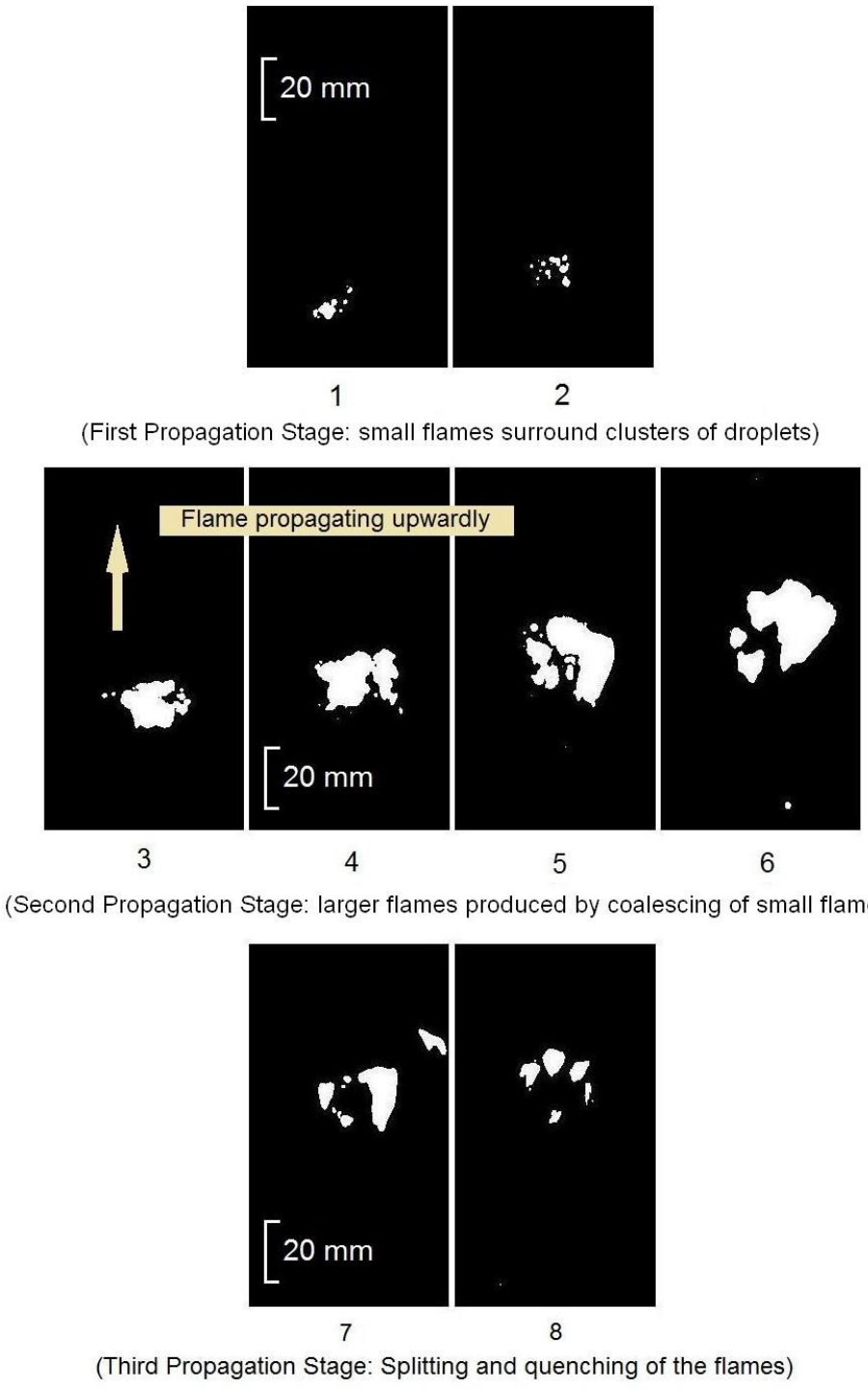

Figure 4-3 Flame propagation in the aerosol by high speed camera (P-NF)

The characteristics of aerosol flames are quite different when compared to the phenomenon of flame fronts flashing through flammable vapors, due to the discrete flame fronts and non-uniform shapes. As seen in Figure 4-3, as the flames moved upward the characteristics of flames changed, which can be classified into three different stages of the flame propagation process. In the first stage, the flames started with individually burning droplets or small flames surrounding clusters of droplets in lower positions (Figures 4-3 [1] and [2]). During the second stage the small flames moved up, and quickly coalesced into larger flames with a bright yellow color (Figures 4-3 [3] to [6]). In the third stage the flames continued to move upward, split into smaller flames, and finally quenched at the top, near the grounded aluminum mesh.

The different stages of flame propagation in P-NF aerosols were also exhibited by different rates of change in the flame size as they moved up. As seen in Figure 4-4, the flame size continued to increase (13.38 cm^2/s) in the first stage, but when the propagation developed into the second stage, a much higher rate of increase in the flame size (98.19 cm^2/s) was observed as small flames coalesced and developed into larger flames. In the third stage, the total area of the flames shrank at a rate of -79.25 cm^2/s, which corresponds with the large flames splitting into smaller flames before quenching at the top. Different combustion modes of flames in aerosol systems have also been reported by previous researchers (Hayashi & Kumagai, 1974; Hayashi et al. 1981; Aggarwal, 1997). Among the three stages of flame propagation, i.e., the second stage which is characterized by large yellow flames and rapid flame size expansion, is

considered to be the most hazardous scenario of aerosol flames and may result in more severe damage to the plant environment if it occurs on a large scale.

Figure 4-5 shows the moving trend of the flame propagation distance as a function of time. There is a good linearity in the trajectories of the travel distance (0.28 m/s as the slope of linear fitted line), indicating a stable propagation speed through different stages of flame development.

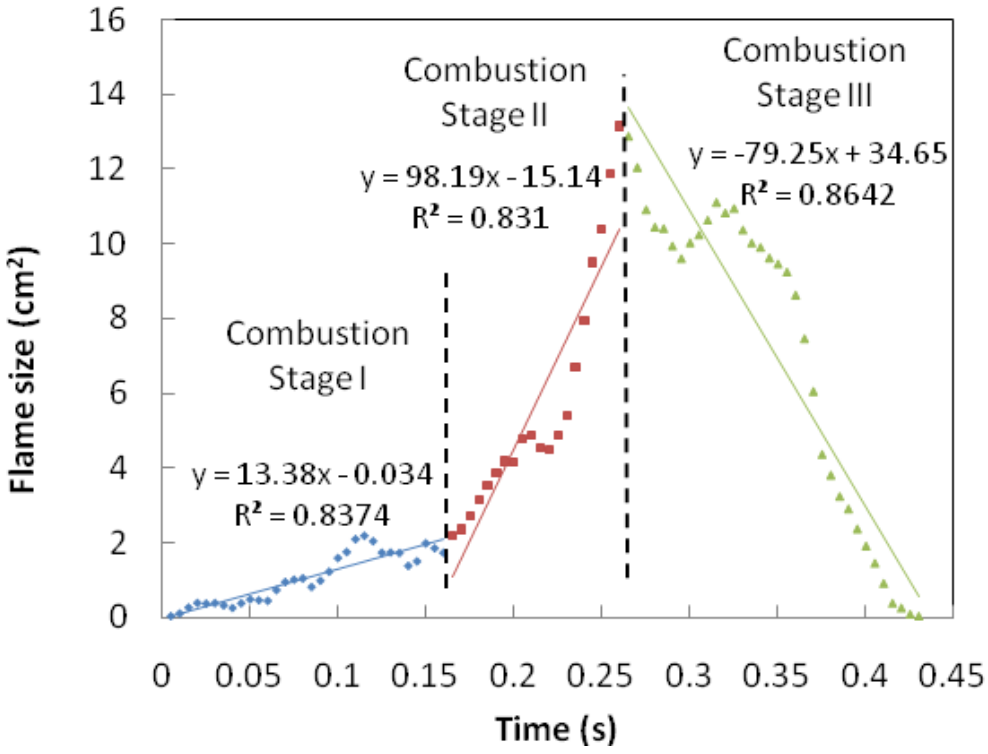

Figure 4-4 Propagation analysis of a flame in the aerosol system based on visual observation: the flame's size changes as a function of time (P-NF)

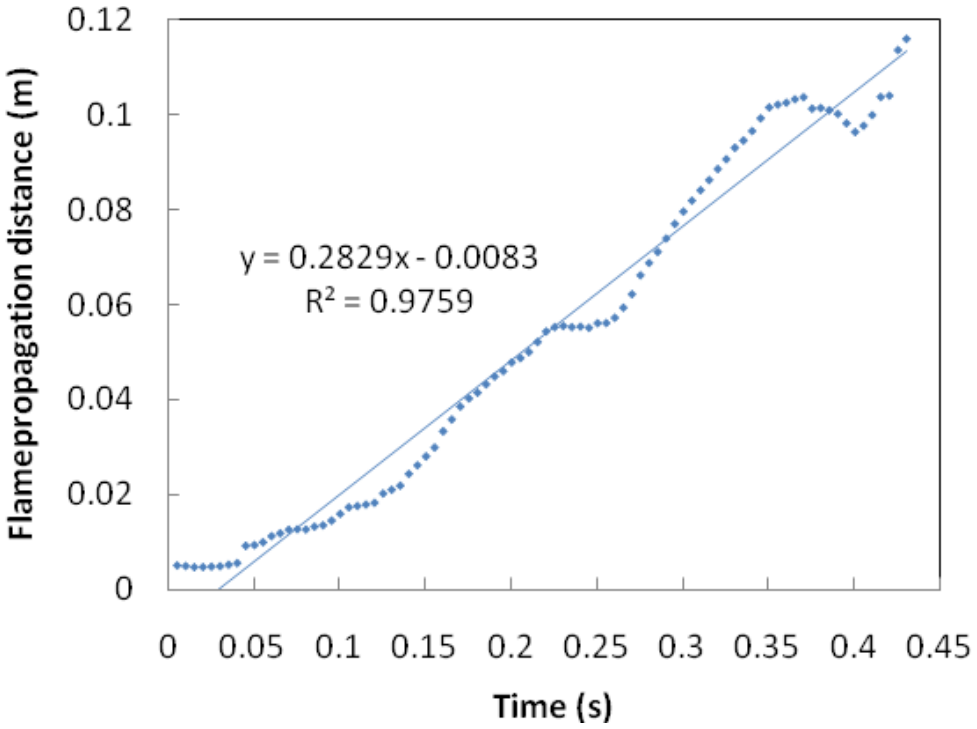

Figure 4-5 Propagation analysis of a flame in the aerosol system based on visual observation: the flame's position changes as a function of time (P-NF)

Flame characteristics in aerosols of different properties

Observation of the flames in the aerosol systems was carried out with four different produced droplet sizes. Part of the calculated values of flame propagation speed and flame size is tabulated in Table 4-1. The average flame propagation speed and flame size for different droplet sizes are shown in Figure 4-6. As the produced droplet size increases, both the flame propagation speed and the flame size in the aerosol systems decreases slightly. Compared with values of the laminar flame front velocity in the flammable gaseous mixtures (Glassman & Yetter, 2008), values of the newly defined flame propagation speed in aerosols are relatively slow.

Table 4-1 Flame propagation speed and flame size in P-NF aerosols

Flame No.	Produced droplet size (μm)	Speed (m/s)	R-square for the flame speed (m/s)	Flame size (cm^2)
1	89.07	0.52	0.966	2.63
2	89.07	0.45	0.984	2.76
3	89.07	0.36	0.914	0.84
4	89.07	0.28	0.969	0.89
5	89.07	0.26	0.948	0.77
6	85.91	0.37	0.965	1.41
7	85.91	0.32	0.990	2.03
8	85.91	0.35	0.933	1.85
9	85.91	0.28	0.976	4.54
10	85.91	0.43	0.905	1.55

Table 4-1 Continued

Flame No.	Produced droplet size (µm)	Speed (m/s)	R-square for the flame speed (m/s)	Flame size (cm^2)
11	86.14	0.26	0.925	1.96
12	86.14	0.35	0.992	3.45
13	86.14	0.44	0.957	2.02
14	86.14	0.43	0.984	1.96
15	86.14	0.59	0.949	1.49
16	82.99	0.33	0.985	2.09
17	82.99	0.54	0.968	2.32
18	82.99	0.36	0.982	2.04
19	82.99	0.45	0.960	2.84
20	82.99	0.55	0.992	1.92

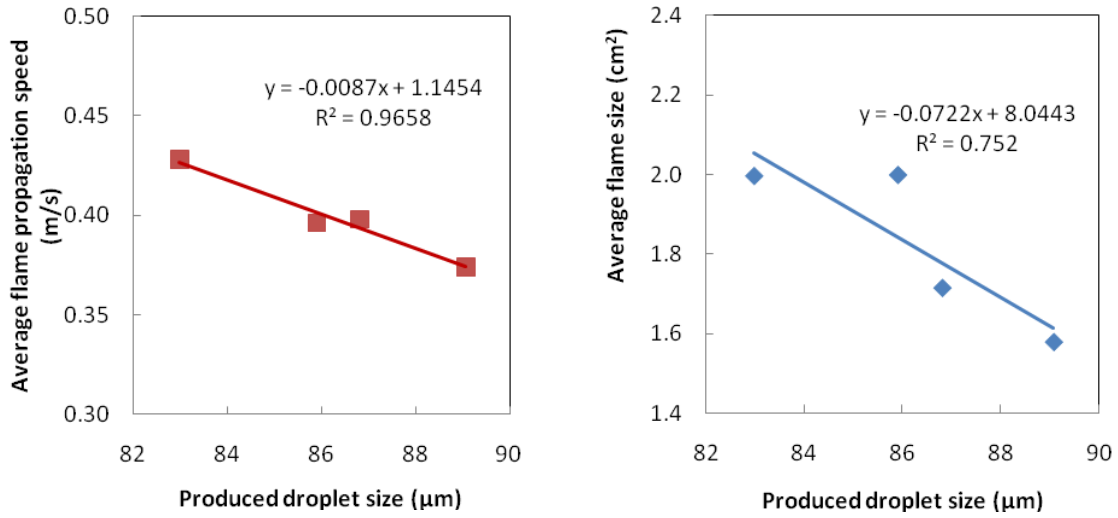

Figure 4-6 Influence of produced droplet size on average flame propagation speed and average flame size. (a) Average flame propagation speed against change in produced droplet size of P-NF aerosols; (b) average flame size against change in produced droplet size of P-NF aerosols

Flame characteristics in aerosols by HT-D fluid

Ignition tests of aerosols by the HT-D heat transfer fluids were carried out. Flames in the HT-D aerosols were captured by a high speed camera, and the flame pictures were analyzed using ImageJ software following the procedure introduced above for the P-NF aerosols. Some of the calculated values of flame propagation speed and flame size are tabulated in Table 4-2. Compared with the flames in the P-NF aerosols, the flames in HT-D aerosols tend to have higher flame propagation speeds and smaller flame sizes.

Table 4-2 Flame propagation speed in HT-D aerosols

Flame No.	Produced droplet size (μm)	Speed (m/s)	R-square for the flame speed (m/s)	Flame size (cm^2)
1	118.64	0.55	0.925	0.53
2	118.64	0.45	0.783	0.53
3	118.64	0.98	0.904	0.69
4	111.28	0.54	0.999	1.16
5	111.28	0.42	0.976	0.72
6	111.28	1.02	0.983	0.65
7	111.28	0.94	0.970	0.76
8	111.28	0.54	0.987	1.69

Propagation of a flame in the HT-D aerosol is shown in Figure 4-7. Different burning modes are also observed for the flame in HT-D aerosol. But unlike the P-NF flame in Figure 4-3, the flame in HT-D aerosol does not follow the propagation process of three-stage sequence. Instead, the different burning modes appear alternatively as the flame propagated upwardly. For example the droplet cluster burning mode was observed in Figure 4-7[1], [4], and [9]; the global flame mode was observed in Figure 4-7[2]-[3], [6]-[7], and [10]-[12]. The rest of the pictures show both burning modes.

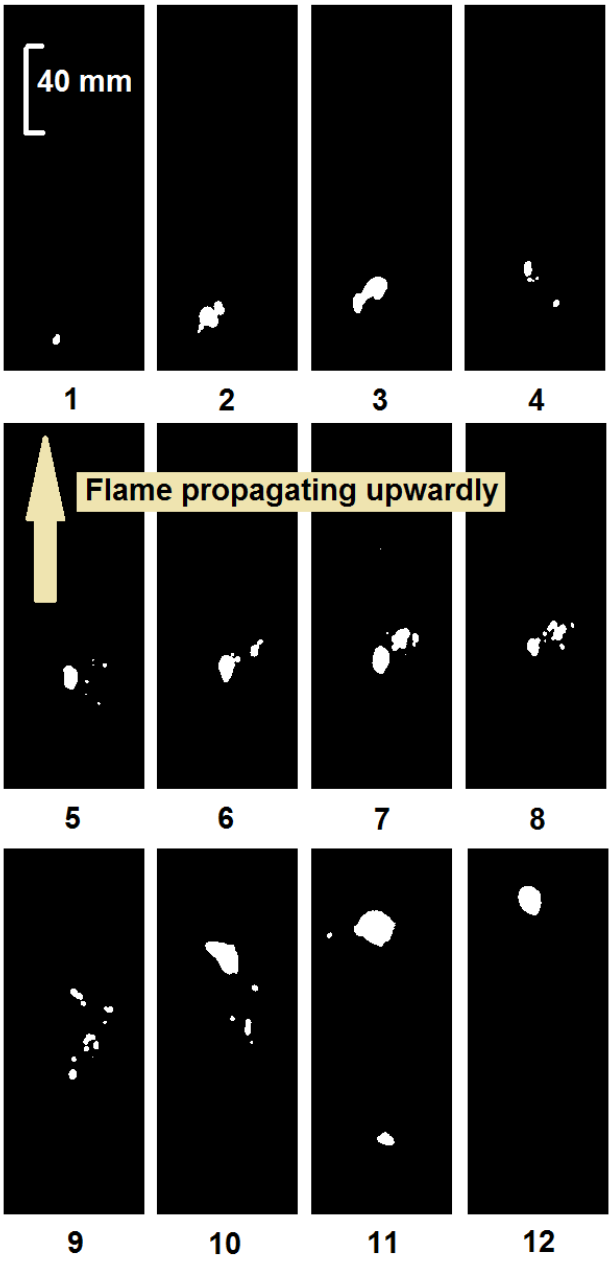

Figure 4-7 Flame propagation in the aerosol by high speed camera (HT-D)

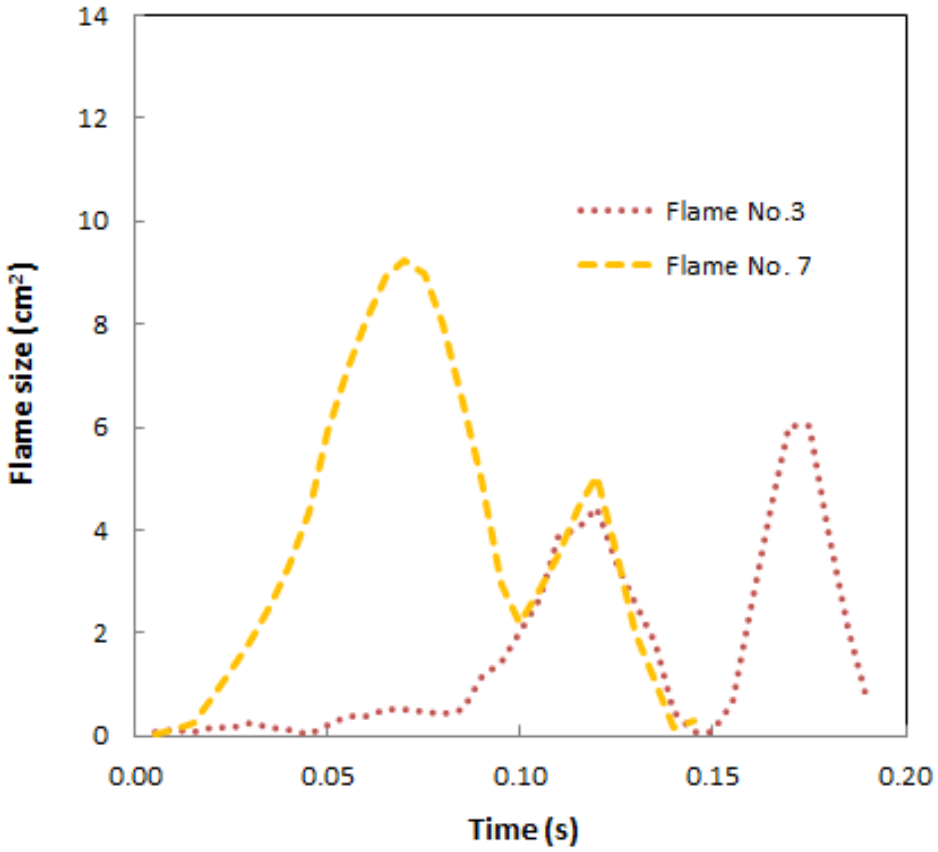

Figure 4-8 Propagation analysis of a flame in the aerosol system based on visual observation: the flame's size changes as a function of time (HT-D)

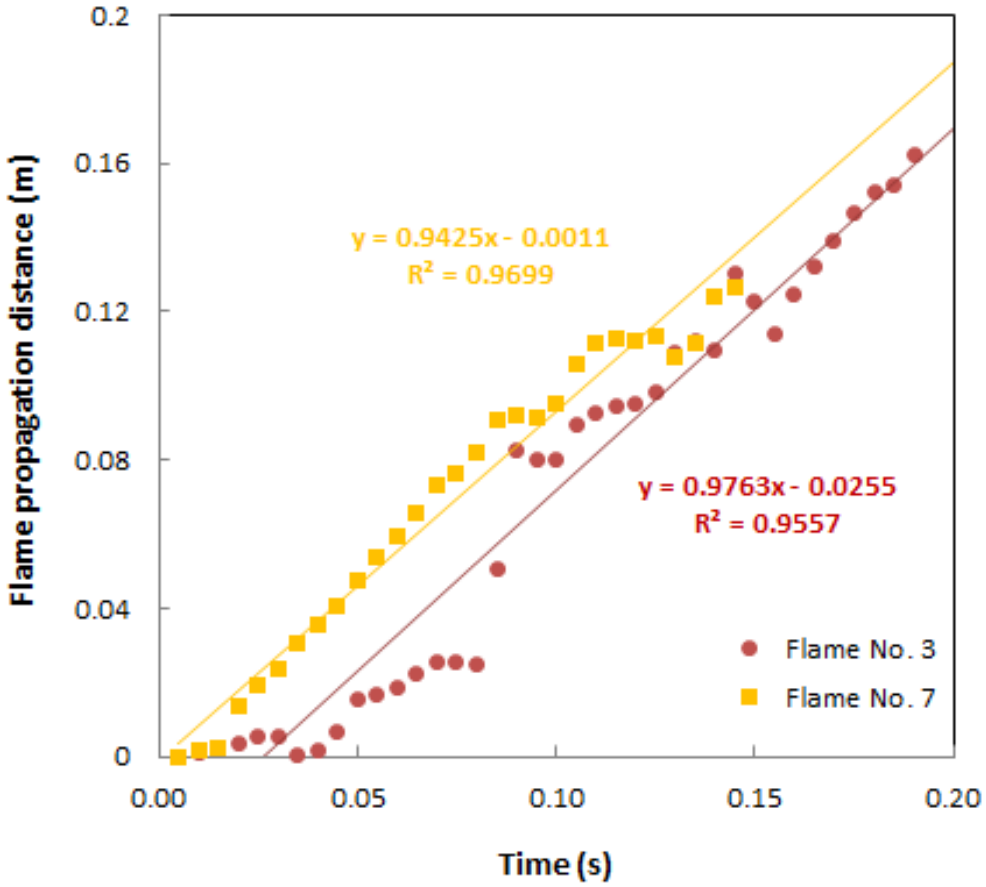

Figure 4-9 Propagation analysis of a flame in the aerosol system based on visual observation: the flame's position changes as a function of time (HT-D)

The alternative appearance of different burning modes in the flame propagation process is also shown by the flame size changing pattern in Figure 4-8. Instead of one peak pattern for the P-NF aerosol in Figure 4-4, there are two peaks for each flame in HT-D aerosols. The sizes of the HT-D aerosol flames pulsated during the flames' upward propagation. The appearances of the climax flame sizes are not limited to the middle section of the aerosol system in the Stage II propagation region of the P-NF

flame, illustrated in Figure 4-2. The HT-D aerosol flames have stable flame propagation speeds as indicated by the good linearity of the flame trajectories in Figure 4-9.

The possible explanation for the difference between the flames in the P-NF and HT-D aerosols are the combining effects from two factors, the aerosol droplet size and the droplet spacing. Chan (Chan & Jou, 1988; Chan & Wu, 1989) provided an explanation for similar phenomena observed in his experiments using monodisperse tetralin aerosols. Under the same equivalence ratio, there exists a transition range of droplet size. When droplet size is below the transition range, the smaller droplet size not only enhances the droplet evaporation rate, but also reduces the droplet spacing. The burning mode in aerosols becomes similar to the burning mode in homogeneous mixtures. The burning mode takes the form of large global flames. When the droplet size is above the transition range, the droplet spacing becomes significantly larger, and the fuel vapor mainly concentrates on the area around a single droplet. Although the fuel vapor concentration in the area around a single droplet can be even higher than the equivalence ratio, the fuel vapor concentration in the space between the droplets is very low. The burning modes tend to be individual burning droplets or burning droplet clusters. When the droplet size falls into the transitional range, the combined effects of both the droplet size and droplet spacing result in a variation of the burning modes between burning droplet clusters and a large global flame.

For P-NF aerosols, the droplet sizes range from 85 μm to 95 μm in the ignition test environment. For this size range, the middle section of the aerosol system is capable of supporting the global flames burning mode, or the second stage of the flame propagation

process, observed in Figure 4-3. For HT-D aerosols, the droplet sizes range from 110 μm to 130 μm. Under the same fuel-air equivalence ratio, the larger droplet sizes result in larger spacing between droplets. Therefore, the phenomenon of burning mode transition appears in the HT-D aerosol. As the flame propagated upward, the burning mode kept changing between burning droplet clusters and a global flame.

Accompanying the phenomenon of burning mode transitions for the flames in HT-D aerosols are the two phenomena, higher flame propagation speed and reduced flame size, which kept pulsating along the flame's propagation. The higher upward flame propagation speed in HT-D aerosols is due to the enhanced propagation speed of the flame's upward flame front. This is similar to the phenomenon of enhanced flame front speed which was observed by Chan and Jou (1988) and Atlzer (Atzler et al. 2007). Because of the alternating pattern of the burning modes, the flame front speed took a pulsating pattern, exhibiting another result similar to other experiments.

The phenomenon of enhanced burning speed is unique to aerosol burning and is not yet fully understood, although different researchers have studied the phenomenon theoretically (Polymeropoulos, 1984; Greenberg et al. 1999) and proposed different mechanisms. The burning speed enhancement may appear when the droplet size must be within a certain range, because droplets that are too small burn in the mode close to the flames in homogeneous mixtures. Droplets that are too large may not be able to support the continuous propagation of the flames due to the large spacing between droplets. When the droplet size is within the range, the higher fuel vapor concentration around droplets enhances the combustion reaction, and the fuel vapor concentration in the space

between droplets can still support the propagation of the flame through ignition of the neighboring droplets.

On the other hand, the sizes of the global flames in the HT-D aerosols are smaller compared to those in the P-NF aerosols. Although enhanced upward flame front propagation speed favors a faster expansion of the flame size, the phenomenon of the flame speed enhancement only happens for the upward flame front, because droplets are coming down from the top and running into the upward flame front directly. Expansion of the flame fronts in other directions, where droplets were not directly running, is limited by the larger spacing between droplets. The heat radiation and conduction from the flame fronts of droplets in these directions in the nearby space are not as significant as those of the flames in P-NF aerosols. This results in a smaller flame size with a higher flame propagation speed.

Flame detection by laser diffraction technique

As observed in the ignition tests above, the discrete flame front and the irregular flame shape make it hard to apply classical flame front theory, which assumes a plane shape flame front. Still, trials for a new method of detecting flames in aerosols using the laser diffraction technique are carried out and results are shown below.

Figure 4-10a is a typical pattern of the droplet size and transmission data from the laser diffraction analysis when a global flame appears in a P-NF aerosol and the flame front propagates into the laser beam detection area.

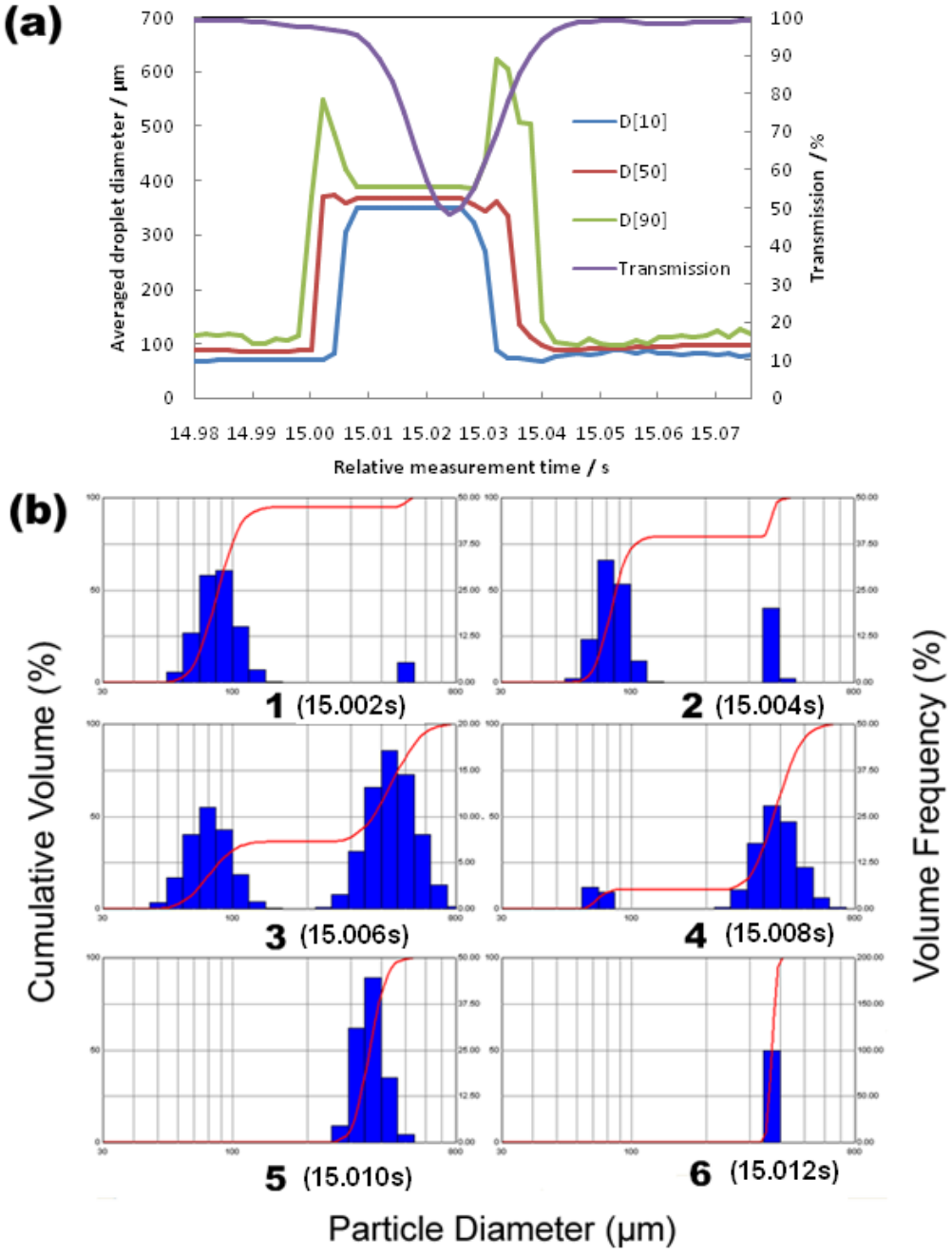

Figure 4-10 Typical aerosol combustion flame LDA measurement profile. (a) Transmission and droplet size data along time during aerosol ignition (3 ml/h flow rate, 8.5kV applied voltage); (b) particle size distribution during the aerosol ignition, number 1, 2, 3, 4, 5, and 6 corresponding to relative time at 15.002s, 15.004s, 15.006s, 15.008s, 15.010s, and 15.012s respectively in (a)

The time between each data point in Figure 4-10a is 0.002s. Before and after the pattern both the droplet size and transmission lines remain flat, indicating stability in the un-burnt droplet size. Upon the appearance of the aerosol combustion flame, the changing pattern appears with a rapid increase in droplet size data lines and significant decrease in the transmission line. One of the characteristic features in the pattern are the two $D_{[90]}$ peaks at the start and end of the pattern, and another feature is the flat-line region between the two $D_{[90]}$ peaks where the $D_{[10]}$, $D_{[50]}$ and $D_{[90]}$ values remain constant. The pattern is recognized as a combustion pattern to identify the occurrence of global flame propagation events in aerosol.

Detailed droplet size distributions for the process of flame appearance in Figure 4-10a are shown in Figure 4-10b. In Figure 4-10b, the numbers under every diagram indicate their relative positions in the pattern along time in Figure 4-10a. In the begining, the sizes of most of the droplets ranged from 50 to 110μm, as shown in Figure 4-10b[1]. The emergence of a size band around 500μm gradually led to the appearance and formation of a new droplet size distribution around the larger size area, accompanied by the disappearance of the initial droplet size distribution, as indicated by Figure 4-10b[1] to [4]. Then, from Figure 4-10b[5] to [6], the second distribution became significantly narrower until there was only one size band around 375μm. Then from time 15.012s to 15.030s, the droplet size distribution remained exactly the same as in Figure 4-10b[6] with constant $D_{[10]}$, $D_{[50]}$ and $D_{[90]}$ values. The flame pattern started disappearing at 15.032s as the droplet size distribution histogram changed in a way quite similar to Figure 4-10b, but in a reverse sequence from [6] to [1].

Although the electrospray technique used in the current work has a good control over the aerosol droplet size distribution, it is impossible to maintain an identical droplet size distribution for any two different measurements. However, similar flame patterns with flat regions of consistent droplet size and the same distribution histogram, as shown in Figure 4-10a from 15.012s to 15.030s, occurred in different ignition tests when flames propagate through the laser beam. The aerosol combustion propagation can bring about steep refractive index gradients for the materials within the laser beam detection area. The refractive index gradients can be due to phenomena generated by aerosol combustion, such as shock waves, changing heat and mass transfer, and changing pressure. All of these factors can result in unreliable droplet size data by laser diffraction analysis using Mie theory. So long as changes in the LDA measurement data during the flame front propagation is distinguishable as compared to data for un-burnt aerosol droplets, laser diffraction using Mie theory can be applied in the aerosol combustion flame detection, as in the current work. The flat region in Figure 4-10a corresponds to the situation when the laser beam penetrates the global flame. The unchanging pattern may be explained by the fact that laser beams probe the plasma phase of the flame. The pattern recognized in Figure 4-10a corresponds to the flame running into and leaving the laser measurement zone. The high peaks in the $D_{[90]}$ line may be related to the light scattering pattern by the individually burning droplets on the boundary of the flame.

The appearance of an aerosol combustion flame was captured by a high speed digital camera and is shown in Figure 4-11. The Red arrow in Figure 4-11a represents the position of the laser beam, its width corresponding to the diameter of the intersection

of the laser beam. The time interval between every two pictures is 0.019s. Before the appearance of the flame, the average $D_{[3][2]}$ and droplet volume concentration are 79.20μm and 2.77×10^{-5}%, respectively. It can be observed from Figure 4-11a to Figure 4-11h, that small flames first appeared 20-30mm above the ignition flame tip, then they coalesced into a larger flame (Figure 4-11i). The flames ran into the laser beam at Figure 4-11g. At the moment of Figure 4-11j was taken, the flame should have covered the whole intersection area of the laser beam. Flame length is visually observed as the distance between the highest point on the upper flame boundary and the lowest point on the lower flame boundary. The flame front propagation speed is measured as the distance the flame front propagated upward per unit time. The flame front propagation speed and flame length based on these pictures are shown in Figure 4-12a. During the 0.057s time period from Figure 4-11g to Figure 4-11j, the flame propagation speed ranges from 0 to 0.5m/s. The flame propagation speeds measured in the current work are also close to the speed values measured by Ballal and Lefebvre (1981) using iso-octane aerosols.

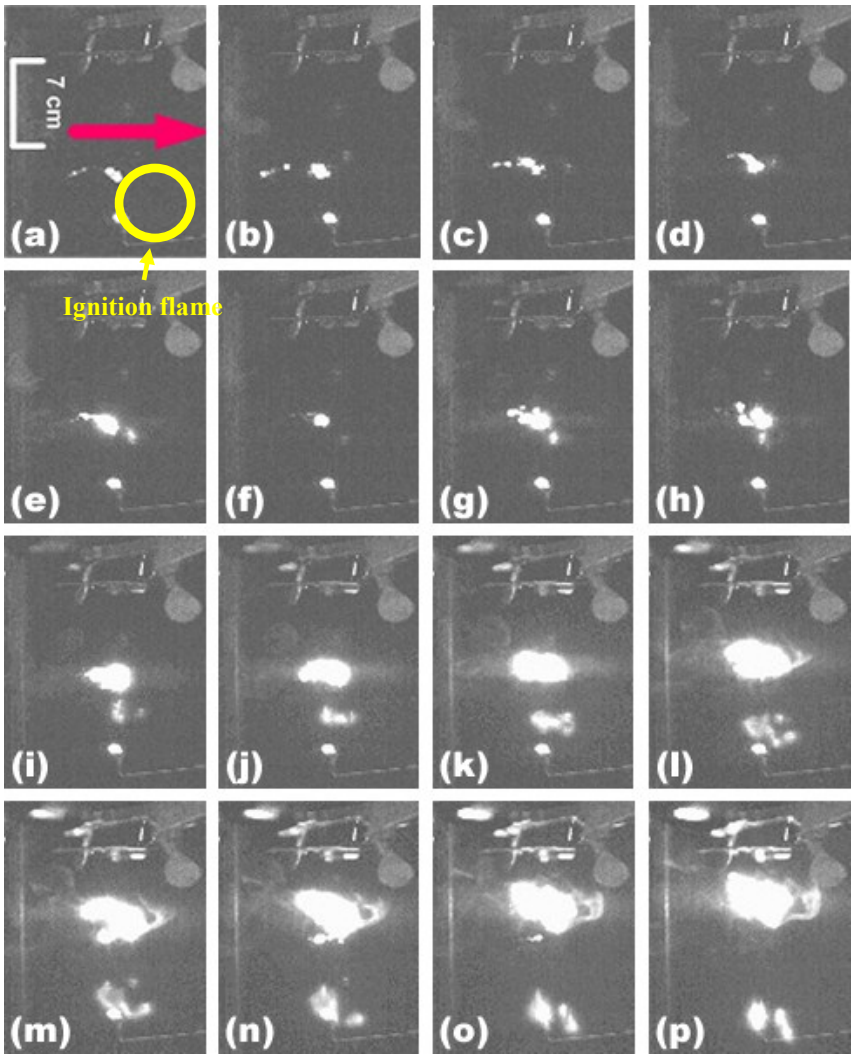

Figure 4-11 Aerosol combustion and propagation as recorded by fast camera

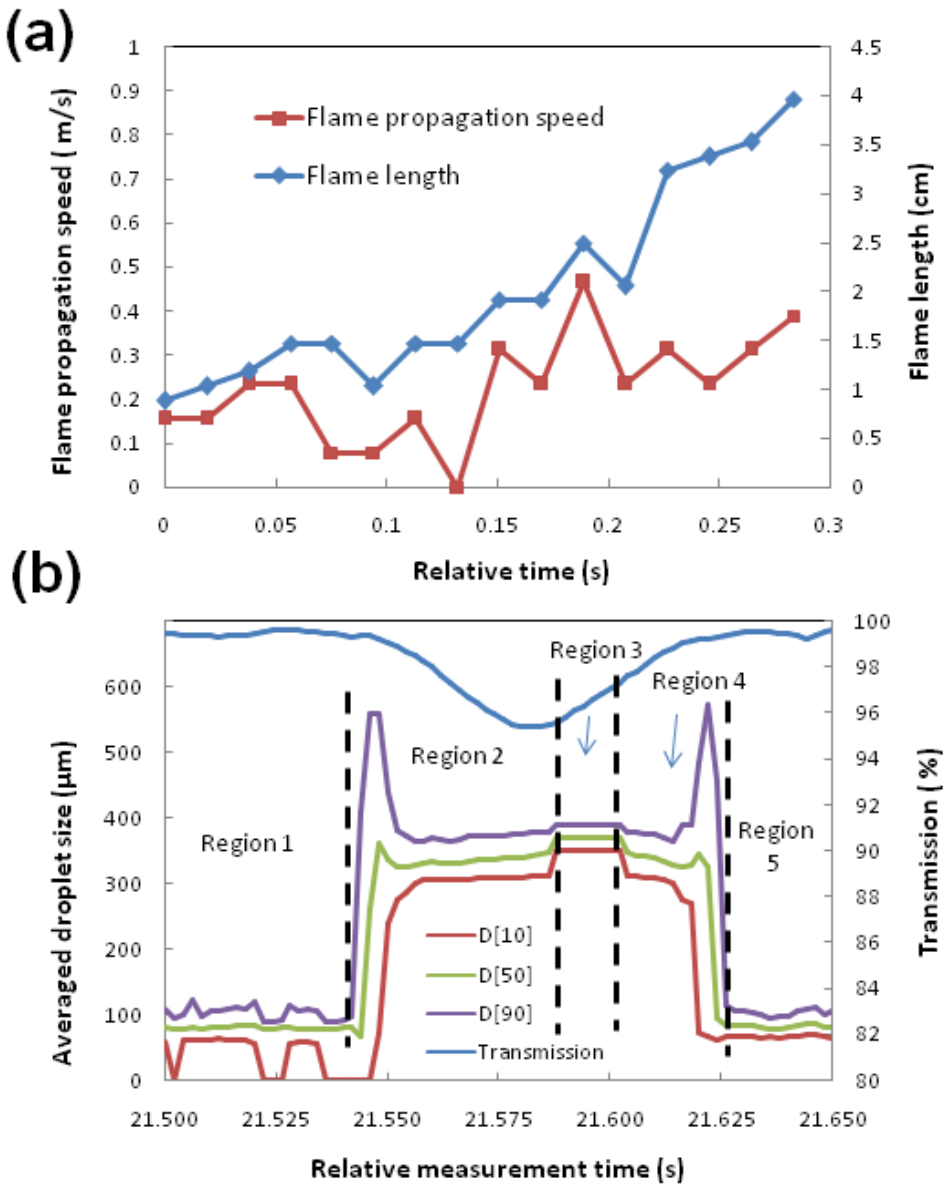

Figure 4-12 Aerosol flame propagation velocity and LDPA droplet size measurement pattern. (a) Aerosol combustion flame length and propagation speed measured by a high speed camera; (b) aerosol combustion flame detected by LDPA

The flame pattern detected by LDPA for the flame propagation process in Figure 4-11 is shown in Figure 4-12b and is divided into five regions. Region 1 corresponds to the period before the flame front reaches the laser beam detection region. Region 2 represents the "cutting-through" period, when the flame front reaches the laser beam region until the intersectional area of the laser beam is completely covered by the flame. Region 3 represents the whole coverage period when the flame moves upwardly. Region 4 represents the period when lower boundary of the flame leaves the laser beam region, and Region 5 represents the period after the flame leaves the laser beam region. As calculated from Region 2, the "cutting-through" period lasted from 21.548s to 21.588s, or 0.050s, which is close to the observed 0.057s period based on the pictures Figure 4-11g to Figure 4-11j. The reason for the difference between the values from the two methods may lie in the errors in the visual observation of the flame front propagation due to the observation angle and the calculation of the flame speed based on the visual observation.

It should be pointed out that the droplet size information in the flame propagation patterns are no longer reliable, because of the various types of particles formed in aerosol combustion, and the large variations in the refractive indices of the materials along the laser beam pathway.

FURTHER DISCUSSION

The motivation for exploring a different flame characterization method, rather than measurement of the traditional flame front speed, lies in the difficulty in applying

the classical concept of flame front velocity to the flame propagation in aerosols. According to the classical combustion theory, the flame front velocity is defined as the velocity at which unburned gases move through the combustion wave in a direction normal to the wave front (Aggarwal, 1997). In addition, the values of flame front speed were found to vary considerably with different test methods in the previous studies. For instance, the velocity of the flame front was found to reduce with the existence of fuel droplets as compared to other experiments performed using a fuel vapor system with the same fuel concentration (Ballal & Lefebvre, 1981; Myers & Lefebvre, 1986; Hayashi & Kumagai, 1974; Hayashi et al. 1981). In other studies, the flame front velocity in the aerosol system was found to be higher than that in the gaseous mixtures, and the phenomenon of flame speed oscillation was also reported (Suard et al. 2001; Suard et al. 2004; Lawes et al. 2002; Atzler et al. 2007; Greenberg et al. 1999). The seemingly contradictory results actually arose due to the complexity of flame characteristics in the aerosol system. For the case of flames in the current aerosol system, there was little uniformity or even discreteness in the flame shapes, followed by the observation of different stages of flame propagation. This observation is similar to Hayashi's finding that the seemingly continuous flame actually consists of smaller flames supported by evaporating droplets. Based on the current findings, it appears that the fuel-air reaction zone as defined in classical combustion theory can be found inside the flame, as opposed to existing only in the outer area of the flame. Fuel vapor is continuously evaporating from the aerosol droplets inside the flame to support the reaction zones inside the flame.

Considering the potentially higher fuel burning rate and the relatively slow propagation speed of flames in aerosols (< 0.6 m/s), it is reasonable to assume, based on the current results, that there can be more severe consequences due to the heat release of aerosol flames caused by the accidental release of industrial fluids, as compared to the consequences of flash fires of vapor mixtures. Therefore, there is a need to investigate the actual heat release rate from the aerosol flames, taking into account the scaling effects, before any further conclusions can be made.

Based on the current findings, it appears that the fuel-air reaction zone as defined in classical combustion theory can be found inside the flame in the second stage of propagation, as opposed to existing only in the outer area of the flame. Fuel vapor is continuously evaporating from aerosol droplets inside the flame to support the reaction zones inside the flame, which may contribute to a higher energy release rate from the flame. Considering the relatively slow propagation speed of flames in aerosols (< 0.6 m/s), it is reasonable to assume that there can be more severe consequences due to the heat release of aerosol flames caused by the accidental release of industrial fluids, as compared to the consequences of flash fires of vapor mixtures. Therefore, there is a need to investigate the actual heat release rate from the second stage aerosol flames, taking into account the scaling effects, before any further conclusions can be made.

SUMMARY

The work in this chapter focuses on characteristics of flame propagation in aerosols and how they are influenced by the presence of fuel droplets in the systems. Major findings in the chapter are listed below:

1. Flames in aerosols are characterized by non-uniform shapes and discrete flame fronts, making it difficult to apply the classical flame front theory to characterize the flame propagation process.
2. For the aerosols produced by P-NF heat transfer fluids, three stages of flame propagation with different burning modes have been observed. The second stage, the burning mode of a global flame with rapid size expansion, is considered the most hazardous scenario caused by aerosol combustion.
3. For aerosols created by the HT-D heat transfer fluid, the modes of burning droplet clusters and the global flames appeared alternatively as the flames propagated upwardly.
4. The appearance of different burning modes are related to aerosol droplet size and droplet spacing. Droplet size in the P-NF aerosols ranges from 80 μm to 90 μm. The middle section of the aerosol droplet system is capable of supporting the burning mode of larger global flames. Droplet size in the HT-D aerosols ranges from 110 μm to 130 μm. Larger spacing between the droplets results in the alteration in the flame burning modes.
5. The flame size in P-NF aerosols decreased as droplet size became larger. Flames in the HT-D aerosols tend to have smaller size than the flames in the

P-NF aerosols. The larger droplet size and the larger droplet spacing in the HT-D aerosols limited the expansion rate of flame fronts except in the upward front.

6. The flame propagation speeds in the HT-D aerosols are higher than those of the flames in the P-NF aerosols. The enhanced propagation speed of the overall flame is mainly due to the enhanced propagation speed of the upward flame front. Larger droplet size and spacing have profound influences on the appearance of the phenomenon, which is not yet fully understood.
7. The laser diffraction technique was used to detect the flame propagation process. The measured flame front speed agrees well with the upward flame front speed based on visual observations. The flame front speed by laser diffraction analysis may only represent the local changes in the position of the upward-propagating flame front. Further tests and validations are needed before future application of the new method.

CHAPTER V

THEORETICAL STUDY ON FACTORS INFLUENCING FLAME CHARACTERISTICS IN AEROSOLS *

INTRODUCTION

In Chapter IV, different combustion behaviors were observed for aerosols from heat transfer fluids. Flames in the P-NF aerosols went through three propagation stages. The second stage of the large global flames happened in the middle section of the aerosol system. Flames in the HT-D aerosols exhibit the phenomenon of alternative transitions between different burning modes. Although the experimental observations have been related to aerosol droplet size, it is necessary to gain more insight into the mechanisms inside the phenomena. In this chapter, numerical methods are used to find potential explanations on the mechanisms. The aerodynamic droplet evaporation modeling for the P-NF aerosols studies droplet movement and evaporation behaviors in aerosol system. Modeling can provide information on the distribution of vapor fuel concentration in the aerosol system. The non-dimensional controlling parameter analysis tries to find the parameters which result in the difference in burning modes between the aerosols by two types of heat transfer fluids.

---

* Part of this chapter is reprinted from "Study on flame characteristics in aerosols by industrial heat transfer fluids" by Lian, P., Ng, D., Mejia, A. F., Cheng, Z., and Mannan, M. S. (2011). *Industrial & Engineering Chemistry Research*, *50*, 7644-7652, Copyright 2011, with permission from American Chemical Society.

DYNAMIC DROPLET EVAPORATION MODELING

Model description

Previous studies have shown that the flame characteristics of aerosol combustion are determined by the droplet evaporation (Maragkos & Bowen, 2002; Hayashi et al. 1981). The evaporation of droplets give rise to the fuel vapor concentration in the aerosol system, which may influence the flame front propagation speed. Subsequently, evaporation of droplets moving inside the flame determines the amount of fuel that is supplied by the droplets to support the combustion reactions, which may increase the fuel burning rate and influence propagation process of the flames. Furthermore, droplet evaporation is related to droplet size and movement speed. To study this relationship, a simplified one-dimensional model is used to simulate a droplet's evaporation behavior during its downward travel in the space below the grounded mesh with a height of 100 mm (Figure 5-1), where the aerosol flames moved upward. And the fuel vapors evaporated in two different conditions are studied. The fuel vapor in gaseous phase of the aerosol system before flames appear is based on the movement and evaporation of the simulated droplets in the space without flames, while the evaporated fuel vapor inside the flame is based on the movement and evaporation of the simulated droplets inside the flame. The main differences between the movement of the droplets inside and outside the flames lie in the different gaseous phase temperatures surrounding the droplet and its liquid phase temperature in the models. The model details and the values of the physical properties are listed below.

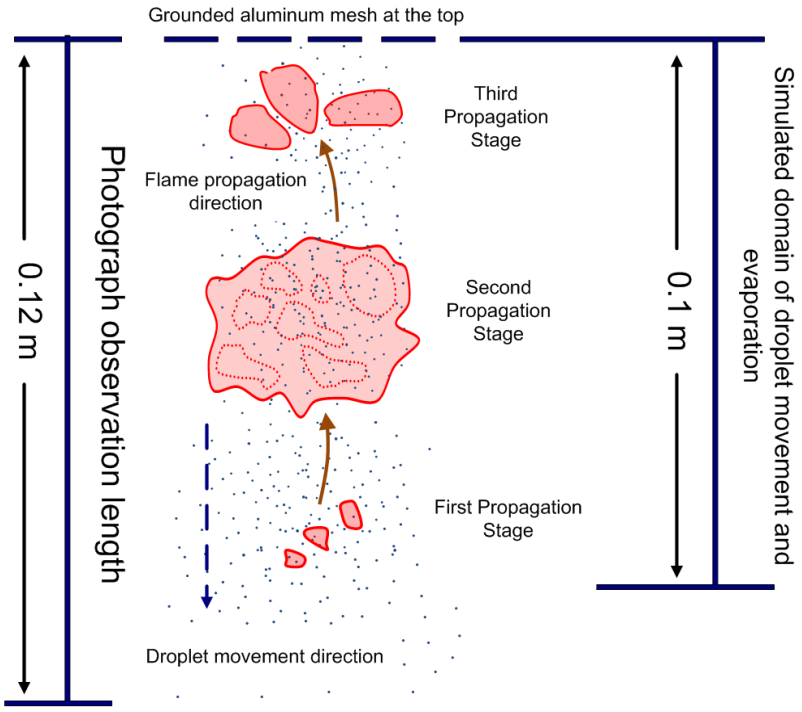

Figure 5-1 Schematic illustration on the simulated domain of droplet movement and evaporation in the P-NF aerosols

The movement of the droplets and the change in their diameter due to evaporation, both inside and outside the flame, are governed by the following equations (Abramzon & Sirignano, 1989):

$$\frac{dY_S}{dt} = v_S \tag{5-1}$$

$$\frac{dv_S}{dt} = -\frac{3C_D}{2R}\left(\frac{\rho_\infty}{\rho_l}\right){v_S}^2 + g \tag{5-2}$$

$$\frac{dR}{dt} = -\frac{\dot{m}}{4\pi\rho_l R^2} \tag{5-3}$$

where Y_s is the vertical position of the droplet's center, v_s is the velocity, C_D is the drag coefficient, R is the radius, ρ_l is the density of the liquid fuel (881 kg/m^3 at 298 K; 670 kg/m^3 at 623 K), ρ_∞ is the density of air (1.2 kg/m^3), g is the gravitational constant (9.8 m/s^2), and $\dot{m}$ is the evaporation rate (kg/s). Using the velocity measurement of droplets created by electrospray from a previous study (Deng et al. 2006), and considering the differences in droplet size, the initial droplet velocity was assumed to be 3 m/s at the top mesh position.

To calculate the droplet evaporation rate $\dot{m}$, the convective droplet vaporization model by Sirignano (2010) is used:

$$\dot{m} = 4\pi \frac{\lambda R}{C_{Pl}} \ln(1+B_H)\left[1+\frac{k}{2}\frac{\mathrm{Pr}^{1/3}\,\mathrm{Re}^{1/2}}{F(B_H)}\right] \tag{5-4}$$

where λ is the thermal conductivity of liquid (0.1056 W/Km at 298 K; 1.7307 W/Km at 623 K), C_{pl} is the specific heat of liquid fuel (1439 J/kgK at 298 K; 3511 J/kgK at 623 K), B_H is the non-dimensional energy transfer number, k is the non-dimensional positive coefficient (k=0.848), P_r is the Prandtl number, R_e is the Reynolds number, and $F(B_H)$ is the universal function following the form of the correlation (Abramzon & Sirignano, 1989):

$$F(B_H) = (1+B_H)^{0.7}\,\frac{\ln(1+B_H)}{B_H} \quad \text{for } 0 \le B_H \le 20,\ 1 \le \mathrm{Pr} \le 3 \tag{5-5}$$

The non-dimensional energy transfer number B_H follows the form (Williams, 1990):

$$B_H = \frac{1}{H_{evp}}\left[C_{pl}\left(T_\infty - T_L\right)\right] \text{ (For cases without flame)} \tag{5-6}$$

$$B_H = \frac{1}{H_{evp}}\left[C_{pl}\left(T_\infty - T_L\right) + \frac{Qy_{O,\infty}}{\delta}\right] \text{ (For cases in the flame)} \tag{5-7}$$

where H_{evp} is the heat of evaporation (210 kJ/kg), T_∞ is the gaseous phase temperature (2473 K in flame, 298.15 K without flame), T_L is the droplet liquid temperature (623 K in flame, 298 K without flame), Q is the heat of combustion (46,300 kJ/kg), $y_{O,\infty}$ is the oxygen concentration in air ($y_{O,\infty}$ = 0.21), and δ is the stoichiometric coefficient (δ = 37.5). The Prandtl number P_r follows the form (Abramzon & Sirignano, 1989):

$$P_r = \frac{C_{pl}\mu}{\lambda} \tag{5-8}$$

The Reynolds number R_e follows the form(Abramzon & Sirignano, 1989):

$$R_e = \frac{2\rho_\infty \left|v_\infty - v_s\right| R_S}{\mu_g} \tag{5-9}$$

The droplet drag coefficient C_D follows the form (Williams, 1990):

$$C_D = 27R_e^{-0.84} \tag{5-10}$$

The behavior of evaporating droplets was further studied using numerical modeling. The study focused on two different aspects of fuel vapor concentration due to the droplet evaporation, i.e., the fuel vapor concentration in the aerosol system before

flames appear and the concentration of fuel droplets evaporating inside the flame, and how they are affected by the droplet size and movement velocity.

Evaporated fuel vapor in aerosols before flames appear

As the aerosol droplets traveled down from the nozzle tip in the aerosol system, they continued to evaporate and produce a certain fuel vapor concentration prior to encountering the flame. To understand the formation of the fuel vapor concentration in the aerosol system, the movement and evaporation behaviors of a single droplet were studied using numerical modeling, and results are shown in Figure 5-2. As the droplet travelled down from the nozzle tip, its diameter, velocity, and evaporation rate all kept decreasing with time and travel distance. Initially the droplet velocity decreased at a high rate during the first 0.05 s period, corresponding to the first 0.35 m distance traveled. Then the droplet velocity stabilized, indicating that the forces exerted on the droplet reached a state of balance between the gravitational force and the drag force with the air. The droplet evaporation rate followed a decreasing trend similar to that of the velocity, suggesting a strong dependency of the droplet evaporation rate on its movement velocity. The droplet evaporation rate can be enhanced by higher droplet velocity due to effects of the convective mass and heat transfer, or convective droplet vaporization (Sirignano, 2010).

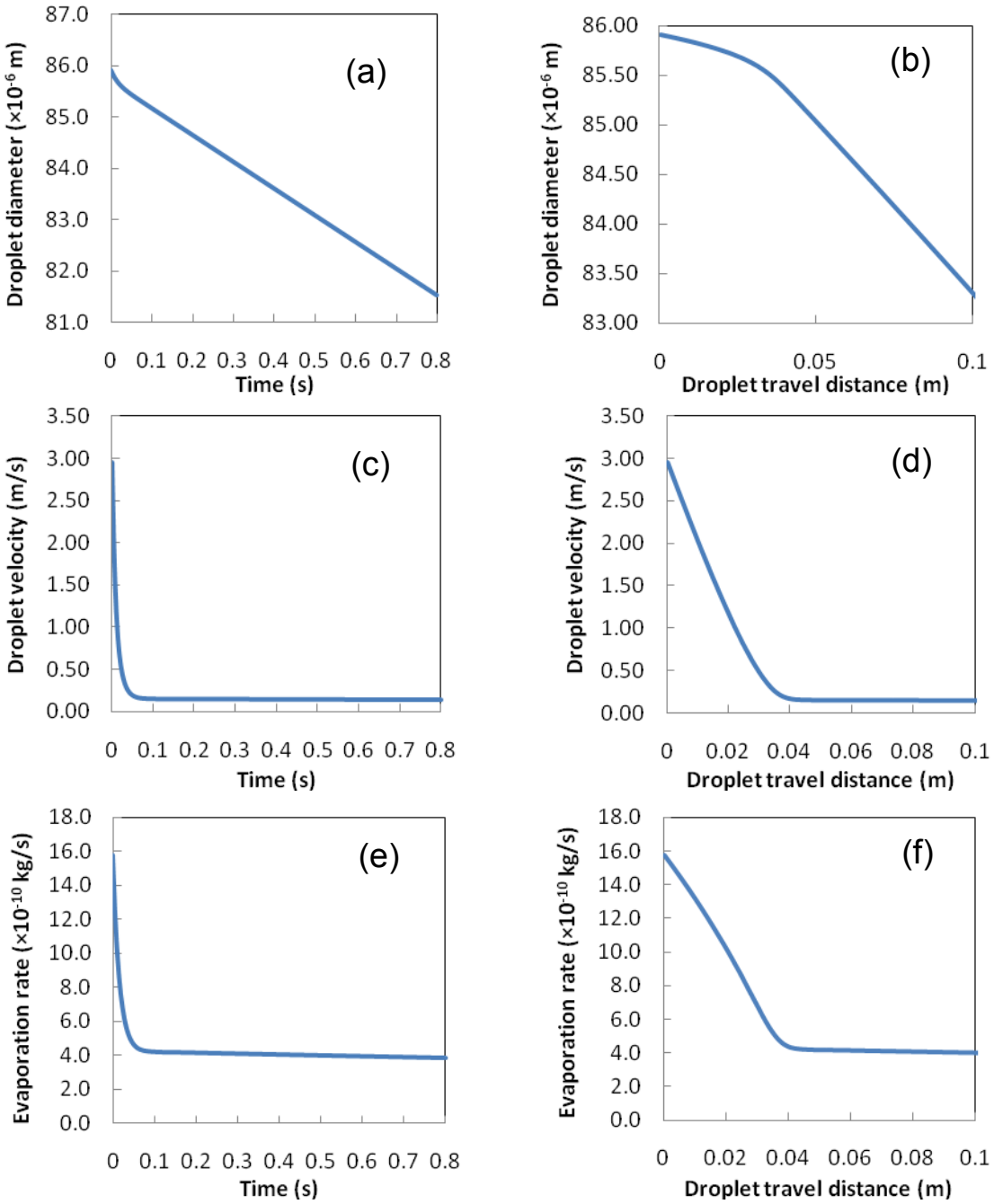

Figure 5-2 Movement and evaporation behavior of a single droplet in the aerosol system before encountering the flames. (a) Droplet diameter as a function of time; (b) droplet diameter as a function of travel distance; (c) droplet velocity as a function of time; (d) droplet velocity as a function of travel distance; (e) droplet evaporation rate as a function of time; (f) droplet evaporation rate as a function of travel distance

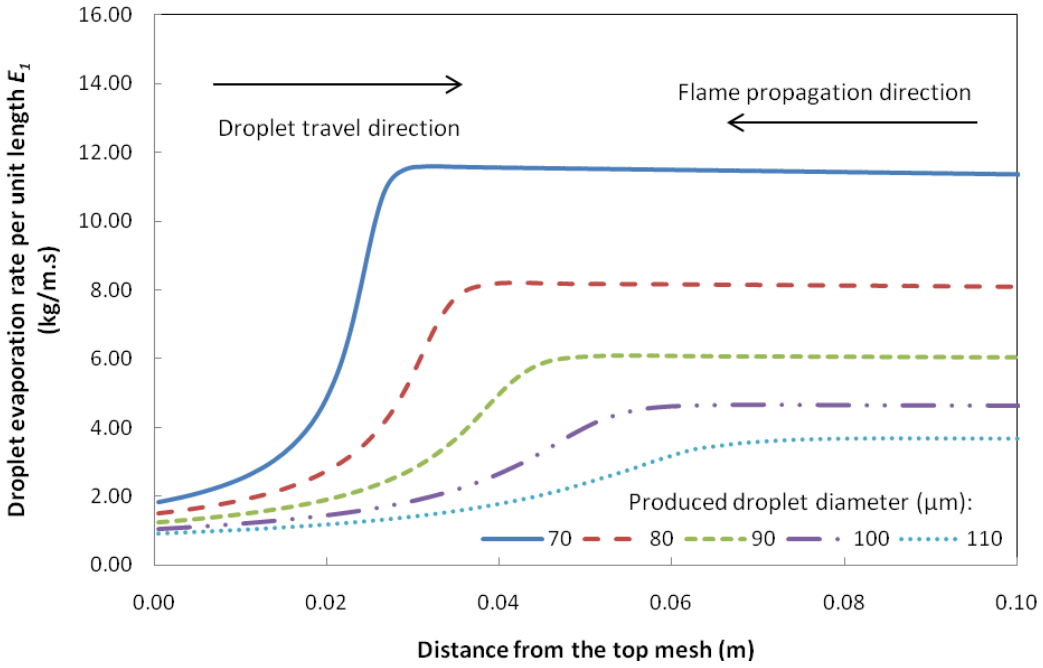

Figure 5-3 Droplet evaporation rate per unit length, E_1, against the distance from top of the aerosol system

The amounts of fuel vapor generated at different heights were then calculated. Since the droplet moves in a downward vertical direction, the fuel vapor concentration in the aerosol system is assumed to be one-dimensionally distributed along the vertical axis of the system. The amount of fuel vapor at a specific height in the aerosol system is proportional to the fuel evaporation rate per unit length $E_1 = \frac{\dot{m} P_S}{U_S}$ from the droplets passing through a certain height. $\dot{m}$, U_S, and P_S are the single droplet evaporation rate, the droplet velocity, and the number of droplets which passed through the height each second. Figure 5-3 shows that the fuel evaporation rate per unit length E_1 increased as

the travel distance from the top became larger, implying that the fuel vapor concentration at the lower positions of the aerosol system (from 40 mm below the top mesh to 100 mm below) have a much higher fuel evaporation rare. The higher amount of fuel vapor in this lower section of the aerosol system may bring about the second stage of flame propagation in the P-NF aerosol as observed in the aerosol ignition tests in Chapter IV.

Fuel vapor evaporation from droplets in the flame

When droplets traveled into the flame, fuel vapor continuously evaporated from the droplets to support the combustion inside the flame. To study the fuel vapors that evaporated from a droplet inside the flame, the numerical model also simulated the droplet's movement and evaporation behaviors inside the flame, as depicted in Figure 5-4. The droplet evaporation rates were much higher (Figures 5-4e and 5-4f) compared to those in Figures 5-2e and 5-2f due to the high temperature of the gaseous phase surrounding the droplet. Moreover, the droplet's diameter and velocity all decreased at much higher rates with time and travel distance as compared to Figure 5-2.

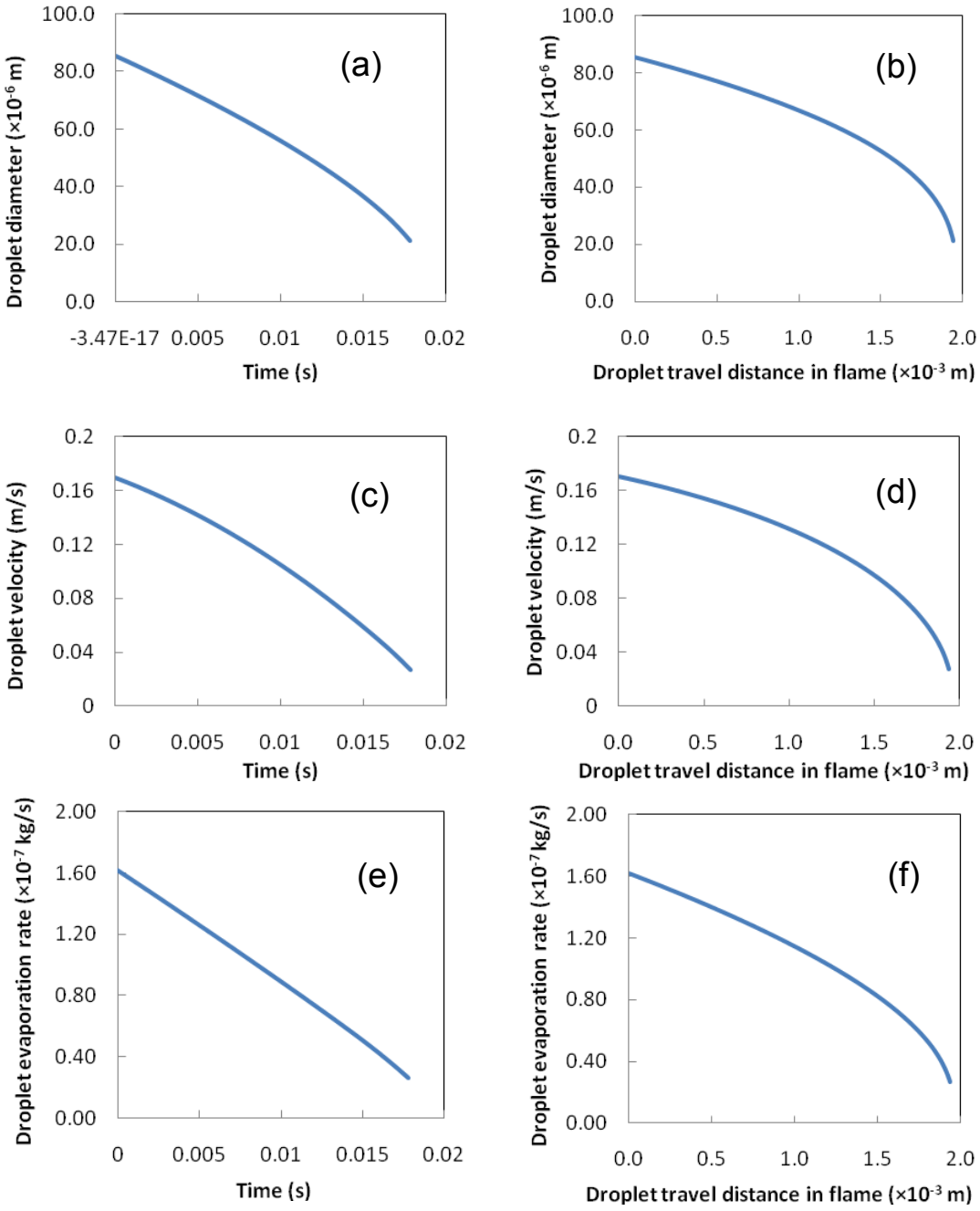

Figure 5-4 Movement and evaporation behavior of aerosol droplets inside flame. (a) Droplet diameter as a function of time; (b) droplet diameter as a function of travel distance in flame; (c) droplet velocity as a function of time; (d) droplet velocity as a function of travel distance in flame; (e) droplet evaporation rate as a function of time; (f) droplet evaporation rate as a function of travel distance in flame

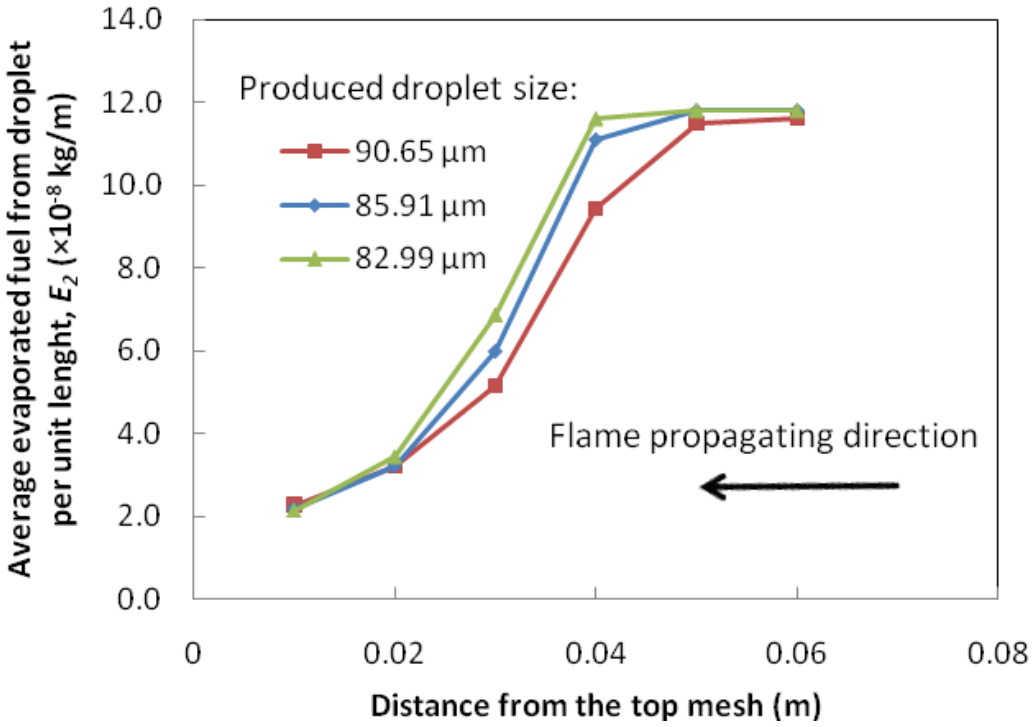

Figure 5-5 Average amount of evaporated fuel from droplet per unit travel distance inside the flame (E_2) against distance the droplet traveled from top of the aerosol system before entering the flame (Y_f)

The amount of evaporated fuel vapor inside the flame is indicated by the amount of the evaporated fuel vapor from the droplet averaged by its travel distance in the flame $E_2 = \frac{M}{L_S}$. M and L_S are the total amount of evaporated fuel from the droplet and the maximum distance traveled by the droplet in the flame. A higher E_2 means larger amount of fuel vapor supplied from the droplet to support the combustion per unit droplet travel distance. E_2 further depends on the travel distance of the droplet before entering the flame Y_f because Y_f influences the size and velocity of the droplet upon

entering the flame (Figure 5-4), as well as its M and L_S values inside the flame. Figure 5-5 shows the trend of average evaporated fuel from droplet per unit travel distance in the flame E_2 for different Y_f. E_2 increased as the travel distance Y_f became longer, or when the droplet entered the flame at a lower position in the aerosol system. For the flames propagating in the lower space of the aerosol system, a larger amount of fuel vapor was supplied by droplets inside the flame for each unit length the droplet traveled in the flame to support the combustion, which might be another reason for the formation of the second stage of observed flame propagation in the aerosol systems.

Based on the aerodynamic droplet evaporation modeling, the three sections in the P-NF aerosols, the upper, middle, and lower section, have different conditions, which can be the reason for the appearances of the global flames in the middle section of the aerosol system.

1) In the upper section, aerosol droplets have a higher velocity, which enhances the liquid fuel evaporation rate. But the shorter residence time of the droplet in this section reduces the amount of evaporated fuel vapor, as compared to the other two sections. Moreover, higher turbulence may arise from the droplet's velocity. These factors result in the global flame's quenching in the upper section.
2) In the middle section of the P-NF aerosol, droplet movement is significantly slowed down. The droplet's residence time becomes longer, which increases the amount of fuel that evaporates from the droplets. The middle section has a higher fuel vapor concentration before the upwardly propagating flames enter

the section. When flames from the lower section rise into the section, the higher fuel vapor concentration enhanced the flames' size expansion. The droplets, which run into the flames, provide a larger amount of fuel vapor to support the reaction zones inside the flame. The global flames appear in the middle section.

3) In the lower section, the amount of evaporated fuel from the droplets in the section are similar to that in the middle section, but the turbulence due to the heat from the pilot ignition flame below the section may dilute the fuel vapor concentration. This means that the rate of the flame size expansion of the burning droplet clusters, which originated from the pilot flame, are relatively slow compared to flames in the middle section.

NON-DIMENSIONAL CONTROLLING PARAMETER ANALYSIS

Through analysis of the droplet evaporation behaviors in the P-NF aerosols, appearance of the global flame burning mode in the middle section of the aerosol system can be due to the favorable conditions in the section, as discussed in the previous section. However, the phenomenon of the burning mode alternating, which happened in the HT-D aerosols with larger droplet sizes, cannot simply be explained by the droplet evaporation model. The phenomenon reflects the profound influences of various parameters, including droplet size, droplet spacing, and liquid fuel volatility. In order to further understand the aerosol combustion phenomena as depicted in the current experimental system, involvement of other undetermined parameters should be studied,

leading the equation to become quite complicated. However, if the variables related to the aerosol combustion process can be assigned into a few non-dimensional functional groups, then the complex mechanisms of the aerosol combustion process can be understood through the relationship between different non-dimensional groups. In order to understand the mechanisms behind the flame propagation process, non-dimensional parameter analysis is used here. The flames in both P-NF and HT-D aerosols are included in the analysis. The purpose is to identify the possible explanations of the difference in burning modes of aerosols created by different fluids.

Selection of the dimensionless variables may be arbitrary, but particular variables that can depict the role of different phenomena involved in the aerosol combustion process are preferred. The following variables have been selected to influence certain factors in the analysis: the flame propagation speed u, the average flame area A, the original aerosol droplet size in the non-ignition environment d_1, droplet size in the ignition environment d_2, droplet volume concentration n, kinematic viscosity of the heat transfer fluids μ, density of the fluid ρ, average molecular weight M, and the fluid vapor pressure P. All of these parameters can be described by a maximum of three units: mass, length, and time. From the π theorem, three dimensionless variables will be sufficient to describe the observed phenomenon.

In this research, three parameters are designated as the basic parameters: ΔV (m3), ρ (kg/m3), μ (m2/s), where ΔV reflects the volume of evaporated liquid fuel, and $\Delta V = (d_1^3 - d_2^3)n$. The remaining three parameters are grouped within the three basic parameters.

The flame propagation speed can be nondimensionalized as:

$$U^* = \frac{u\sqrt{\Delta V}}{\mu} \tag{5-11}$$

The flame area can be nondimensionalized as:

$$A^* = A(\Delta V)^{-2/3} \tag{5-12}$$

A third dimensionless variable containing the molecular weight is shown below:

$$M^* = \frac{M}{\Delta V \rho} \tag{5-13}$$

Variable M* represents the contribution of evaporated fuel vapor to the flame propagation process, by considering the average molecular weight of an oil divided by mass of the evaporated liquid fuel from the droplet.

Similarly, a fourth dimensionless variable containing the liquid fuel vapor pressure can be constructed as:

$$P^* = \frac{P\Delta V^{2/3}}{\mu^2 \rho} \tag{5-14}$$

Variable P* represents the volatility of the aerosol droplet, determined by vapor pressure of the liquid fuel and droplet surface area.

An empirical model for the relationship between U*, M* and P* can be obtained by performing a multiple linear regression analysis as shown below:

$$U^* = 2875.5(M^*)^{-0.46}(P^*)^{0.068} \tag{5-15}$$

Similarly, an empirical model for the relationship between A*, M* and P* is given as follow:

$$A^* = 369.4(M^*)^{0.39}(P^*)^{-0.33} \tag{5-16}$$

Based on relationships **[5]** and **[6]**, it can be inferred that higher liquid volatility in the aerosol droplets and smaller amounts of evaporated fuel tend to increase the flame propagation speed. The flame propagation speed is inversely proportional to the flame area, where larger amounts of evaporated fuel and lower liquid volatility resulted in a greater combustion flame area. The results are in agreement with findings in the aerosol ignition tests in Chapter IV. The HT-D aerosols have higher flame propagation speeds. The liquid HT-D fluid has a larger volatility, which is shown by comparing the aerosol droplet size in the ignition tests and in the non-ignition environment (Figure 5-6). There are larger decreases in the droplet size for the HT-D aerosols than for the P-NF aerosols. Considering the droplet size range, larger volumes of liquid fuels evaporated from the HT-D droplets because of the heat from the approaching flame front propagating in the aerosol system.

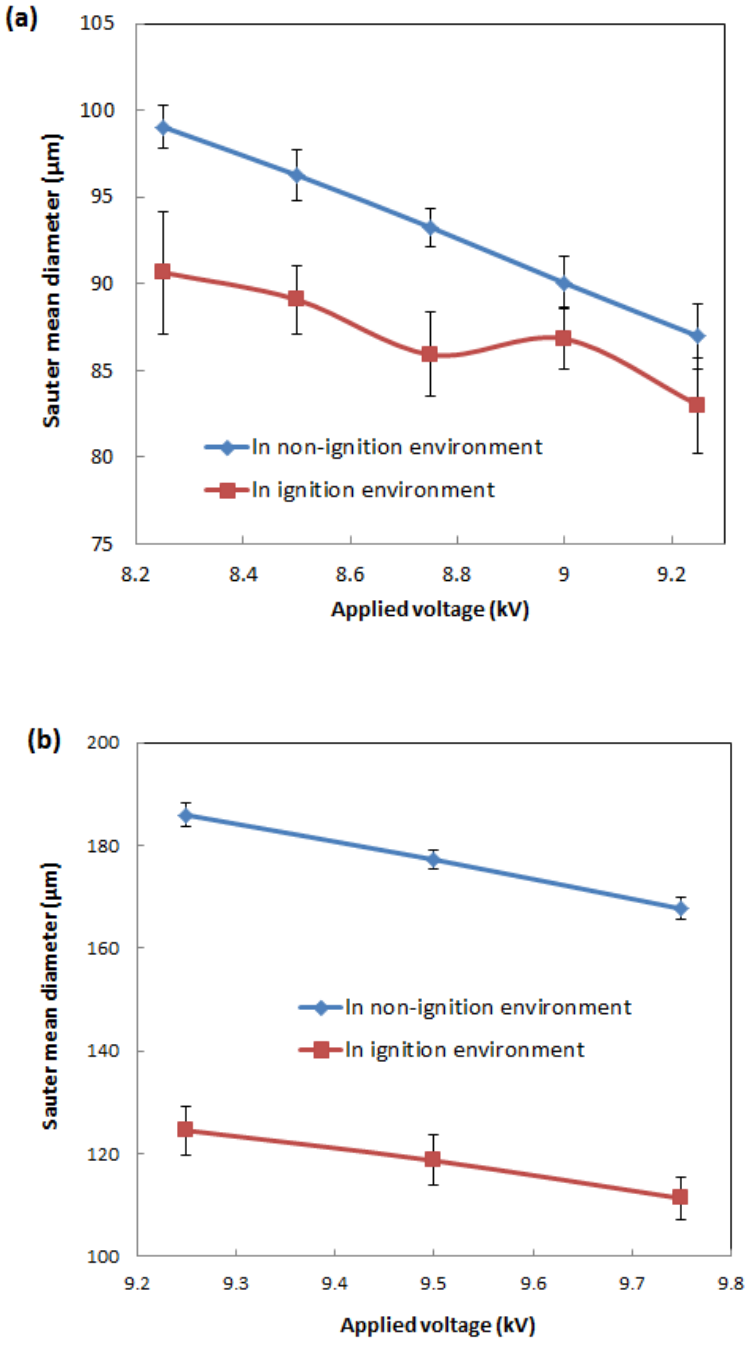

Figure 5-6 Comparison of unburned droplet size in the ignition and non-ignition environments. (a) P-NF aerosols; (b) HT-D aerosols

It can also be seen from Figure 5-6 that the amounts of evaporated fuel vapor in the HT-D aerosol systems should be higher than those in the P-NF aerosol system, which seems to be contradictory to the findings from relationships **[5]** and **[6]**. The seeming contradiction actually reveals the importance of the distribution of the fuel vapor concentration in the aerosol system, and its contribution to the appearance of the unique phenomena of burning mode alternations and flame speed enhancement in the HT-D aerosols.

The overall fuel vapor concentrations in the HT-D aerosols are higher than in the P-NF aerosols because of the higher liquid volatility. But the fuel vapors are not evenly distributed in the HT-D aerosols. They tend to stay in the areas surrounding the droplets, and the fuel vapor concentration around the droplets may be even higher than that in the P-NF aerosols. But the fuel vapor concentration in the space between droplets is lower than that in the P-NF aerosols because of the larger droplet size and spacing between the droplets in the HT-D aerosols. This uneven distribution of the fuel vapor concentration may result in a situation where the areas with conditions favorable to the burning mode of global flames exist intermittently in the aerosol system depending on positions of the droplets. Flames which are propagating in the aerosol system change burning modes upon encountering different conditions, exhibiting the pulsating pattern of the flame size change along the propagation routes. The variation in the burning modes also brings about the enhanced flame front propagation speed, which may get accelerated by the locally higher fuel vapor concentration around droplets.

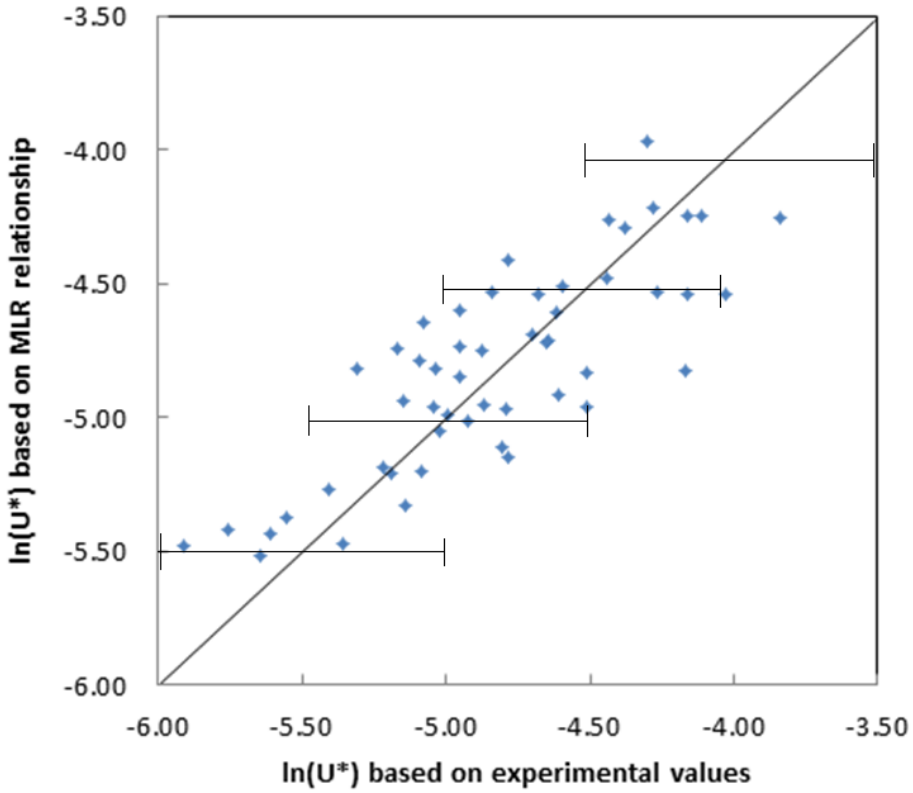

Figure 5-7 Comparison of experimental and model-predicted *U values** (x-error bars indicate ± 0.5 ln(*U**))

Comparison of the U* based on experimental values and the U* predicted by regression analysis is shown in Figure 5-7. Most of the data stay around approximately 10% the y=x line. Scattering of the data is mainly attributed to statistical fluctuations in the data in the combustion process, and the errors introduced during the process such as determination of the droplet size in the ignition environment, and calculation of the flame area based on the image processing.

SUMMARY

Through theoretical analyses it can be concluded that droplet evaporation, and the subsequent distribution of the fuel vapor concentration in the aerosol system, plays the most important role in the aerosol burning modes and the characteristics of the flames, as observed in the ignition tests. The droplet evaporation behaviors and the fuel vapor distribution are further related to aerosol droplet size, droplet spacing, movement velocity, and the liquid volatility.

1) The fuel vapor concentration in the aerosol system should be high enough to support the large global flames, as in the middle section of the P-NF aerosols. This requires smaller droplet sizes and smaller spaces between droplets, so that the fuel vapor concentration can support the global flames not only in the surrounding areas of the droplets but also in the space between droplets, and the flame size expansion is facilitated.

2) Larger droplet size and droplet spacing may hinder the appearance of global flames. When the liquid fuel has certain level of volatility, a unique situation may appear, similar to what happened with the HT-D aerosols, which creates an uneven distribution of fuel vapor in the system. The local high vapor fuel concentration around the droplets favor the global flame mode, while the space between the droplets does not have sufficient fuel vapor to support the global flame mode. Because of this variation in the burning mode combined with enhanced flame propagation speed may occur.

3) Turbulence induced by droplet movement may dilute the fuel vapor concentration in the aerosol system, which may also hinder the flame size expansion and appearance of the global flame mode. High turbulence can result in quenching a flame.

CHAPTER VI

PREDICTION OF AEROSOL MINIMUM IGNITION ENERGY

INTRODUCTION

In the process industry, flammable aerosols can be formed from the pressurized release of hydrocarbon liquids, and are considered one of the major forms of hazardous materials influencing safety in the process industry (Aggarwal, 1997; Bowen & Shirvill, 1994; Bowen et al. 1997; Maragkos & Bowen, 2002). The flammability of aerosols is still not fully understood. Compared with gaseous flammable mixtures, data on aerosol flammability is rather scarce. One reason for this is the huge complexity of the aerosol ignition process, and the difficulty of carrying out experiments with setups sophisticated enough to account for various factors in the process (Ballal & Lefebvre, 1981). Aerosol ignition tests were limited to aerosols formed by a small group of hydrocarbons, including iso-octane, diesel oil, n-decane, n-heptane, methanol, etc. (Hayashi & Kumagai, 1974; Hayashi et al. 1981; Myers & Lefebvre, 1986; Singh, 1986; Danis, 1987; Atzler & Lawes, 1998; Atzler et al. 2007; Lawes et al. 2002). The minimum ignition energy, the most important indicator for aerosol flammability is limited to data obtained in the above-listed studies. Predicting the flammability of aerosols formed by industrial hydrocarbons is still a problem for the process industry. Finding a theoretical method for the prediction of the minimum ignition energy of an aerosol is important to prevent industrial aerosol fire hazards.

Flammability of aerosols is closely related to the ignition process of aerosols. For gaseous mixtures, the ignition process involves the concept of flame front propagation speed, which is one of the most important topics in classical combustion theory and has been widely studied by researchers for a long time. The flame front propagation speed, or flame speed, is defined as the velocity at which unburned gases move through the combustion wave in the direction normal to the wave surface (Glassman & Yetter, 2008). According to the classical Mallard and Le Chatelier Theory, the laminar flame speed for the gaseous phase is obtained under the condition of mass, energy and momentum balance of both burned and unburned materials inside the flame front. A fully developed flame front meeting the requirements of such conditions is considered necessary for successful ignition. Although the flame speed theories are applied in ignition-related topics for gaseous mixtures, flame front propagation speed in aerosols is not fully understood, due to complications with the existence of liquid droplets (Polymeropoulos, 1984; Greenberg et al. 1999; Suard et al. 2001; Suard et al. 2004). The flame speed theory is rarely applied in aerosol ignition and flammability research.

The main purpose of the work in this chapter is to develop an integrated model applying the flame front propagation theory to the aerosol ignition process, and use the model to predict the minimum ignition energy of aerosol. The integrated model coupled the flame speed development process, which is based on the flame front propagation theory in aerosols, to the flame kernel growth model, which is applied in spark ignition modeling for flammable mixtures. Changes in the thermodynamic properties of the flame kernel during the flame front development process are modeled. By identifying the

minimum kernel temperature as the criterion for successful ignition, the aerosol minimum ignition energy can also be found. The dependency of the minimum ignition energy on aerosol properties, such as droplet size and fuel-air equivalence ratio, can also be studied. The model for prediction of the minimum ignition energy of aerosols is of practical importance considering the scarcity of relevant experimental data. It is also of theoretical importance as the connection is established between aerosol flammability and the flame propagation theory in aerosols.

MODEL DESCRIPTION

Singh (1986) experimentally determined the minimum spark ignition energy of tetralin aerosols in a laminar gas flow. The aerosol droplet size was between 6.7 μm and 40 μm. To make results from the current model comparable to the data obtained in Singh's work, tetralin is used as the fuel and its properties as inputs for the model.

The integrated model consists of three major components to account for different phenomena in the aerosol ignition process:

1. The flame kernel growth model;
2. Droplet evaporation in the flame front;
3. Initiation and development of the propagating flame front around the flame kernel.

The initial values for the variables and values for the constants used in the model are listed in the table on page 137.

The flame kernel

A successful spark ignition process is considered comprised of two major stages, as illustrated in Figure 6-1. The first stage involves the creation and growth of a plasma kernel by the electric spark discharge. A spark channel of electron flow is initially established between the two electrodes from the electric breakdown, and a plasma kernel containing ionized species from the original gas phase molecules is formed. The plasma kernel then goes through a constant mass expansion with additional electric energy input. The first stage happens in a very short period of time depending on the spark discharge duration (usually within the first 2 ms). The first stage also includes the emission of a shock wave. According to the study on characteristics of spark discharges, the radius of the plasma kernel can grow from below 1 mm to 2 mm, and its temperature can grow from 7000 K to as high as 70000 K (Eisazadeh-Far et al. 2010). The pressure in the kernel, upon pressure wave emission, will drop to the ambient pressure during the kernel's constant mass expansion.

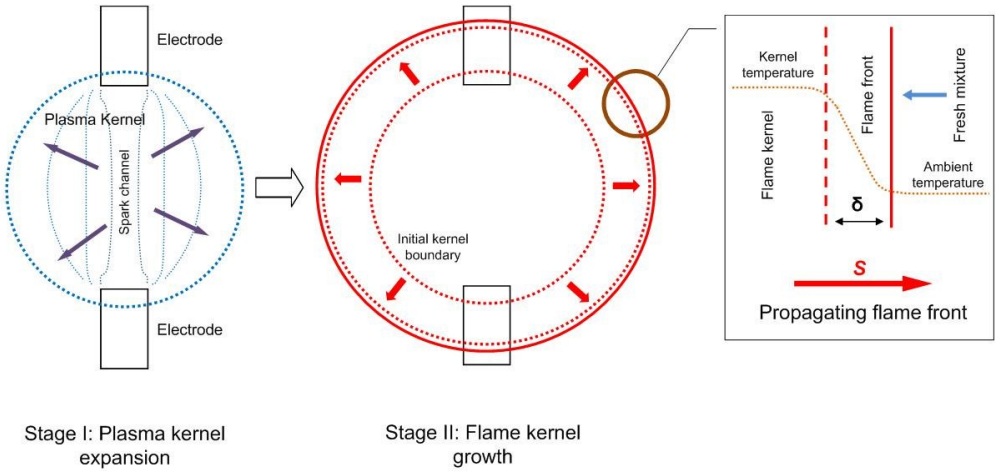

Figure 6-1 Schematic illustration of the flame kernel growth

The second stage involves the growth of the flame kernel. At the beginning of the second stage, the combustible mixtures surrounding the hot plasma kernel ignite and a propagating flame front is produced. During the second stage, to distinguish this kernel from the plasma kernel in the previous stage, it is called the flame kernel. The flame kernel undergoes a constant pressure expansion with the flame front developing on its outskirt. The mass of the kernel continues to increase subsequently as more fresh mixtures go through the flame front and are converted into burned products. Because the combustion and the flame front start in this second stage, the current model starts at the beginning of this second stage and focuses on the growth of the flame kernel. The initial condition of the flame kernel is the same as the final condition of the plasma kernel at the end of its expansion in the first stage, which can be based on the results in literature

(Eisazadeh-Far et al. 2010). The flame kernel grows until a fully developed flame front is established and is capable of propagating through the aerosol mixture.

A spherical flame kernel is assumed (Pischinger & Heywood, 1990; Dulger et al. 1994). Equations (6-1) and (6-2) are the mass and energy balances for the flame kernel. Major energy items considered in the energy balance include the combustion heat release rate Q_{comb}, heat conduction loss to the surrounding environment Q_{cond}, droplet evaporation heat Q_{vap}, and the heat to raise the temperature of the fresh mixture entering the flame front Q_{cp}. Electric energy input is assumed to have stopped within the previous stage. It is assumed that the ignition happens in an area with relatively low turbulence, similar to Singh's tests. The heat loss due to turbulent diffusion is also neglected.

$$\frac{dM}{dt} = \rho_u A S \tag{6-1}$$

$$\frac{dT}{dt} = \frac{Q_{comb} - Q_{cond} - Q_{vap} - Q_{cp}}{C_{pa} M} \tag{6-2}$$

$$Q_{comb} = \frac{dM}{dt} \frac{\rho_{fl} v_f H_c}{\rho_u M_f} \tag{6-3}$$

$$Q_{cond} = k_a A \frac{T - T_{am}}{\delta} \tag{6-4}$$

$$Q_{vap} = \frac{dM}{dt} \frac{\rho_{fl} E_{vap} v_f}{\rho_u M_f} \tag{6-5}$$

$$Q_{cp} = \frac{dM}{dt}\frac{\rho_{fl} C_{pf} v_f}{\rho_u M_f}(T - T_{fb}) + \frac{dM}{dt}\frac{\rho_a C_{pa}}{\rho_u}(T - T_{am}) \tag{6-6}$$

M and T are kernel mass (kg) and temperature (K), ρ_u is the density of unburned mixture (kg/m^3), A is the kernel outer surface area, and S is the flame front propagation speed (m/s), which will be introduced below in detail. Initial conditions of the kernel temperature and volume are based on data by Eisazadeh-Far (Eisazadeh-Far et al. 2010), which are listed in Table 6-1.

Following the ideal gas law, the kernel volume expansion rate is expressed as follows:

$$\frac{dV}{dt} = \frac{V}{T}\frac{dT}{dt} + \frac{dM}{dt}\frac{RT}{P} \tag{6-7}$$

Droplet evaporation

Upon encountering the flame front, the aerosol droplets evaporate into fuel vapor and participate in the chemical reaction. To calculate the droplet evaporation rate $\dot{m}_e$ (kg/s), the convective droplet vaporization model by Sirignano (2010) is used:

$$\dot{m}_e = 4\pi \frac{k_{fl} R_s}{C_{pf}} \ln(1 + B_H)\left[1 + \frac{k'}{2}\frac{\mathrm{Pr}^{1/3}\,\mathrm{Re}^{1/2}}{F(B_H)}\right] \tag{6-8}$$

R_s is initial radius of aerosol droplets and B_H is the non-dimensional energy transfer number, which follows the form (Abramzon & Sirignano, 1989):

Table 6-1 Variables and constants in the flame kernel model

Variable/ Constant	Value	Meaning
M	* 1×10^{-13}-5×10^{-11}	Kernel mass (kg)
T	* 35000-70000 K	Kernel temperature (K)
V	* 5×10^{-12}-3×10^{-9}	Kernel volume (m^3)
ρ_u	** 1.124-1.272	Unburned mixture density (kg/ m^3)
C_{pa}	1012	Heat capacity of air (J/kg K)
ρ_{fl}	970	Liquid tetralin density (kg/m^3)
v_f	0.0769	Stoichiometric coefficient of tetralin
H_c	5.60×10^6	Combustion heat of tretralin (J/mol)
M_f	0.132	Molecular weight of tetralin (kg/mol)
k_a	0.025	Thermal conductivity of air (W/K m)
T_{am}	298.15	Ambient temperature (K)
C_{pf}	217.44	Heat capacity of tetralin (J/mol K)
T_{fb}	480.7	Tetralin's boiling point (K)
P	101325	Ambient pressure (Pa)
k_{fl}	0.2	Thermal conductivity of liquid tetralin (W/K m)
k'	0.848	Non-dimension coefficient for droplet evaporation rate
H_{evp}	5.86×10^4	Evaporation heat of tetralin (J/mol)
μ_a	1.78×10^{-5}	Viscosity of air (Pa s)
ρ_a	1.184	Air density (kg/m^3)
v_s	0.05	Droplet velocity (m/s)

* Initial value

** Depends on fuel-air equivalence ratio

$$B_H = \frac{1}{H_{evp}}\left[C_{pf}\left(T_{am} - T_{fb}\right)\right] \tag{6-9}$$

$F(B_H)$ is the function based on B_H:

$$F(B_H) = (1 + B_H)^{0.7}\,\frac{\ln(1 + B_H)}{B_H} \text{ (for } 0 \le B_H \le 20,\ 1 \le \Pr \le 3) \tag{6-10}$$

The Prandtl number P_r follows the form:

$$P_r = \frac{C_{pa}\mu_a}{k_a} \tag{6-11}$$

The Reynolds number R_e follows the form:

$$R_e = \frac{2\rho_a v_s R_S}{\mu_a} \tag{6-12}$$

Flame front propagation speed

The flame front develops around the flame kernel. Its propagation speed follows the asymptotic form, which means that after a certain period of time, the increase in the flame front propagation speed will slow down as it approaches a certain value. The asymptotic form of flame speed development has been observed experimentally by Atzler (Atzler et al. 2007) and Eisazadeh-Far (Eisazadeh-Far et al. 2010).

$$S = S_{La}\left[1 - \exp\left(-\frac{t}{\tau_c}\right)\right] \tag{6-13}$$

S_{La} is the laminar flame speed in the aerosol droplet system, and τ_c is a characteristic time scale based on thermodynamic properties of the mixtures and the reaction kinetics in the flame zone. τ_c is taken as the sum of the characteristic time for droplet evaporation and the chemical reaction in the flame zone. S_{La} and τ_c will be introduced as follows.

The laminar flame speed S_{La} is the value that the flame speed will gradually approach following the asymptotic form of development. It is the speed of the flame front under the ideal steady-state propagation mode in the aerosol droplet system, when the mass, energy and momentum balances in the flame front are achieved. It is readily available but can be computed following the steps below. According to the analysis by Ballal and Lefebvre (1981) and Polymeropulos (1984), it is assumed that in the fully developed flame front, the equilibrium of three characteristic time values is established:

$$t_q = t_e + t_c \tag{6-14}$$

t_q, t_e and t_c are the characteristic time for flame zone quenching, fuel droplet evaporation, and chemical reaction in the vapor phase, respectively.

The characteristic time for the flame zone quenching is expressed as follows:

$$t_q = \frac{\delta^2}{\alpha_g} \tag{6-15}$$

δ is the thickness of the flame front, and a_g is the thermal diffusivity.

It is assumed that droplet evaporation happens in the flame front, and the droplets evaporate completely. The vapor fuel concentration produced by droplet evaporation outside the flame front is neglected because of the low vapor pressure of tetralin at ambient conditions (Singh, 1986). The time it takes the liquid fuel to evaporate can be expressed in a form similar to Ballal's definition:

$$[Fuel\ evaporation\ time] = \frac{[Mass\ of\ fuel\ in\ a\ droplet]}{[Droplet\ evaporation\ rate]}$$

Based on the droplet evaporation rate described above, the characteristic time for fuel droplet evaporation is expressed as follows:

$$t_e = \frac{2R_s^2 C_{pf} \rho_{fl}}{3k_{fl} \ln(1+B_h)\left[1+\frac{bP_r^{1/3} R_e^{1/2}}{2F(B_h)}\right]} \tag{6-16}$$

The characteristic time for the chemical reaction is based on characteristics of the combustion reaction in the gaseous phase.

$$t_c = \frac{\alpha_g}{S_{Lg}^2} \tag{6-17}$$

a_g is the thermal diffusivity, and S_{Lg} is the laminar flame front propagation speed in the gas phase mixtures. S_{Lg} data for certain fuels can be found in literature and it usually changes in a quadratic shape along the fuel-air equivalence ratio, as shown in Figure 6-2.

Because the corresponding S_{Lg} data for tetralin are not currently available, an S_{Lg} expression in the quadratic form based on the S_{Lg} data for dihydropyran (Glassman & Yetter, 2008) is used in the current work:

$$S_{Lg} = -1.633\Omega^2 + 3.369\Omega - 1.183 \tag{6-18}$$

Ω is the fuel-air equivalence ratio, defined as the ratio of the overall fuel-to-oxygen ratio in the aerosol to the stoichiometric fuel-to-oxygen ratio. For the equivalence ratio of 0.6-1.0, the S_{Lg} data for dihydropyran is between 0.3-0.6 m/s, typical range of the laminar flame speed for major group of hydrocarbons.

Then Equation (6-14) can be expressed as:

$$\frac{\delta^2}{\alpha_g} = \frac{2R_s^2 C_{pf}\rho_{fl}}{3k_{fl}\ln(1+B_h)\left[1+\dfrac{bP_r^{1/3}R_e^{1/2}}{2F(B_h)}\right]} + \frac{\alpha_g}{S_{Lg}^2} \tag{6-19}$$

Based on Equation (6-19), the expression for δ can be obtained with:

$$\delta = \left[\frac{\alpha_g R_s^2 C_{pf}\rho_{fl}}{3k_f\ln(1+B_h)\left(1+\dfrac{bP_r^{1/3}R_e^{1/2}}{2F(B_h)}\right)} + \frac{\alpha_g^2}{S_{Lg}^2}\right]^{\frac{1}{2}} \tag{6-20}$$

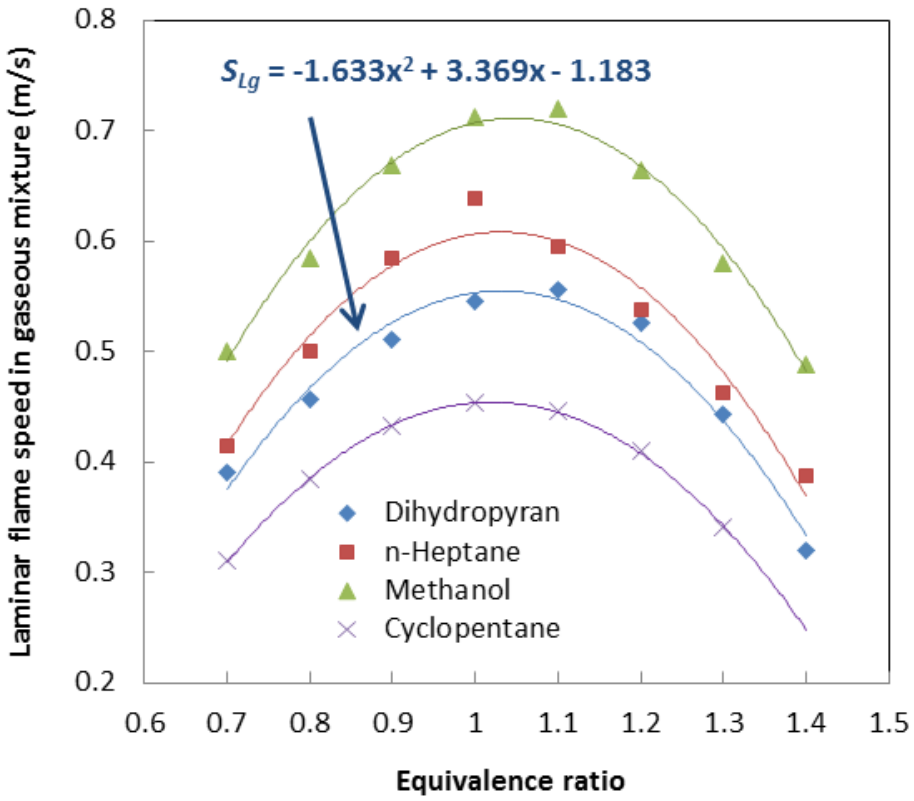

Figure 6-2 Laminar flame speed in gaseous mixtures S_{Lg} (Glassman & Yetter, 2008)

Then they can be computed as follows and applied to Equation (6-13) for the computation of flame front speed *S* around the flame kernel.

$$S_{La} = \frac{\alpha_g}{\delta} = \left[\frac{R_s^2 C_{pf} \rho_{fl}}{3k_f \alpha_g \ln(1+B_h)\left(1+\frac{bP_r^{1/3} R_e^{1/2}}{2F(B_h)}\right)} + \frac{1}{S_{Lg}^2} \right]^{-\frac{1}{2}} \tag{6-21}$$

$$\tau_c = t_q = t_e + t_c \tag{6-22}$$

By assuming that the flame front propagation speed in the aerosol systems will follow the asymptotic form, a flame front propagation will always be developed in the current model along the flame kernel growth. The kernel energy balance will play an important role in determining if the seemingly already developed flame front can become truly self-sustainable. Thus the kernel temperature will be used as the key indicator of whether the flame front meets the requirement of the energy balance for continuous propagation through ignition of fresh mixtures entering the flame front, as will be discussed below.

MODELING RESULTS AND DISCUSSION

Flame propagation speed in aerosols

According to the current model, the speed of the flame front around the kernel takes the asymptotic form. After a certain period of time, the flame speed will approach

the constant laminar flame speed, S_{La}, for the aerosol system. The laminar flame speed of an aerosol is the rate of flame propagation through the aerosol droplet system under ideal steady-state conditions. It corresponds to the steady-state propagation mode of a fully developed flame front, which satisfies both the energy balance in the propagating flame zone and the requirements specific to the aerosol system, including droplet evaporation and fuel chemical kinetics. The laminar flame speed S_{La} depends on the aerosol droplet size and fuel-air equivalence ratio, as shown in Figure 6-3. When the droplet diameter is 0 μm, $S_{La} = S_{Lg}$. The flame propagation speed decreases as the droplet size in the aerosol becomes larger. In regards to droplet size, the flame propagation speed of an aerosol with a higher fuel-air equivalence ratio is higher. The trend is similar to previous experimental data (Ballal & Lefebvre, 1981; Polymeropulos, 1984).

The flame kernel growth

Using the model described above, growth of the flame kernel is carried out in aerosols where tetralin is the fuel in the liquid droplets. Figure 6-4 shows the characteristics of the kernel development process along time, including the development of the flame front propagation speed, the kernel mass, radius, and temperature.

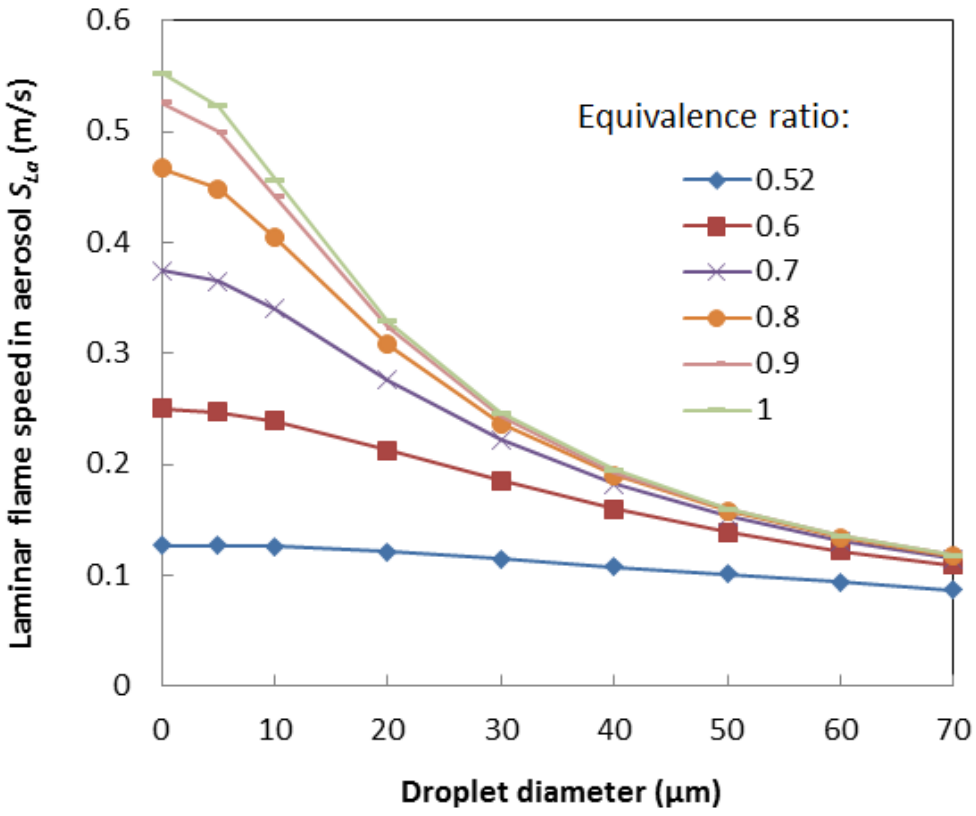

Figure 6-3 Laminar flame speed in aerosols S_{La} (tetralin aerosol)

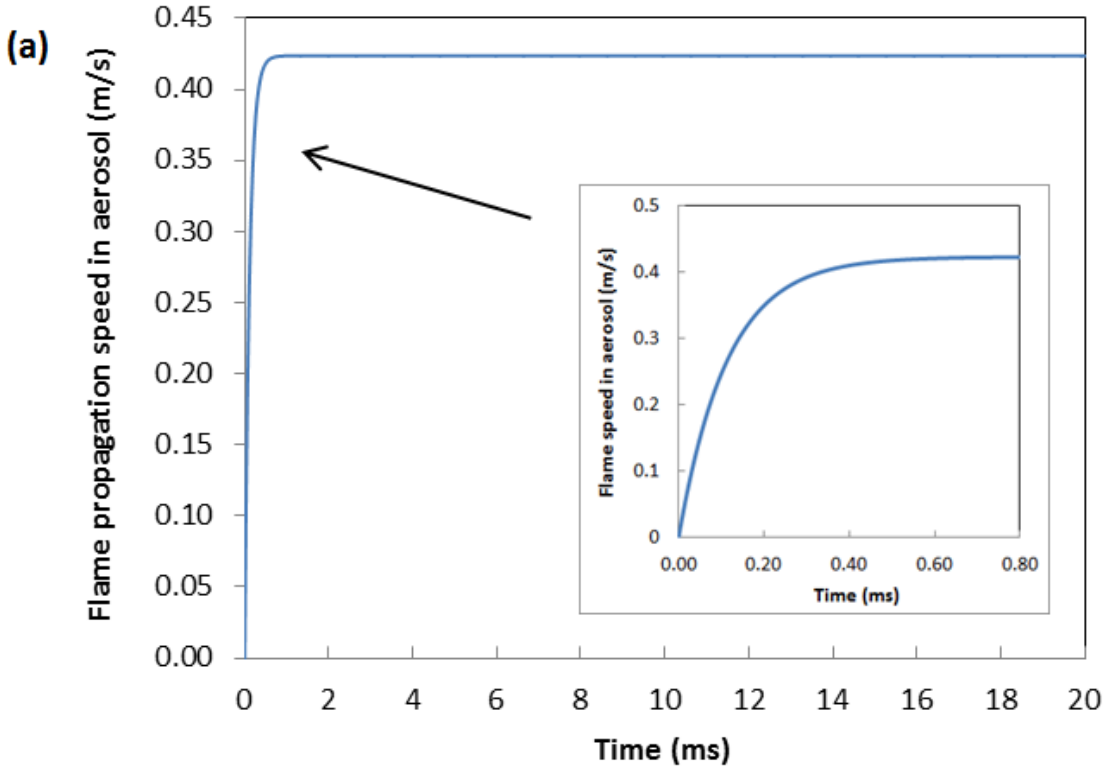

Figure 6-4 Properties of the flame kernel during growth. (a) Flame propagation speed as function of time; (b) kernel mass as function of time; (c) kernel temperature as function of time; (d) kernel radius as function of time (tetralin aerosol, 12 µm droplet diameter, 1.0 fuel-air equivalence ratio)

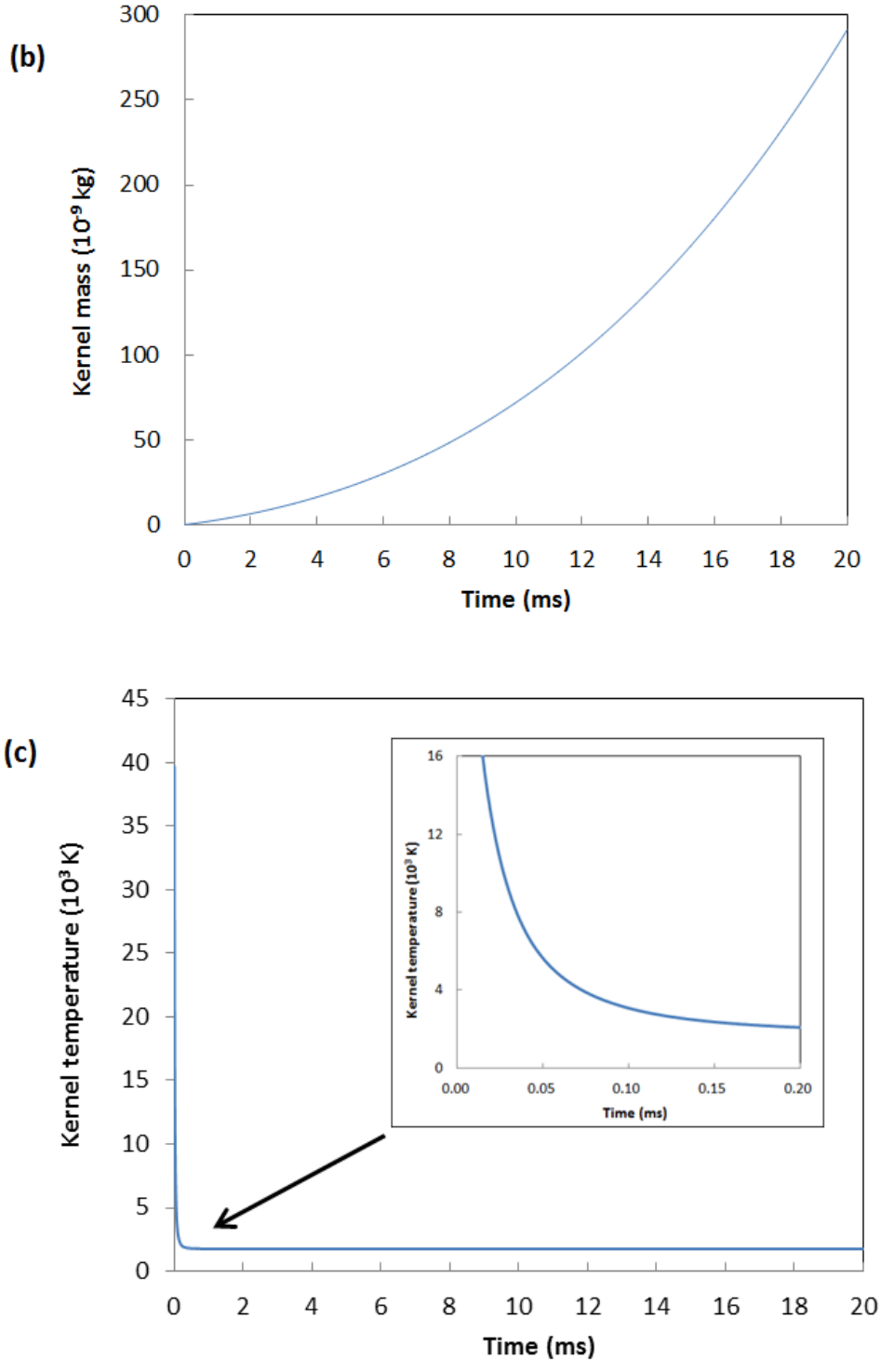

Figure 6-4 Continued

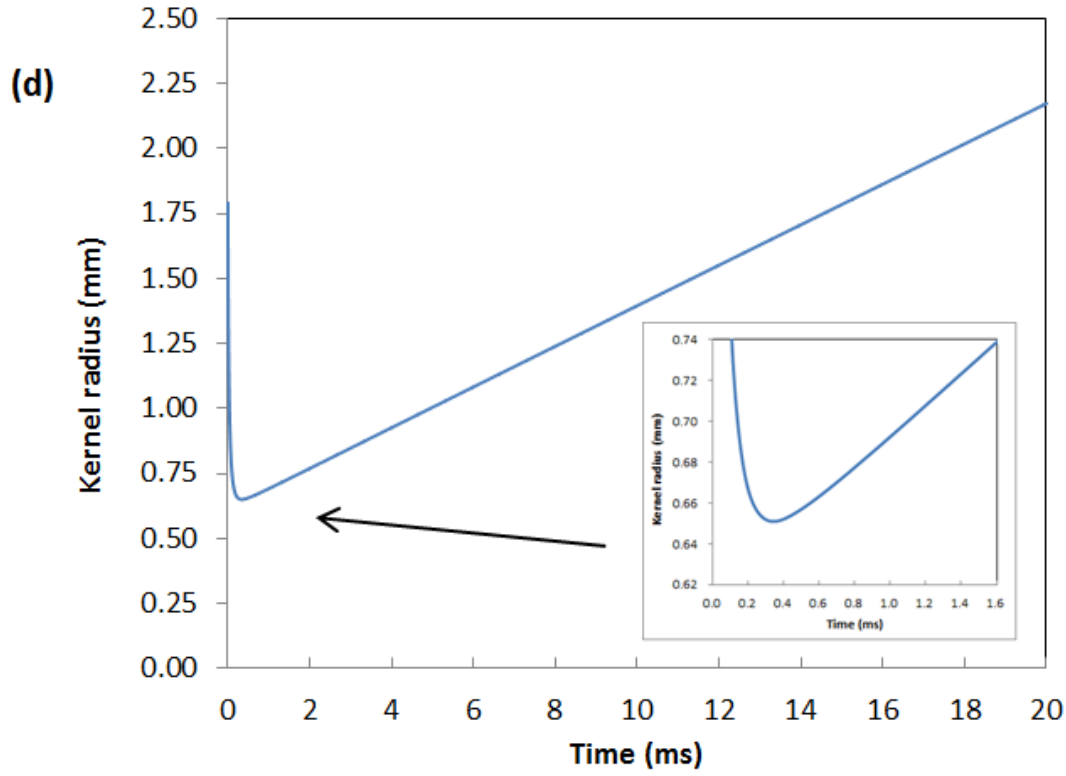

Figure 6-4 Continued

The flame front speed increases quickly within the first 0.6 ms, from 0 to the laminar flame speed (Figure 6-4a). The propagating flame front causes the kernel mass to increase along time (Figure 6-4b). The kernel temperature decreases sharply within the first 0.2 ms before becoming stable. Then, it gradually approaches a certain quasi-steady state value (Figure 6-4c). The kernel volume also drops within the first 0.4 ms until reaching a minimum value. The kernel radius then turns to increase along time (Figure 6-4d).

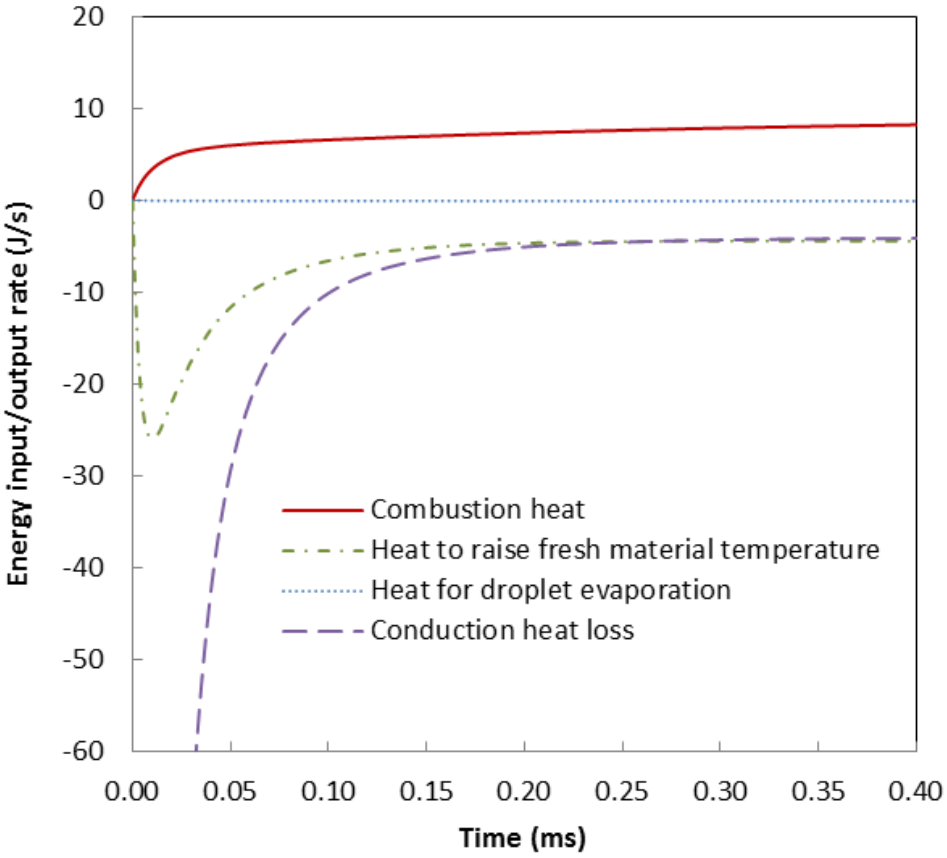

Figure 6-5 The energy terms along time during the kernel growth period

Characteristics of the kernel growth exhibit influences from both the thermodynamic changes in the kernel and the evolving flame front around the kernel. Analysis of the energy balance of the kernel, shown in Figure 6-5**,** can help to understand characteristics of the kernel development process. The energy items include the combustion heat release, conduction heat loss, the energy to heat up fresh mixtures in the kernel and the liquid fuel evaporation heat. During the first 0.2 ms, the heat loss that is conducted from the kernel to its surrounding is very large because the kernel

temperature at the end of the plasma growth in the first stage of the spark ignition is extremely high. During this time the flame front around the kernel has not been fully developed, when the energy lost through heat conduction and the energy used to heat up the fresh mixture into the kernel are significantly larger than the combustion heat of the fuel carried by the fresh mixtures into the kernel. This results in a sharp decrease in kernel temperature causing the kernel radius to shrink during the first 0.2 ms.

As the kernel temperature drops, the conduction heat loss also decreases rapidly. With the development of the flame front around the kernel outskirts, as represented by the rapidly growing flame speed, more fresh mixtures around the kernel encounter the flame front and are converted into kernel mass, assisting the kernel mass in growing larger. The kernel's radius starts to grow after reaching a minimum value. The combustion heat release rate also increases since more fuel is burned as a larger volume of fresh mixture is added into the kernel mass. The combustion heat gradually increases to such a level that it balances all the other energy items, and the kernel temperature stabilizes. Compared with other energy items, the energy for liquid fuel evaporation is small (within 1 J/s).

Minimum ignition energy of aerosols

To determine the aerosol’s minimum ignition energy, the first step is to identify the information in the modeling results which can be the criterion for successful ignition. Based on of the basic assumption of the model and the modeling results, the ignition criterion can be identified in the kernel temperature change, as discussed below.

The current model assumes that the speed of flame front around the kernel will approach the constant laminar flame speed for the aerosol system. As described above, the kernel also reaches a quasi-steady state of growth, when the kernel temperature becomes quite stable as it approaches a quasi-steady value (Figure 6-4c). This quasi-steady kernel temperature is the temperature in the fully developed flame front under the energy equilibrium state, when energy generated in the flame front balances with energy losses. In classic combustion theories, flame front temperature is important for the successful ignition of fresh mixtures. There exists an ignition temperature for the flame front below which the ignition of fresh mixtures will be hindered. Following that concept, there is also a minimum ignition temperature for the flame front in aerosol systems. When the computed temperature in the flame front is below this minimum value, the flame front will not be able to support the continuous ignition of the fresh mixture, and the flame kernel will ultimately quench without a self-sustainable flame front. It is necessary to identify this minimum ignition temperature.

The quasi-steady kernel temperature is determined mainly by the fuel-air equivalence ratio, as shown in Figure 6-6. The quasi-steady kernel temperature is lowered by decreasing the fuel-air equivalence ratio (Figure 6-6a), because the equivalence ratio determines the amount of fuel and related combustion heat that is generated in the flame front. A lower equivalence ratio reduces the amount of fuel in the flame front, thus reducing the flame front temperature. When the equivalence ratio is lowered to a minimum value, the quasi-steady kernel temperature can be identified as the minimum ignition temperature. The lower flammability limit for tetralin in the vapor

form is 0.84%, corresponding to a minimum fuel-air equivalence ratio of 0.52 (Glassman & Yetter, 2008). For a 0.52 equivalence ratio, the quasi-steady kernel temperature is 1073 ± 3 K for droplet sizes in the range of 10-100 μm (Figure 6-6b). The temperature 1073 K is identified as the minimum ignition temperature for tetralin aerosols. The inflammable region in Figure 6-6a and 6-6b represents a condition where the fuel concentration becomes insufficient.

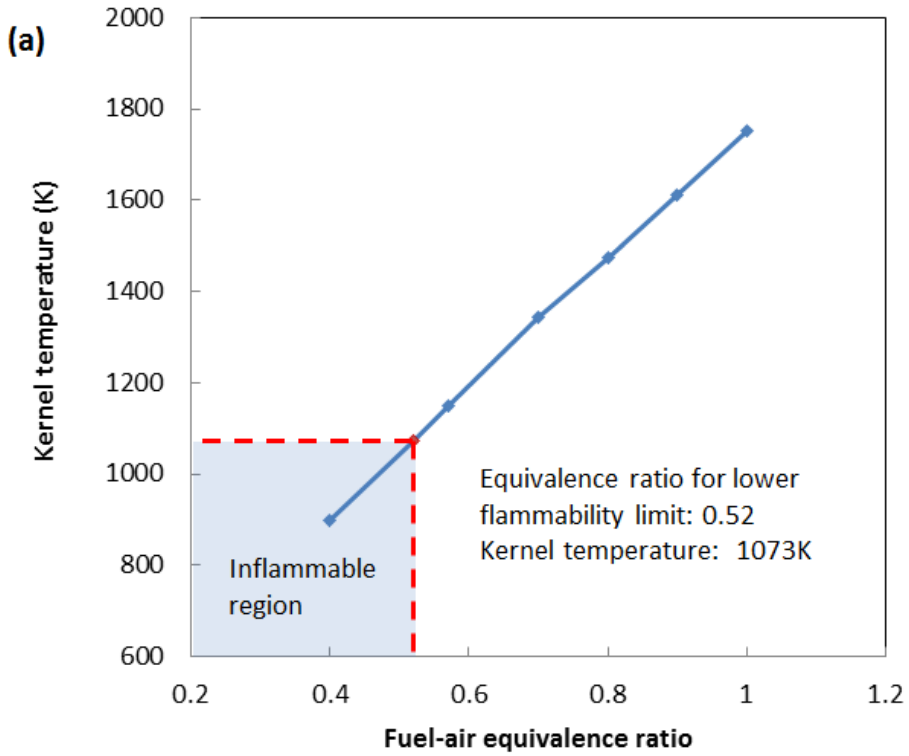

Figure 6-6 Identification of the minimum kernel temperature as ignition criterion. (a) Influence of equivalence ratio on quasi-steady kernel temperature; (b) influence of droplet size on quasi-steady kernel temperature (ignition energy 25 mJ)

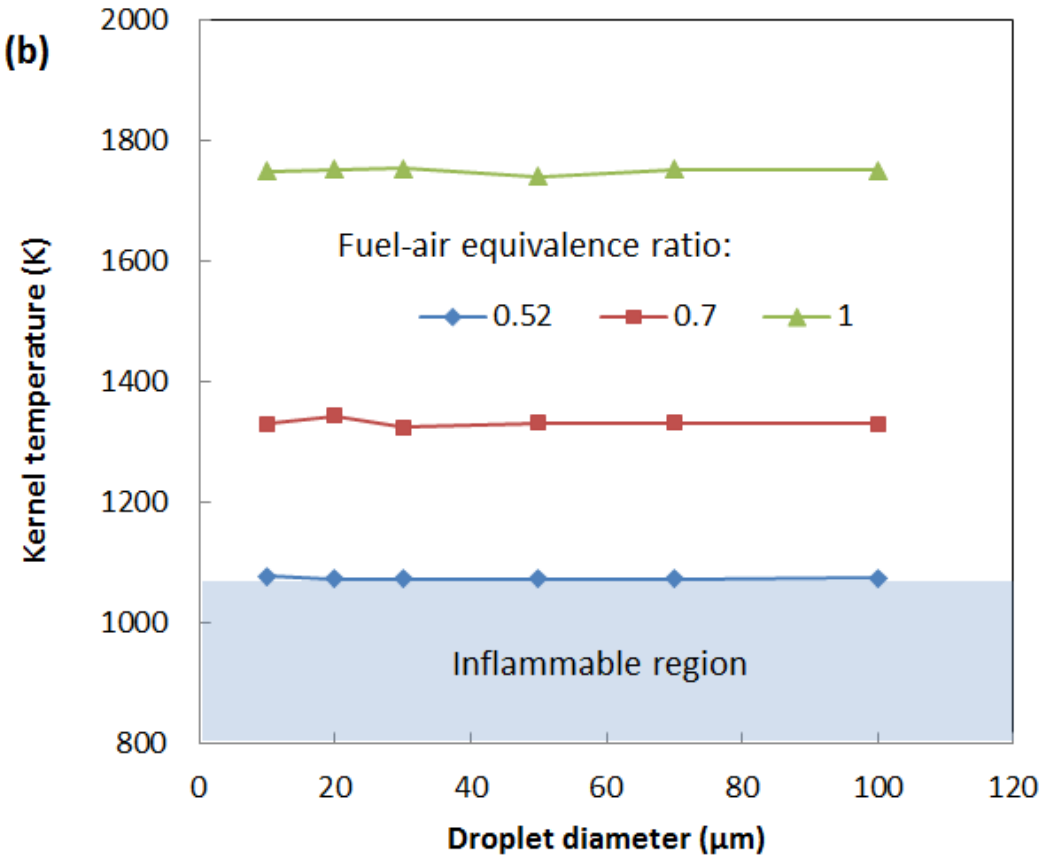

Figure 6-6 Continued

Based on previous analysis, the temperature in the fully developed flame front must be higher than the criterion 1073 K to enable continuous propagation of the flame front in a tetralin aerosol. This concept can be extended to the entire kernel growth period. The kernel temperature must remain above the criterion temperature throughout its growth to realize ignition. If not, the modeled flame kernel growth and aerosol

ignition is not valid since the flame front will quench at a certain point due to the low temperature of the flame front.

Ignition energy is defined as the energy in the initial flame kernel, which is the internal energy in the plasma kernel at the end of the first stage of spark ignition. The ignition energy is calculated as the energy to raise the air inside the kernel to the flame kernel's initial temperature. When the ignition energy drops to a certain level, a local minimum appears in the kernel temperature during the kernel growth, as shown in Figure 6-7a. The local minimum temperature decreases as the ignition energy lowers. Appearance of the local minimum temperature can be explained as follows. The heat loss from the kernel with a lower initial energy results in a faster drop in kernel temperature compared to kernels of higher energy. But, in the current model, it is assumed that the flame front always develops around the kernel with the flame speed assuming a specific pattern along time. Calculation of the flame speed is not based on the instant energy balance in the flame kernel. A faster temperature drop can result in the temperature dropping to a minimum value before the heat input rate increases due to the fuel combustion of the flame front, which helps to increase the kernel temperature back to a quasi-steady temperature with a fully developed flame front appearing later.

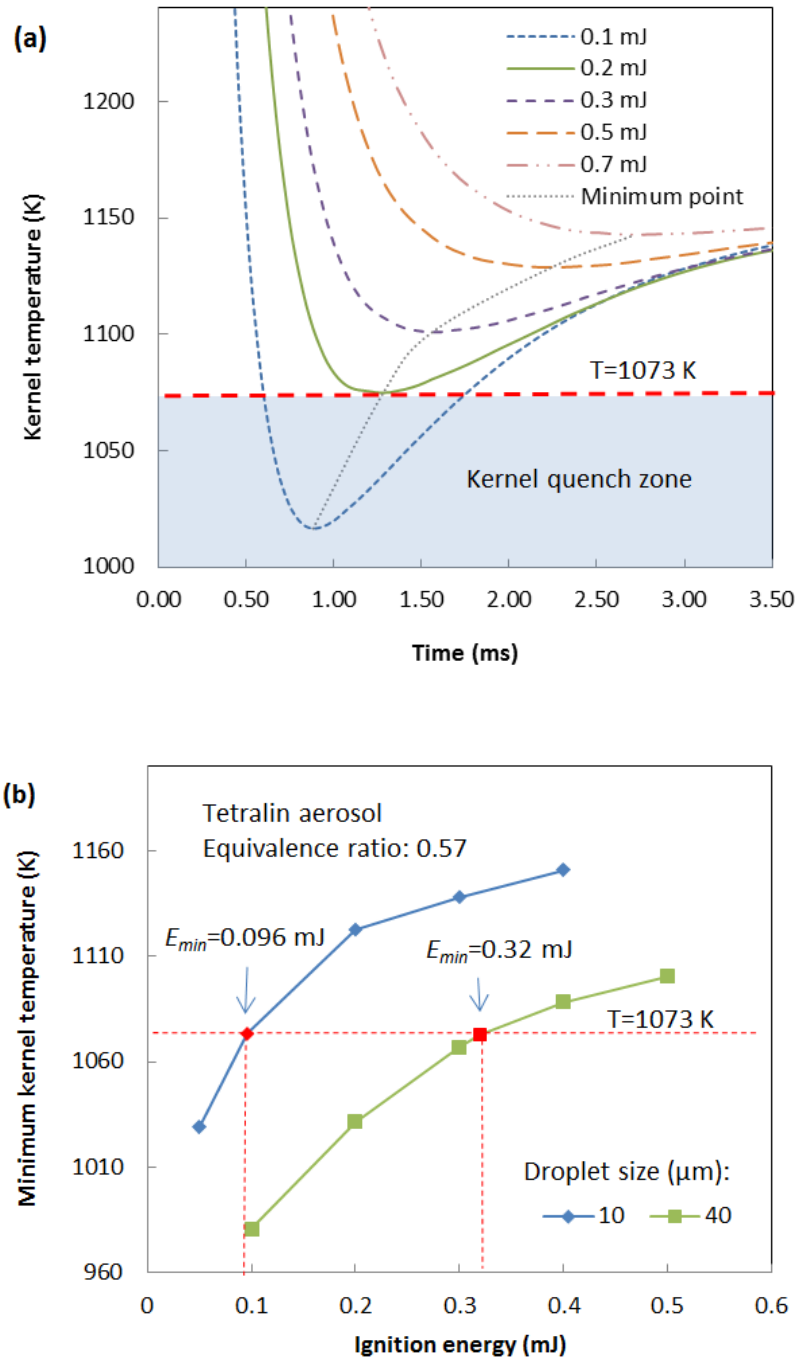

Figure 6-7 Identification of aerosol minimum ignition energy. (a) Appearance of the minimum kernel temperature during the kernel temperature drop (tetralin aerosol, equivalence ratio 0.57, 30 µm droplet diameter); (b) influence of ignition energy on the minimum kernel temperature (tetralin aerosol, equivalence ratio 0.57)

Applying the principle of minimum ignition temperature, when the local minimum temperature drops to below the ignition criterion temperature 1073 K, the energy balance in the developing kernel cannot match the flame speed development pattern, and the flame front, together with the flame kernel, will actually quench instead of developing further. Since the kernel temperature dropped below 1073 K, further kernel development would be invalid. The minimum ignition energy for a tetralin aerosol is the ignition energy which produces a minimum kernel temperature of 1073 K. As shown in Figure 6-7b, the minimum ignition energy E_{min} is 0.096 mJ for tetralin aerosol of 0.57 equivalence ratio, 10 μm droplet diameter, and 0.32 mJ for tetralin aerosol of 0.57 equivalence ratio, 40 μm droplet diameter.

The minimum ignition energy, as obtained by the current method, is influence by both the equivalence ratio and aerosol droplet size. Figure 6-8a shows that the minimum ignition energy decreases significantly as the equivalence ratio increases from 0.57 to 1.0. Figure 6-8b indicates that the minimum ignition energy is higher for an aerosol of same equivalence ratio but with larger droplet sizes. These trends are in agreement with observations in previous research on aerosol ignition (Singh, 1986; Danis, 1987; Aggarwal, 1997).

The minimum ignition energy is also influenced by initial kernel temperature, as shown in Figure 6-8c. A higher initial kernel temperature results in a higher E_{min} because of the increase in conduction heat loss during the flame kernel development period. Larger amounts of initial energy are required in the initial flame kernel to maintain the local minimum kernel temperature above the 1073 K, thus increasing the minimum

ignition energy. The initial temperature of the flame kernel, or the final temperature of the plasma kernel in the first stage of spark ignition, depends on the characteristics of the spark discharge in the first stage. The current results agree with previous research that a spark discharge mode which can bring about a plasma kernel of the same energy with a lower temperature can reduce the minimum ignition energy (Ballal & Lefebvre, 1975; Singh, 1986; Dulger et al. 1994). Although the current model starts by the second stage of the spark ignition process, by changing the initial kernel temperature, characteristics of the first stage and its influence on aerosol ignition energy can be reflected.

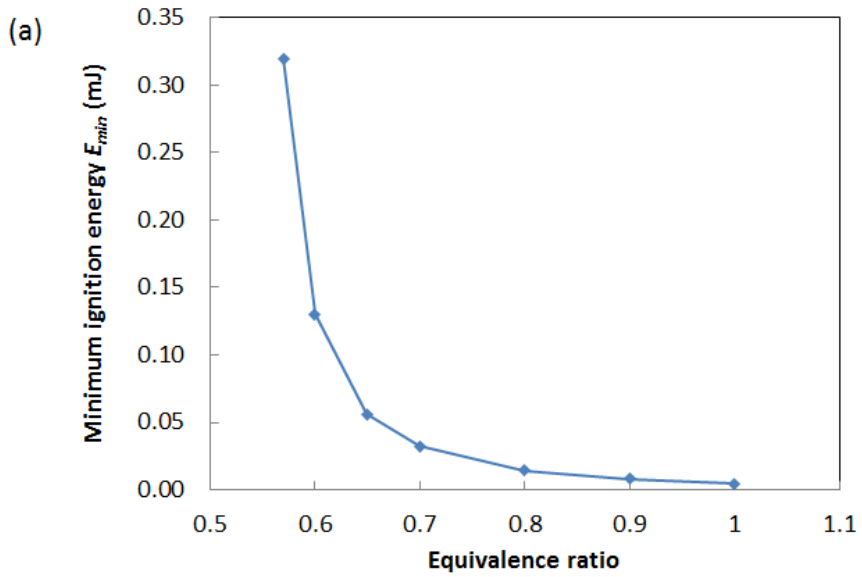

Figure 6-8 Factors influencing the minimum ignition energy of tetralin aerosol. (a) Aerosol minimum ignition energy as function of equivalence ratio (tetralin aerosol, 40 μm droplet diameter); (b) aerosol minimum ignition energy as function of aerosol droplet size (tetralin aerosol, equivalence ratio 0.57); (c) influence of initial kernel temperature on aerosol minimum ignition energy

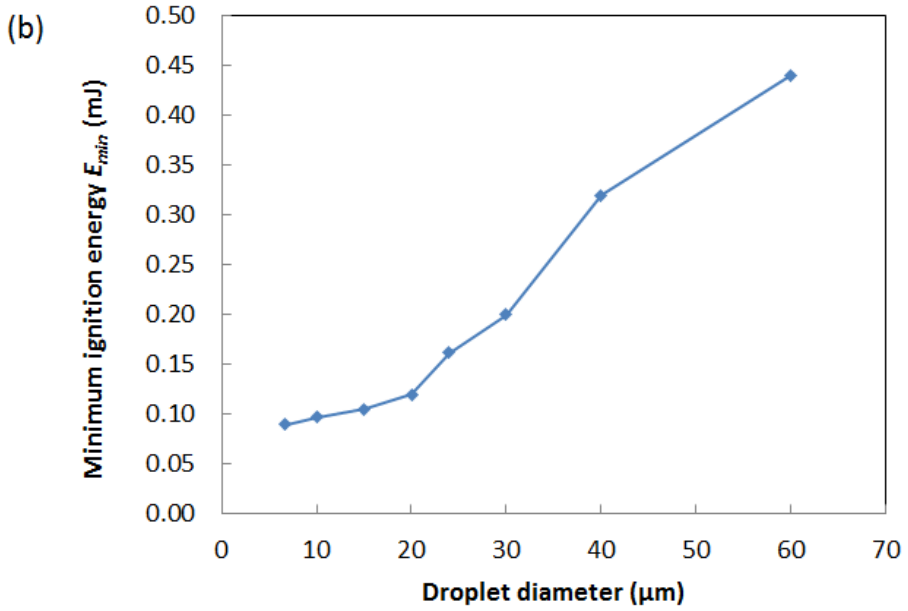

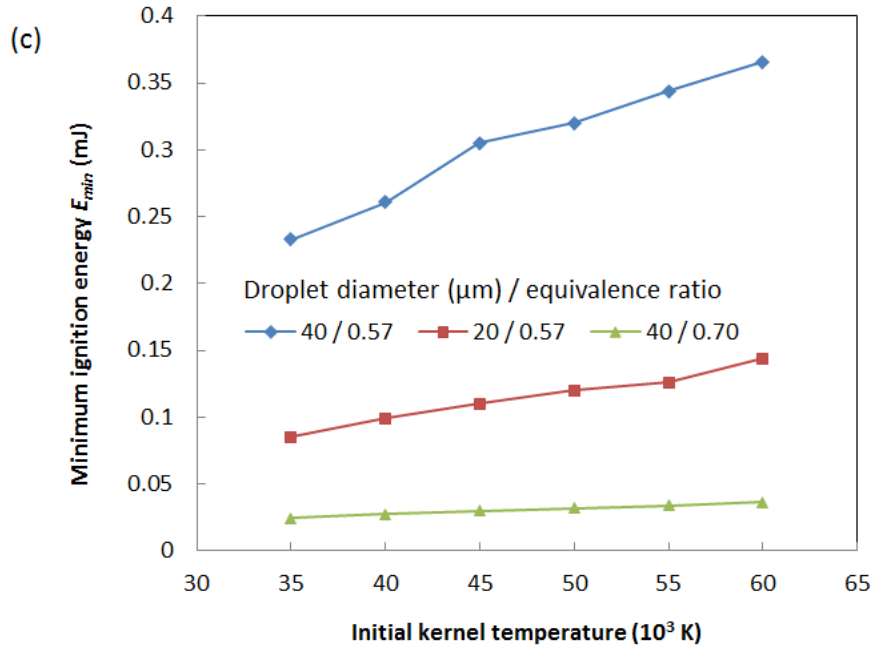

Figure 6-8 Continued

Further discussion

The minimum ignition energy in the current work can be defined as the minimum energy in the initial flame kernel needed to keep the kernel temperature above the criterion temperature throughout the kernel growth when the flame front follows the asymptotic pattern to the laminar flame propagation speed for the aerosol. The concept is similar to Ballal's definition (Ballal & Lefebvre, 1979) of E_{min} as the amount of energy needed to raise a spherical volume of air with diameter of d_q up to stoichiometric flame temperature. d_q is the quenching distance, the minimum diameter of the spherical volume of the kernel needed to be able to self-sustainably develop and propagate through an aerosol mixture. The current model improves this concept by considering information on the dynamic kernel development processes created in recent years (Dulger et al. 1994; Sher et al. 1995; Thiele et al. 2000; Eisazadeh-Far et al. 2010), and further coupling it with the flame front propagation theory.

The E_{min} values predicted by the current model are lower compared to the experimental data. For example, the minimum ignition energy by Singh's tests (1986) is 3.0 mJ for tetralin aerosol of 0.57 equivalence ratio and 40 μm droplet diameter. The minimum ignition energy by current model is 0.32 mJ. Another example is the 0.7 mJ minimum ignition energy for n-heptane of 1.0 equivalence ratio (Glassman & Yetter, 2008). There is a difference in the meaning of E_{min} obtained experimentally and the E_{min} as defined in the current work. The minimum ignition energy from experimental tests is usually obtained through electric spark ignition tests. The ignition energy is based on voltage and current measurements of spark generation from the circuit. As discussed in

the literature, during the original spark discharge and the subsequent plasma kernel expansion, a large portion of the electric energy was consumed in ways other than being stored in the plasma kernel, such as conduction heat loss to the electrodes, radiation heat loss, heat loss by turbulent diffusion, energy taken away by the shock wave upon spark discharge, etc. (Ballal & Lefebvre, 1979; Singh, 1986; Pischinger & Heywood, 1990; Dulger et al. 1994). Although there have been discussions on which energy terms are more significant, it has been agreed that only a certain portion of the measured electric energy inputs are eventually stored in the kernel and used to initiate the flame (Thiele et al. 2000). The current E_{min} values refer to this energy which is stored in the kernel to initiate the flame front. It is smaller than the experimentally recorded spark ignition energy.

There is another reason for the current minimum ignition energy being lower than Singh's experimental data. Singh's minimum ignition energy is based on 50% ignition frequency. In Singh's tests, the minimum ignition energy was obtained following this procedure: under the same fuel-air equivalence ratio and droplet size, 100 electric sparks of the same recorded energy were generated in the aerosol. The number of successful ignitions was recorded, and the percent of successful ignition was calculated as ignition frequency. The ignition energy which can produce a 50% ignition frequency was defined as the minimum ignition energy. The minimum ignition energy in Singh's tests refers to a condition when aerosol ignition is still possible. The minimum ignition energy, as computed in the current work, can be seen as the theoretical limit for ignition to be possible in an aerosol with the corresponding properties. The aerosol system cannot be

ignited using energy below the current E_{min} value. The agreement between general trends of the E_{min} values of current models and the experimental E_{min} data implies the value of using the current method for predicting aerosol flammability.

The minimum ignition energy obtained in experimental tests includes the energy losses which happened in the first stage of the plasma kernel, and can be influenced by factors related to the first stage. In the current method, influences from these factors on the minimum ignition energy are simplified to the changing initial kernel energies with different initial kernel temperatures. With this simplification, the current model has the potential to be further extended to aerosol ignition scenarios by other ignition sources, such as open flames and hot walls, since the ignition by various types of sources are assumed to initiate from flame kernels with certain levels of energy.

SUMMARY

In this study, modeling of the flame kernel growth during the spark ignition of aerosols is carried out, and the aerosol minimum ignition energy is predicted using the minimum ignition temperature as the criterion. The major findings and conclusions are as follows:

1. The minimum ignition energy of aerosols is predicted using an integrated model applying the flame front propagation theory to the process of a flame kernel in the aerosol droplet system. It is assumed that the flame front speed around the flame kernel will follow the development pattern of an asymptotic form, and will approach the steady-state propagation speed, namely the

laminar flame speed for aerosol S_{La}. The minimum ignition temperature is defined as the temperature in the fully developed flame front in the aerosol with an equivalence ratio corresponding to the fuel's lower flammability limit. For tetralin aerosol, the minimum ignition temperature is 1073 K. The minimum ignition energy of tetralin aerosols is defined as the initial energy in the flame kernel which can produce a minimum kernel temperature of 1073 K during the kernel's growth period. The minimum ignition energy E_{min} as calculated by the model is influenced by the aerosol equivalence ratio and droplet size. Higher equivalence ratios up to 1.0 significantly reduce the E_{min}, while larger droplet sizes require higher E_{min}. The trends are in agreement with previous experimental observations, which implies the potential value of using the current method for predicting the aerosol minimum ignition energy.

2. The minimum ignition energy values obtained in the current work are lower compared to previous experimental data. The current model focuses on the flame kernel growth in the second stage of the spark ignition process. The minimum ignition energy values obtained in the current model are the minimum energy in the initial flame kernel for the ignition to be possible in an aerosol with a certain equivalence ratio and droplet size. The minimum ignition energy obtained in previous tests also includes the energy lost during the plasma kernel expansion in the first stage of the spark ignition process.

CHAPTER VII

CONCLUSIONS

This dissertation has presented research on the combustion behaviors of flammable aerosols, which can be formed in the process industry through the pressurized release of fluids during loss of containment scenarios.

The current work tried to study the characteristics of flame propagation in aerosols and how they are influenced by the presence of fuel droplets in the systems. Flames in aerosols are characterized by non-uniform shapes and discrete flame fronts, making it difficult to apply the classical flame front theory to characterize the flame propagation process. For the aerosols produced by P-NF heat transfer fluid, the burning mode of a global flame with rapid size expansion was observed in the middle section of the aerosol system and is considered the most hazardous scenario caused by aerosol combustion. For aerosols created from the HT-D heat transfer fluid, different burning modes appeared alternately as the flames propagated upwardly. And the upward flame front propagation speed was accelerated.

Appearances of different burning modes are related to aerosol droplet size and droplet spacing. Droplet size in the P-NF aerosols ranges from 80 μm to 90 μm. The middle section of the aerosol droplet system is capable of supporting the burning mode of larger global flames. The flame size in P-NF aerosols decreases as the droplet size became larger. The HT-D aerosols have larger droplet size and droplet spacing, which limited the expansion rate of flame fronts except the upward front and reduced the flame

size. The enhanced upward flame front propagation speed in the HT-D aerosols is a complicated phenomenon which has not yet been fully understood. Larger droplet size and droplet spacing have profound influences on the appearance of the phenomenon.

Through theoretical analyses, it can be concluded that droplet evaporation plays an important role in the aerosol burning modes and the characteristics of the flames. The droplet evaporation behaviors and the fuel vapor distribution are further related to aerosol droplet size, droplet spacing, movement velocity, and the liquid volatility. The fuel vapor concentration in the aerosol system should be high enough to support the large global flames, as in the middle section of the P-NF aerosols. This requires the smaller droplet size and smaller space between droplets. Larger droplet size and droplet spacing may hinder the appearance of global flames. But when the liquid fuel has certain level of volatility, an uneven distribution of fuel vapor in the system was created, as in the HT-D aerosols. The local high vapor fuel concentration around the droplets favors the global flame mode, while the space between the droplets does not have sufficient fuel vapor concentration. So the unique phenomenon of burning mode variations with enhanced flame propagation speed may happen. Turbulence induced by droplet movement may dilute the fuel vapor concentration in the aerosol system, which may also hinder the flame size expansion and appearance of the global flame mode.

Considering the safety measures that should be taken in the process industry to avoid aerosol fire hazards, factors influencing aerosol droplet size during pressurized release of industrial fluids should be considered to prevent the formation of flammable aerosols, and safety measures should be taken to avoid the scenarios of fine atomization

of leaked fluids. It was found that distribution of the evaporated fuel concentration prior to encountering the flame can create either global flame scenarios with a high heat release rate or accelerated flame front speed, depending on produced droplet size. Both cases are capable of bringing about significant impacts on the surrounding environment. Until the droplets have fully evaporated, their presence in the aerosol system increases the potential severity of the aerosol fire hazards. Due to the effects droplet size on flame propagation, safety measures should be taken in the process industry to avoid the scenarios of fine atomization of leaked fluids which produces ultra-fine droplet sizes.

Moreover, results of the current work also suggests considering the factors influencing the movement or dispersion of aerosol droplets in the assessment of potential fire hazards of flammable aerosols, because the droplet movement also influences distribution of droplets, the fuel vapor concentration in aerosols and the subsequent combustion characteristics of the flames in aerosols. The factors affecting aerosol formation and dispersion may include distance from the fluid releasing source, turbulence and non-uniformities in the flow and the rate of mixing of fuel and air. Efforts are underway to address these factors and their impacts on aerosol combustion.

Also, there is a need to further develop a method to characterize the flammability of the aerosols. Using an integrated model, the minimum ignition energy values of aerosols are predicted. The aerosol minimum ignition energy is influenced by the fuel-air equivalence ratio and the droplet size. Higher equivalence ratios up to 1.0 significantly reduce the minimum ignition energy, while larger droplet sizes require a higher minimum ignition energy. The trends are in agreement with previous experimental

observations. Considering the safety measures that should be taken in the process industry to avoid ignition of flammable aerosols, the knowledge on properties of the aerosol which can be formed in specific process areas can help determine the minimum ignition energy to characterize the aerosol's flammability. Because of this, proper classification of the area can be carried out, which considers the hazards from the flammable aerosols in the area.

REFERENCES

Abramzon, B., & Sirignano, W. A. (1989). Droplet vaporization model for spray combustion calculations. *International Journal of Heat Mass Transfer*, *32*, 1605-1618.

Aggarwal, S. K. (1997). A review of spray ignition phenomenon. In *33rd AIAA/ASME/SAE/ASEE Joint Propulsion Conference & Exhibit*, Seattle, WA.

Almekinders, J. C., & Jones, C. (1999). Multiple jet electrohydrodynamic spraying and applications. *Journal of Aerosol Science*, *30*, 969-971.

Atzler F, & Lawes M. (1998). Burning velocities in droplet suspensions. In *ILASS-Europe'98*, Manchester, UK.

Atzler, F., Demoulin, F. X., Lawes, M., Lee, Y., & Marquez, N. (2007). Flame speed oscillations in combustion of two-phase mixtures. *Rev. Téc. Ing. Univ. Zulia*, *30*, 23-32.

Ballal D. R., & Lefebvre A. H. (1975). The influence of spark discharge characteristics on minimum ignition energy in flowing gases. *Combustion and Flame*, *24*, 99-108.

Ballal D. R., & Lefebvre A. H. (1979). Ignition and flame quenching of flowing heterogeneous fuel-air mixtures. *Combustion and Flame*, *35*, 155-168.

Ballal, D. R., & Lefebvre, A. H. (1981). Flame propagation in heterogeneous mixtures of fuel droplets, fuel vapor and air. *Eighteenth Symposium (International) on Combustion. The Combustion Institute, 18*, 321-328.

Bocanegra, R., Galan, D., Marquez, M., Loscertales, I. G., & Barrero, A. (2005). Multiple electrosprays emitted from an array of holes. *Journal of Aerosol Science*, *36*, 1387-1399.

Bowen P. J., & Shirvill L. C. (1994). Combustion hazards posed by the pressurized atomization of high-flashpoint liquids. *Journal of Loss Prevention in the Process Industries*, *7*, 233-241.

Bowen P. J., Bull D. C., Prothero A., & Rowson J. J. (1997). Deflagration of hydrocarbon aerosol fuels. *Combustion Science and Technology*, *130*, 25-47.

Burgoyne, J. H., & Cohen, L. (1954). The effect of drop size on flame propagation in liquid aerosols. *Proceedings of the Royal Society*, *225*, 375-392.

Chan, K. K., & Jou, C. S. (1988). An experimental and theoretical investigation of the transition phenomenon in fuel spray deflagration 1. The experiment. *Fuel*, *67*, 1223-1227.

Chan, K. K., & Wu, S. R. (1989). An experimental and theoretical investigation of the transition phenomenon in fuel spray deflagration 2. The model. *Fuel*, *68*, 139-144.

Chigier, N. A., & McCreath, C. G. (1974). Combustion of droplets in sprays. *Acta Astronautica*, *1*, 687-710.

Chigier, N. (1983). Group combustion models and laser diagnostic methods in sprays: A review. *Combustion and Flame*, *51*, 127-139.

Chigier, N. (1991). *Combustion measurements*. New York: Hemisphere Pub. Corp.

Chiu, H. H., Kim, H. Y., & Croke, E. J. (1982). Internal group combustion of liquid droplets. *Nineteenth Symposium (International) on Combustion, the Combustion Institute*, *19*, 971-980.

Danis, A. M. (1987). Spark ignition of monodisperse fuel sprays. Ph.D. Dissertation, Drexel University (Philadelphia, PA).

de la Mora, J. F. (2007). The fluid dynamics of Taylor cones. *Annual Review of Fluid Mechanics*, *39*, 217-43.

Deng, W., Klemic, J. F., & Li, H. (2006). Increase of electrospray throughput using multiplexed microfabricated sources for the scalable generation of monodisperse droplets. *Journal of Aerosol Science*, *37*, 696-714.

Deng, W., & Gomez, A. (2007). Influence of space charge on the scale-up of multiplexed electrosprays. *Journal of Aerosol Science*, *38*, 1062-1078.

Duby, M., Deng, W., Kim, K., Gomez, T., & Gomez, A. (2006). Stabilization of monodisperse electrosprays in the multi-jet mode via electric field enhancement. *Journal of Aerosol Science*, *37*, 306-322.

Dulger M., Sher E., & Chemla F. (1994). Simulation of spark created turbulent flame development through numerical stochastic realizations. *Combustion Science and Technology*, *100*, 141-162.

Eichhorn, J. (1955). Careful! Mists can explode. *Petroleum Refiner*, *34*, 194-196.

Eisazadeh-Far K., Parsinejad F., Metghalchi H., & Keck J. C. (2010). On flame kernel formation and propagation in premixed gases. *Combustion and Flame*, *157*, 2211-2221.

Elkotb, M. M. (1982). Fuel atomization for spray modeling. *Progress in Energy and Combustion Science, 8*, 61-91.

Faeth, G. M. (1977). Current status of droplet and liquid combustion. *Progress in Energy and Combustion Science*, *3*, 191-224.

Faeth, G. M. (1983). Evaporation and combustion of sprays. *Progress in Energy and Combustion Science*, *9*, 1-76.

Faeth, G. M. (1990). Structure and atomization properties of dense turbulent sprays. *Twenty-Third Symposium (International) on Combustion, the Combustion Institute*, *23*, 1345-1352.

Faeth, G. M., Hsiang, L. P., & Wu, P. K. (1995). Structure and breakup properties of sprays. *International Journal of Multiphase Flow*, *21*, Suppl. 99-127.

Faeth, G. M. (1996). Spray combustion phenomena. *Twenty-Sixth Symposium (International) on Combustion, the Combustion Institute*, *26*, 1593-1612.

Febo, H. L. (1995). Heat transfer fluid mist explosion potential: An important consideration for users. In *AIChE Loss Provention Symposium*, Norwood, ME.

Febo, H. L., & Valiulis, J. V. (1996). Recognize the potential for heat-transfer-fluid mist explosions. *Chemical Engineering Progress*, *92*, 52-55.

Glassman, I., & Yetter, R. A. (2008). *Combustion* (4^{th} ed.). Elsevier.

Greenberg J., McIntosh A., & Brindley J. (1999). Instability of a flame front propagating through a fuel-rich droplet-vapor-air cloud. *Combustion Theory and Modeling*, *3*, 567-584.

Hayashi, S., & Kumagai, S. (1974). Flame propagation in fuel droplet-vapor-air mixtures. *Fifteenth Symposium (International) on Combustion, the Combustion Institute*, *15*, 445-452.

Hayashi, S., Ohtani, T., Iinuma, K., & Kumagai, S. (1981). Limiting factor of flame propagation in low-volatility fuel clouds. *Eighteenth Symposium (International) on Combustion, the Combustion Institute*, *18*, 361-367.

Health and Safety Executive (HSE) (2000). *Offshore hydrocarbon releases statistics. Offshore technology report OTO 2000 112*. Bootle, Merseyside, UK: HSE.

Hinze, J. O. (1955). Fundamentals of the hydrodynamic mechanism of splitting in dispersion processes. *AIChE Journal*, *1*, 289-295.

Hsiang, L. P., & Faeth, G. M. (1995). Drop deformation and breakup due to shock wave and steady disturbances. *International Journal of Multiphase Flow*, *21*, 545-560.

Jaworek, A., Balachandran, W., Lackowski, M., Kulon, J., & Krupa, A. (2006). Multi-nozzle electrospray system for gas cleaning processes. *Journal of Electrostatics*, *64*, 194-202.

Jaworek, A. (2007). Micro- and nanoparticle production by electrospraying. *Powder Technology*, *176*, 18-35.

Johnson, D. W., & Woodward J. L. (1999). *RELEASE – a model with data to predict aerosol rainout in accidental releases*. New York, NY: Center for Chemical Process Safety/AIChE.

Juan, L. D., & de la Mora, J. F. (1997). Charge and size distributions of electrospray drops. *Journal of Colloids and Interface Science*, *186*, 280-293.

Kim, S. J., Song, Y., Skipper, P. L., & Han J. (2006). Electrohydrodynamic generation and delivery of monodisperse picoliter droplets using a poly(dimethylsiloxane) microchip. *Analytical Chemistry*, *78*, 8011-8019.

Ko, Y., Anderson, R. W., & Arpaci, V. S. (1991). Spark ignition of propane-air mixtures near the minimum ignition energy: Part I. An experimental study. *Combustion and Flame*, *83*, 75-87.

Kono, M., Kumagai, S., & Takai, T. (1977). The optimum condition for ignition of gases by composite sparks. *Symposium (International) on Combustion*, *16*, 757-766.

Krishna, K., Kim, T. K., Kihm, K. D., Rogers, W. J., & Mannan, M. S. (2003a). Predictive correlations for leaking heat transfer fluid aerosols in air. *Journal of Loss Prevention in the Process Industries*, *16*, 1-8.

Krishna, K., Rogers, W. J., & Mannan, M. S. (2003b). The use of aerosol formation, flammability, and explosion information for heat transfer fluid selection. *Journal of Hazardous Materials*, *104*, 215-226.

Krishna, K., Rogers, W. J., & Mannan, M. S. (2004). Consider aerosol formation when selecting heat transfer fluids. *Chemical Engineering Progress*, *100*, 25-28.

Krzeczkowski, S. A. (1980). Measurement of liquid droplet disintegration mechanisms. *International Journal of Multiphase Flow*, *6*, 227-239.

Law, C. K. (1982). Recent advances in droplet vaporization and combustion. *Progress in Energy and Combustion Science*, *8*, 171-201.

Lawes, M., Lee, Y., & Marquez, N. (2002). Enhanced burning rates due to droplet induced flame instabilities. *Proceedings of the 18th Annual Conference on Liquid Atomization and Spray Systems*, *98*, 475-481.

Leung, E. H., & Halliday, D. X. (2010). "Flashburning"-interpreting the presence of heat damage to a suspect's clothing and footwear in the investigation of fires. *Science and Justice*, *50*, 187-191.

Lewis, B., & von Elbe, G. (1987). *Combustion, flames, and explosions of gases*. Orlando, FL: Academic Press.

Lian, P., Mejia, A. F., Cheng, Z., & Mannan, M. S. (2010). Flammability of heat transfer fluid aerosols produced by electrospray measured by laser diffraction analysis. *Journal of Loss Prevention in the Process Industries*, *23*, 337-345.

Maragkos, A., & Bowen, P. J. (2002). Combustion hazards due to impingement of pressurized releases of high-flashpoint liquid fuels. *Proceedings of the Combustion Institute*, *29*, 305-311.

Mejia, A.F., He, P., & Cheng, Z. (2009). Uniform discotic wax particles via electrospray emulsification. *Journal of Colloid and Interface Science*, *334*, 22-28.

Muñoz, M., Planas, E., Ferrero, F., & Casal, J. (2007). Predicting the emissive power of hydrocarbon pool fires. *Journal of Hazardous Materials*, *144*, 725-729.

Myers, G. D., & Lefebvre, A. H. (1986). Flame propagation in heterogeneous mixtures of fuel drops and air. *Combustion and Flame*, *66*, 193-210.

Pidoll, U. v. (2001). The ignition of clouds of sprays, powders and fibers by flames and electric sparks. *Journal of Loss Prevention in the Process Industries*, *14*, 103-109.

Pischinger S, & Heywood J. B. (1990). A model for flame kernel development in a spark-ignition engine. *Twenty-third Symposium (International) on Combustion, The Combustion Institute*, *23*, 1033-1040.

Polymeropoulos, C. E. (1984). Flame propagation in aerosols of fuel droplets, fuel vapor and air. *Combustion Science and Technology*, *40*, 217-232.

Rao, K. V. L., & Lefebvre, A. H. (1976). Minimum ignition energies in flowing kerosene-air mixtures. *Combustion and Flame*, *27*, 1-20.

Regele, J. D., Papac, M. J., Rickard, M. J. A., & Dunn-Rankin, D. (2002). Effects of capillary spacing on EHD spraying from an array of cone jets. *Journal of Aerosol Science*, *33*, 1471-1479.

Rulison, A. J., & Flagan, R. C. (1993). Scale-up of electrospray atomization using linear arrays of Taylor cones. *Rev. Sci. Instrum*, *64*, 683-686.

Schwar, M. J. R., & Weinberg, F. J. (1969). The measurement of velocity by applying schlieren-interferometry to Doppler-shifted laser light. *Proceedings of the Royal Society*, *311*, 469-476.

Sher E., Kravchik T., & Heywood J. B. (1995). From spark ignition to flame initiation. *Combustion Science and Technology*, *108*, 1-30.

Si, B. Q. T., Byun, D., & Lee, S. (2007). Experimental and theoretical study of a cone-jet for an electrospray microthruster considering the interference effect in an array of nozzles. *Journal of Aerosol Science*, *38*, 924-934.

Singh A. K. (1986). Spark ignition of monodisperse aerosols. Ph.D. Dissertation, Rutgers University, the State University of New Jersey (New Brunswick, NJ).

Sirignano, W. A. (2010). *Fluid dynamics and transport of droplets and sprays*. Cambridge, UK: Cambridge University Press.

Snarski, S. R., & Dunn, P. F. (1991). Experiments characterizing the interaction between two sprays of electrically charged liquid droplets. *Experiments in Fluids*, *11*, 268-278.

Suard, S., Nicoli, C., & Haldenwang, P. (2001). Vaporisation controlled regime of flames propagating in fuel-lean sprays. *J. Phys. IV France*, *11*, 301-310.

Suard, S., Haldenwang, P., & Nicoli, C. (2004). Different spreading regimes of spray-flames. *C. R. Mecanique*, *332*, 387-396.

Sukmarg, P., Krishna, K., Rogers, W. J., Kihm, K. D., & Mannan, M. S. (2002). Non-intrusive characterization of heat transfer fluid aerosol sprays released from an orifice. *Journal of Loss Prevention in the Process Industries*, *15*, 19-27.

Tang, K., & Gomez, A. (1996). Monodisperse electrosprays of low electric conductivity liquids in the cone-jet mode. *Journal of Colloids and Interface Science*, *184*, 500-511.

Thiele M., Selle S., Riedel U., Warnatz J., & Maas U. (2000). Numerical simulation of spark ignition including ionization. *Proceedings of the Combustion Institute*, *28*, 1177-1185.

Turetsky, A. Y., Tavolzhansky, V., Chernova, E. A., & Lipatov, G. N. (2000). Features of electrospray of solutions with different physico-chemical parameters. *Journal of Aerosol Science, 31*, S865-S866.

Williams, A. (1973). Combustion of droplets of liquid fuels: a review. *Combustion and Flame*, *21*, 1-31.

Williams, A. (1990). *Combustion of liquid fuel sprays*. Boston, MA: Butterworths.

Wilm, M. S., & Mann, M. (1994). Electrospray and Taylor-cone theory, Dole's beam of macromolecules at last? *International Journal of Mass Spectrometry and Ion Processes*, *136*, 167-180.

Witlox, H. W. M., & Bowen P. J. (2002). *Flashing liquid jets and two-phase dispersion: a review*. Merseyside, UK: Health and Safety Executive.

Woodward, J. L., Cook, J., & Papadourakis, A. (1995). Modeling and validation of a dispersing aerosol jet. *Journal of Hazardous Materials*, *44*, 185-207.

Woodward, J. L., & Papadourakis, A. (1995). Reassessment and reevaluation of rainout and dropl size correlation for an aerosol jet. *Journal of Hazardous Materials*, *44*, 209-23.

VITA

Peng Lian was born in China in 1980. He holds a Ph.D. in chemical engineering from Texas A&M University (2011), M.S. degree in applied chemistry from China University of Petroleum, Beijing (2005), and B.S. degree in applied chemistry from Liaoning University of Petroleum and Chemical Technology (2002). During his Ph.D. studies, he joined the Mary Kay O'Connor Process Safety Center as a graduate researcher with focus on flammability and fire hazard analysis of aerosols formed by industrial hydrocarbon fluids. Previously he worked for China Petrochemical Corporation (SINOPEC) as technical engineer for product development of lubricating oil and grease. Peng Lian's permanent address is: Peng Lian, C/O Dr. M. Sam Mannan, Artie McFerrin Department of Chemical Engineering, Texas A&M University, College Station, TX 77843-3122.